CHAIN DYNAMICS AND LAYERING WITHIN POLYELECTROLYTE MULTILAYER FILMS

A Dissertation

by

VIKTAR SELIN

Submitted to the Office of Graduate and Professional Studies of
Texas A&M University
in partial fulfillment of the requirements for the degree of

DOCTOR OF PHILOSOPHY

Chair of Committee,	Svetlana A. Sukhishvili
Committee Members,	Jodie Lutkenhaus
	Yossef Elabd
	Zhengdong Cheng
Head of Department,	Ibrahim Karaman

December 2018

Major Subject: Materials Science and Engineering

ABSTRACT

The current study is focused on understanding main factors affecting dynamics of polymer chains included within layer-by-layer (LbL) films and impact of chain dynamics on film structure. LbL films, or polyelectrolyte multilayers (PEMs), can be deposited on a variety of substrates such as silicon, glass, plastics, and metals *via* alternating adsorption of oppositely charged polymers. Modification of surfaces with LbL films impart the substrates with new properties and functionalities, such as controlled wettability and uptake of water or capability to retain and/or controllably release small molecules. For many applications of PEMs, specifically for constructing multifunctional films for sequential, multi-step delivery of bioactive compounds, it is critically important to understand and control film structure. There are two possible modes of the PEM growth: linear growth, with a small, constant increase in the film thickness at each dipping step (*l*PEMs), and non-linear growth, with per-cycle film mass increasing with the number of deposited layers (*nl*PEMs). PEMs can switch between linear and non-linear film growth as a function of pH, temperature, or number of deposited layers. My goal was to relate polyelectrolyte chain mobility to the mechanism of PEM film growth and to establish the origin of transitions between linear and non-linear growth regimes. This goal was accomplished in experiments which allowed direct observation of chain displacements and PEM structural evolution upon exposure of these films to solutions at varied pH and ionic strength. My findings widen the fundamental knowledge about the mechanism of LbL growth and can be used for developing theories and modeling of PEM films. Moreover, these results can be useful in designing polyelectrolyte nanoassemblies for

biomedical applications, such as drug delivery coatings for medical implants or tissue engineering matrices.

ACKNOWLEDGEMENTS

I would like to express my sincere gratitude and deep appreciation to my research advisor Professor Dr. Svetlana A. Sukhishvili for her constant encouraging and patience and support at the times of hardship. Her tremendous contributions have been absolutely invaluable and I cannot thank her enough for her understanding in my times of need.

I also would like to thank my committee members, Dr. Lutkenhaus, Dr. Elabd, and Dr. Cheng for their guidance throughout the course of this research. I would also like to thank Dr. John F. Ankner for his insight and contribution to my work.

I thank my group members, Victoria Albright, Hanna Hlushko, Adwait Gaikwad, Parvin Karimineghlani, Raman Hlushko, Qing Zhou, Alex Aliakseyeu, Anja Krieger, and Diana Al Husseini.

Special thanks to my former colleagues Iryna and Alex Zhuk for their constant support and friendship.

Many thanks to Vasily and Benjamin Belov for the widening my knowledge in the variety of topics.

I thank Dr. Hanna Poznjak for the infinite support and help.

The biggest thanks go to my family. I thank my mother who first who supported my goal to pursue Ph.D. in the U.S. and who has been supporting for me the whole time.

CONTRIBUTORS AND FUNDING SOURCES

All work for the dissertation was completed by the student, under the advisement of Dr. Svetlana A. Sukhishvili of the Department of Materials Science and Engineering in collaboration with Dr. John F. Ankner from Oak Ridge National Laboratory.

This work was made possible in part by National Science Foundation under Grant Numbers DMR-1610725 and DMR-0906474.

NOMENCLATURE

AFM	Atomic force microscopy
ATRP	Atom transfer radical polymerization
BPEI	Branched polyethylenimnine
D	Diffusion coefficient
DMA	2-(dimethylamino)ethyl methacrylate
EBiB	Ethyl-2-bromoisobutyrate
FRAP	Fluorescent recovery after photobleaching
HMTETA	1,1,4,7,10,10-hexamethyltriethylenetetramine
LbL	Layer-by-layer
*l*PEM	linear polyelectrolyte multilayers
NR	Neutron reflectometry
PA	Polyanion
PC	Polycation
PDI	Polydispersity index
PDMAEMA	Poly(2-(dimethylamino)ethyl methacrylate)
PE	Polyelectrolyte
PEC	Polyelectrolyte complex
PMAA	Poly(methacrlylic) acid

TABLE OF CONTENTS

Page

LIST OF FIGURES

Page

LIST OF TABLES

Page

1. INTRODUCTION

1.1. Introduction to Layer-by-Layer Technique

The layer-by-layer (LbL) technique is a robust method to construct polyelectrolyte multilayers (PEM) based upon sequential deposition of interacting components.[1] A large variety of interactions can be used such as hydrogen-bonding, covalent, host-guest, electrostatic interactions, etc. with electrostatic interactions being the most widely studied.[2] The large variety of interactions that can be used to deposit LbL films provides flexibility in the choice of components and, therefore, the ability to preprogram functionality of the resulting films (Fig 1-1).

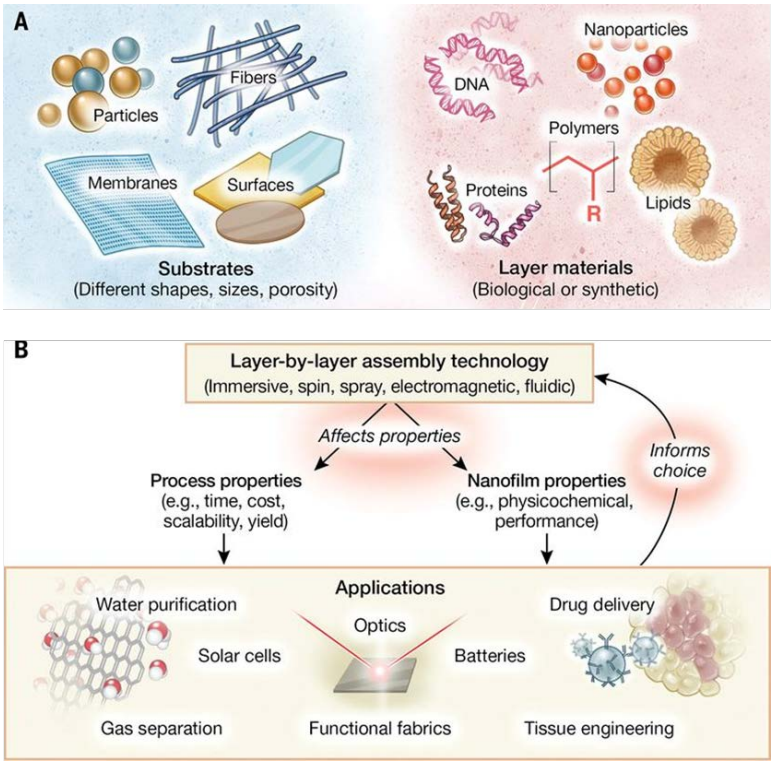

Fig. 1-1. Schematic overview of possible LbL components (A) and possible applications (B). Reprinted from [6] with permission from AAAS.

Thus, as film constituents, multiple components such as polymers, small molecules[3], micelles[4], 2D materials[5] can be used (Fig 1-1A). Using a proper surface pretreatment technique allows growing PEMs on the variety of substrates including silicon[6], titanium[7], polymers.[8-9] As a result, LbL is a powerful and robust technique that may find applications in multiple fields such as gas separation[10], sensors[11] and drug delivery (Fig 1-1B).[12]

In a basic experiment (Fig. 1-2) a pretreated substrate is alternatingly exposed to working solutions of polyelectrolytes, with rinsing steps in between, until the desired number of layers is deposited. There are multiple ways how LbL deposition can be performed. In a classical way, also known as dipping deposition, described by Decher[13], the substrate is alternatively immersed into polymer solutions (Fig. 1-2A). The advantage of this implementation is in its ability to use a substrate of arbitrary size and shape. However, the deposition process sometimes can be very time-consuming. To speed up the deposition process a spin-assisted deposition can be used (Fig. 1-2B). A flat pretreated substrate is fixed on the reactionary stage and working solutions are placed on top of the substrate alternately. The centrifugal force that is a function of a rotating speed alter the structure and properties of resulting PEMs.[14] Such a difference was demonstrated with free-standing films prepared by dip- and spin-assisted deposition of poly(ethylene oxide) and poly(acrylic acid) demonstrated a striking difference in optical properties. Furthermore, Seo *et al.* showed that the opacity of the material made of the dip-assisted film is related to the surface roughness while the transparency of the material made of the spin-assisted film is attributed to the stratified nature of the film.[15]

One more way to deliver solutions to the surface is to use spraying (Fig. 1-2C). Kolasinska *et al.* reported that PEMs prepared by dipping are thicker, denser, and less rough than films assembled by spraying having the same number of layers.[16]

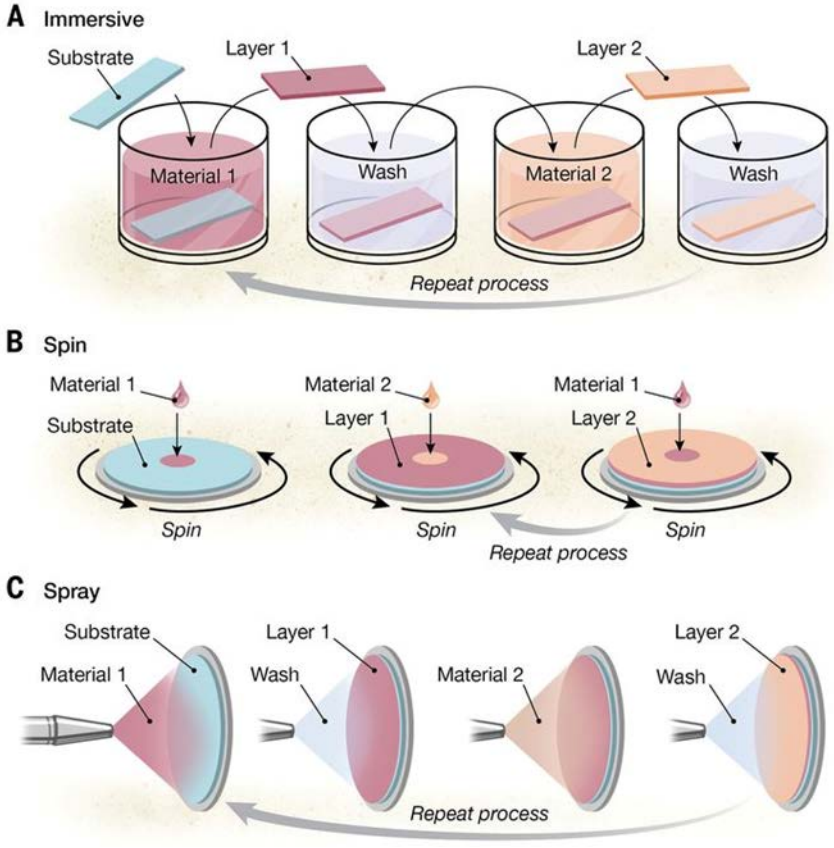

Fig. 1-2. Schematic representation of LbL process using dipping (A), spin-coating (B) and spray-coating (C) techniques. Reprinted from [6] with permission from AAAS.

1.2. Growth Regimes of LbL Films

The literature distinguishes two regimes of PEMs growth – namely, linear and non-linear. The linear regime is dominant and observed for many systems composed of strong polyelectrolytes.[17-18] On the other hand, multilayers composed of polyelectrolyte pairs with weaker binding (such as polypeptides, polysaccharides) are frequently reported to

grow non-linearly.[19-21] Generally, the literature agrees that interaction strength is the main factor that controls growth regime (Fig. 1-3).

Additionally, the growth regime can be controlled by deposition conditions. For example, the growth regime for systems that contain weak polyelectrolytes can be altered by pH adjustments. Such adjustments affect ionization degree of polyelectrolytes causing charge misbalance and as a result weaker binding and non-linear growth.[22-23] Since PEM formed by oppositely charged polymer chains are electrostatic by nature, salt is one more way to affect intrinsic ion pairing and interaction strength. Salt added upon assembly screens the electrostatic charges on the polyelectrolyte chains resulting in a larger thickness.[24-25] However, a further increment of salt concentration may cause a decrease in thickness and even film dissolution.[18, 26] Other deposition variables such as temperature,[27-29] polyelectrolyte molecular weight,[30-31] and chain architecture[32-33] can also be used to affect the PEMs growth.

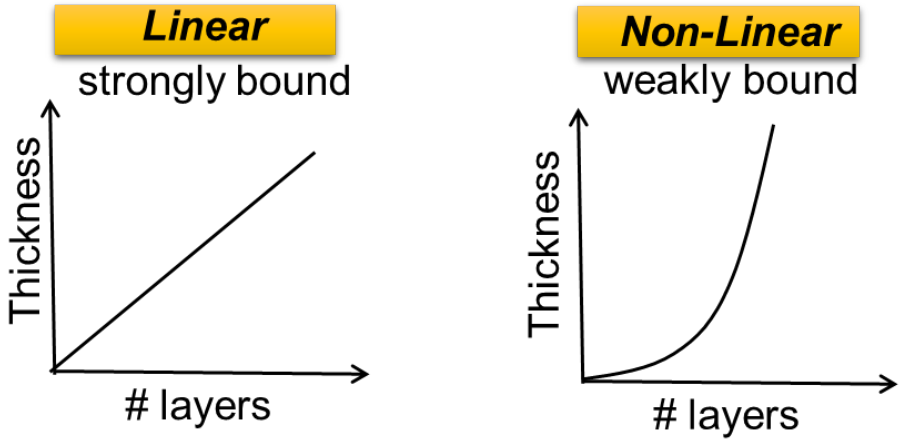

Fig. 1-3. Schematic representation of linear (left) and non-linear (right) growth.

1.3. General Introduction

Assembly of PEM films using the LbL technique has emerged as a powerful means to create a variety of coatings and/or functional nanostructured materials useful in biomedical, sensing, photovoltaics, separation, and photonic applications.[13, 34-37]

LbL technique presents a versatile way to coat the surfaces of a diverse range of materials with nanoscopically structured films.[38] PEMs have found a number of applications, showing particular promise for surface functionalization of biomedical devices to control cell adhesion, antibacterial properties and localized delivery of bioactive molecules.[37,39,40]

Current development of advanced materials for implants, coronary stents, and catheters often involves both organic and inorganic components.[41-44] Such hybrid materials can advantageously combine, for example, the excellent mechanical properties and durability of inorganic materials (such as titanium and ceramics) with the capability of polymers to self-heal or serve as a platform for drug delivery and control cellular proliferation.[45] Traditionally, polymers are deposited on surfaces of biomaterials *via* heat molding or solution casting,[46-48] but controlling the uniformity, thickness, and functionality of the coating using these methods is challenging.[49]

In addition to ionically pairs, cooperative interactions that lie at the heart of many LbL systems — secondary interactions such as hydrogen bonding, van der Waals forces, and hydrophobic interactions — can also play important role in LbL assembly.[50-52] The cooperative type of intermolecular interactions is quite universal and can be applied to metal-protein [53] and hydrogen bonding systems.[54]

Among many external factors that influence assembly and post-assembly behavior of LbL films (such as temperature, solvent, and pH, among others), the effect of salt is most closely related to the electrostatic nature of ionic pairing within PEM films. Stratified *l*PEMs are built from kinetically frozen polyelectrolyte chains, which are stitched together by multiple ionic polymer-polymer associations. Atomic force microscopy (AFM) studies of film surface topography[55-56] and fluorescence recovery after photobleaching (FRAP)[57-58] studies of the diffusion of assembled PE chains reveals an absence of chain motion and rearrangement at low salt concentrations. Addition of salt promotes chain motion as the salt ions break "old" polymer-polymer contacts and allow new ones to form. Such mobility has been observed as AFM-measured film smoothing,[55-56] or as the center-of-mass diffusion of assembled polymer chains as demonstrated by FRAP.[57-59] Post-assembly exposure of PEMs to salt solutions also increases film fuzziness, *i.e.* the degree of interpenetration between individual film layers, as indicated by NR[60-62] and neutral impact collision ion scattering spectroscopy.[63] Yet salt-induced diffusion of PE chains within the bulk of PEM films remains poorly understood quantitatively, with the only experimental results on salt dependence being an AFM topography study of the film surface.[56] Molecular-level information on the structure and dynamics of LbL films has been derived from FRAP and NR experiments,[64-67] but these studies did not explore the functional dependence of polymer chain dynamics and LbL film structure on salt concentration.

While multilayer films are closely related to polyelectrolyte complexes (PECs),[68-69] the layering and anisotropic dynamics of polymer chains[70] raise new questions about the directional dependence of polymer chain motions. However, even for PECs, the salt

dependence of chain dynamics has scarcely been studied, with only one recent report of a stretched exponential dependence of the PEC apparent relaxation time on salt concentration in a rheological experiment.[71] For structured, anisotropic PEM films, McAloney *et al*. observed an exponential dependence of the characteristic time for film surface smoothing on salt concentration.[56] However, for the bulk of PEM films, such dependencies are not reported.

A decrease in the inter-polyelectrolyte binding strength leads to complete loss of film structure and formation of strongly interdiffused, exponentially depositing films.[72] In contrast to the consistent picture showing the role of polyelectrolyte type (i.e. strength of polyelectrolyte "sticky" binding points) and charge density on stratification of LbL films,[61, 73-74] our understanding of the effect of other fundamental parameters of polyelectrolyte chains (such as polyelectrolyte molecular weight) on film structure is still in its infancy.[62,65]

Depending on the binding strength between the components[18, 75], and therefore the mobility of polymer chains during LbL film deposition, two main types of film growth can be distinguished. Namely, linear LbL growth describes those systems that exhibit a constant increment in thickness with deposition of successive bilayers and is usually a characteristic of strongly paired polyelectrolytes and/or nanoparticles[20, 76]. In contrast, non-linear films demonstrate an increase in deposited film mass per deposition step, reflecting the high mobility of chains during deposition and the resulting penetration of the invading component into the film.[19, 77-78] Non-linear growth mode has been predominantly reported for more weakly bound systems, and can be additionally

controlled by several parameters. One of these parameters is polymer molecular weight — a parameter that is directly related to mobility of polymer chains within the films.[59, 79] For ionically paired PEMs, the mobility of chains also can be regulated by the introduction of small ions.[80-81] Moreover, in the case of weak polyelectrolytes, ionization of polymer chains, determined by solution pH and assembly conditions, can also affect chain mobility and film growth.[82-83]

Diffusion of at least one of polyelectrolytes within the film was established as a condition necessary to observe exponential film growth, and a model suggesting "in-and-out" free diffusion of polyelectrolyte chains between film and solution at alternating film deposition cycles was developed.[19, 72, 84] Diffusion of polyelectrolyte chains being limited to a zone close to the film-solution interface was also suggested, and used to explain a transition from exponential to linear film growth after a large number of deposition steps.[85] The "in-and-out" model is widely but not universally accepted; some groups propose an alternative "dendritic and island" explanation for exponential film growth.[86] The only existing mathematical model of exponential film growth[21] assumes diffusion of polyelectrolytes throughout PEMs and consequent film swelling. To assess the validity of such assumptions, it is necessary to measure and quantify chain diffusion and layer intermixing in nonlinear PEMs. Very recently, another mechanism of exponential growth has been proposed by Schlenoff that describes nonlinear deposition as a consequence of the diffusion of ionic binding sites rather than mass diffusion of the polymers.[87] Overall, in spite of an increasing number of experimental reports of nonlinear growth in LbL films, the structure and dynamics of these films are still poorly understood.

For the use of LbL films as drug-delivery coatings, the overall capacity for loading bioactive molecules is especially important, and micron-thick rather than ultrathin films are optimal. At the same time, it is desirable to control film stratification to enable sequential delivery of multiple functional molecules.[88] Addressing this challenge requires a detailed understanding of LbL films that grow non-nonlinearly and feature more mass deposited in fewer steps compared to films grown linearly.[20]

Our goal is to address several unanswered questions regarding chain dynamics within polyelectrolyte multilayers assembled at the conditions where linear or non-linear film deposition occurs. First, we aim to quantitatively explore functional dependences of center-of-mass diffusion of LbL-assembled polyelectrolyte chains on salt concentration in directions parallel and perpendicular to the substrate. While diffusion in the direction perpendicular to the substrate at various salt concentrations will be determined in neutron reflectometry experiments (described in the next chapter), diffusion in the direction parallel to the substrate will be compared with the same system in FRAP experiments. In addition, our goal is to study the molecular weight dependence of the salt-induced film layer intermixing by alternating PMAA chain length. Second, we aim to focus on *nl*PEMs and study the correlation between chain diffusivity, polyelectrolyte deposition time, and film internal structure at different stages of film growth for *nl*PEMs of varying deposition history. To achieve that we will systematically monitor *nl*PEMs growth in a dry state as well as *in situ* by spectroscopic ellipsometry. During these studies, a deposition time of films assembly will not be fixed, and we will explore internal structure and polyelectrolyte ionization at the stages where PEMs are completely saturated with components. Third, we

aim to study the case of the assembly where deposition times were fixed for all layers within the film but varied between different films. We will study swelling of LbL films constructed using fixed deposition time and explore how the internal film structure affects the kinetics of polyelectrolyte chain invasion. Moreover, we aim to explore the effect of layer deposition time on film stability in salt solutions.

2. EXPERIMENTAL PROCEDURES

2.1. Labeling of PAs

Labeling of PMAA with Alexa Fluor® 488 was performed in 0.1 M phosphate buffer at pH 5 as described elsewhere.[89] 5 µL (6.34×10^{-4} mmol) of PMAA solution, 1 mg (5.20×10^{-3} mmol) of 1-ethyl-3-(3-dimethylaminopropyl)carbodiimide hydrochloride and 1.2 mg (5.50×10^{-3} mmol) of N-hydroxysulfosuccinimide sodium salt were mixed in 0.1 M phosphate buffer at pH 5. The solution was continuously stirred for one hour, followed by the addition of 25 µL (4.38×10^{-4} mmol) of Alexa Fluor® 488 dihydrazide in 0.1 M phosphate buffer at pH 5. The reaction was allowed to continue overnight. The solution was then diluted with 0.1 M phosphate buffer solution at pH 7 and dialyzed against 0.01 M phosphate buffer at pH 7 with 0.1 M NaCl for 72 hours, and then against Milli-Q water for 48 hours. The molecular weight cutoff of the dialysis cassettes was 5,000 for $PMAA_{7k}$ and 10,000 for $PMAA_{25k,}$ $PMAA_{105k}$, $PMAA_{145k}$ and $PMAA_{480k}$. The dialysis was terminated when no fluorescence was detected in the outer dialysis water (measured by FCS).

2.2. Synthesis and Quaternization of PCs

2.2.1. PDMA synthesis

Hydrogenated poly(2-(dimethylamino)ethyl methacrylate) (hPDMAEMA) homopolymer was synthesized by atom transfer radical polymerization (ATRP) as previously described[90]. In brief, DMAEMA (1.86 g), EBiB, CuBr, and HMTETA were mixed in 8 mL of 2-propanol, at a molar ratio of 150:1:1:2, respectively. The solution was stirred continuously in an argon atmosphere at room temperature for 12 h. The

polymerization was terminated with liquid nitrogen and the solution diluted with THF. The copper salts were purified by passage through a basic aluminum oxide column. The polymer was precipitated in cold hexane and then dried in a vacuum oven at 25 °C overnight. Gel permeation chromatography (GPC) analysis of hPDMAEMA was performed in DMF with polystyrene (PS) standards.

2.2.2. PDMA quaternization

The Mw and Mw/Mn of the homopolymer were 90 kDa and 1.10, respectively, as determined by GPC. Quaternization of hPDMAEMA to obtain a 100% quaternized polycation with a molecular weight of 95 kDa, abbreviated here as hQPC, was carried out at room temperature. To synthesize hQPC, hPDMAEMA was dissolved in a mixture of ethanol/benzene (v:v = 3:1), and a stoichiometric amount of hydrogenated dimethyl sulfate was added to the solution. The mixture was stirred at room temperature overnight (Fig. A-1). The precipitated product was washed with acetone three times and dried under vacuum overnight. A similar procedure was carried out to synthesize deuterated quaternized polycation (dQPC). To that end, dPDMAEMA was treated with fully deuterated rather than hydrogenated methyl sulfate. The degree of quaternization was determined by 1H-NMR in D2O at pH 9. Briefly, after quaternization with dimethyl sulfate, a new peak at 3.3–3.4 ppm appeared, reflecting successful quaternization of the dimethylamino proton with a methyl group. The absence of a peak C at δ 2.3–2.5 ppm and a peak at δ 4.2–4.4 ppm, which both correspond to dimethylamino protons in hPDMAEMA, indicates complete quaternization of hPDMAEMA homopolymer.

2.3. LbL Films Assembly

LbL films were deposited on silicon wafer substrates (111, Institute of Electronic Materials Technology, Poland) by sequential dipping in 0.2 mg/L PMAA and QPC solutions in 0.01 M phosphate buffer at pH 4.5 or pH 6.0 for 10 min. Prior to film deposition, silicon wafers were cleaned as described elsewhere[81] and primed with a monolayer of BPEI adsorbed from 0.2 mg/mL solution at pH 9 for 15 min. In between polymer deposition steps, the wafers were rinsed twice by immersing in 0.01 M phosphate buffer solutions at pH 4.5 or pH 6.0 for 2 min. Film deposition was terminated after depositing a desired number of layers.

2.4. Characterization Methods

2.4.1. Fluorescence recovery after photobleaching (FRAP)

The effect of molecular weight on the diffusion coefficient of PMAA* within PC/PMAA multilayer films was performed using a homemade FRAP setup with design and optics described earlier.[23, 70, 89] Briefly, the 488 nm wavelength light beam from a Spectra-Physics Stabilite 2017 laser is spatially filtered and expanded three times, attenuated 100 times, reflected from a Chroma Q505LP dichroic mirror and illuminates the back aperture of an Olympus 60× plan apochromat infinity-corrected oil immersion objective with N.A. of 1.45. The fluorescent signal collected from the sample by the same objective passes through the dichroic mirror, is reflected from a Thorlabs BB1-E02 broadband dielectric mirror, and then filtered by a Chroma HQ535/50 narrow band filter and a spatial filter with 10 cm focus length and 15 μm pinhole. This provides the effective optical system magnification of 37.5×, and allows the sample volume lateral size behind

the pinhole to be 0.4 μm. The exact value of a bleaching spot radius (0.239 μm) was determined experimentally by FCS using calibration solution of Alexa 488 Fluor® with the known value of the diffusion coefficient. The FRAP instrument was equipped with a programmable computer-controlled shutter in order to control measurements in required time intervals.

QPC/PMAA PEMs were prepared by LbL assembly within home-built glass cuvettes. A surface priming layer was prepared by injecting BPEI solution at pH 9 into the cells for 15 min, followed by rinsing with Milli-Q water. Alternative depositions of polyelectrolytes were controlled at pH 4.5 and room temperature with two 1 min 0.01 M phosphate/citrate buffer rinsing cycles between the 15 min polymer deposition steps. 60 μl of NaCl solutions were added into glass cells with deposited films and sealed with parafilm. Concentration and pH of NaCl solutions within 0.01 M phosphate/citrate buffer were adjusted to various values depending on the experiment. A spot in the films was bleached for 5 seconds by a focused laser at 1 mW. After the bleaching process, the fluorescence intensity of multilayer films in the bleached zone was recorded every 2 - 60 min (depending on the observed recovery kinetics and a time program) at 1 μW. Since the recovering time required for fluorescence intensity of films in all experiments was much longer than the bleaching time (≥2 hours vs. 5 seconds), a contribution of molecular motion during bleaching to the fluorescence intensity recovery profile was negligible.

2.4.2. Spectroscopic Ellipsometry

Thicknesses and optical constants in both dry and swollen states of PEMs were characterized by a variable angle spectroscopic ellipsometer (VASE, M-2000

UV−visible−NIR (240−1700 nm) J. A. Woollam Co., Inc., Lincoln, NE, USA) equipped with a temperature-controlled liquid cell. For measurements in the liquid cell, the cell geometry dictated that the angle of incidence be 75°. In all experiments, the temperature was set to 25 °C. To avoid effects of absorption in the ultraviolet and near-infrared light region by the buffer solution, the working wavelength band was set to 370.5–999 nm. Prior to deposition of PEM films, the thickness of the oxide layer on the silicon substrate was measured. Dry measurements were carried out at three angles of incidence: 45°, 55°, and 65°.

To fit the ellipsometric data from dry films, a three-layer model was used, in which the first two layers represented the silicon substrate and its oxide layer, and the third layer represented the PEM film. The polymer layer was treated as a Cauchy material of thickness d, having a wavelength-dependent refractive index $n(\lambda) = A + B/\lambda^2 + C/\lambda^3$, where A, B, and C are fitting coefficients, and λ is the wavelength. The film extinction coefficient was assumed to be negligible ($k = 0$). Thickness d and the three coefficients A, B, and C were fitted simultaneously.

For *in situ* ellipsometry experiments, a silicon wafer with a pre-deposited film of known dry thickness was placed into a liquid cell. The cell was then filled with 0.01 M buffer at pH 6.0 and a thickness measurement was taken. The measurements were finalized after a constant wet thickness was reached and then by removing the sample from the cell, drying with nitrogen flow, and measuring the dry thickness again. To fit the ellipsometric data for the in situ measurements, a four-layer model was used. An additional layer represents the semi-infinite buffer solution and was also treated as a

transparent Cauchy medium, with a wavelength-dependent refractive index $n_{buf}(\lambda) = A_{buf} + B_{buf}/(\lambda)^2 + C_{buf}/(\lambda)^3$, where A_{buf}, B_{buf}, and C_{buf} are fitting coefficients, and λ is the wavelength. For the buffer solutions, A_{buf}, B_{buf}, and C_{buf} were determined prior to in situ experiments by measuring $n_{buf}(\lambda)$ for a bare, clean silicon wafer installed in the liquid cell containing 0.01 M phosphate buffer at pH 6.0. After completion of the in situ measurements, the dry thicknesses of the films were measured again to assure that the thicknesses used in the swelling experiments were consistent with the independently measured dry film thicknesses obtained in the film growth experiments. In all experiments, the coefficients A, B, C were consistent within 5%.

2.4.3. Fourier-transform infrared spectroscopy (FTIR)

To study ionization of PMAA chains within PEM films, $PMAA_{11}^{4min}$ and $PMAA_{11}^{24min}$ films were deposited onto undoped silicon wafers (University Wafer, Inc., Boston, MA, USA) and FTIR spectra were recorded with a Tensor II spectrophotometer (Bruker Optic GmbH, Ettlingen, Germany). For each sample, 96 scans were recorded between 600 and 4 000 cm^{-1} with 4 cm^{-1} resolution with the standard Bruker OPUS/IR software (version 7.5), using an interferogram of a bare silicon wafer as a background. To obtain and study QPC_{12}^{4min} and QPC_{12}^{24min} films, one additional layer of the polycation was deposited on top of $PMAA_{11}^{4min}$ and $PMAA_{11}^{24min}$ multilayers.

2.4.4. Neutron reflectometry (NR)

Samples prepared for NR studies were assembled using two different designs. In the first design, used for observing the uptake and penetration of dQPC chains into hydrogenated matrices, films were assembled using 8 and 24 min immersions

($PMAA_{11}^{8min}$ and $PMAA_{7}^{24min}$, respectively). Scattering densities (SLDs) for the hydrogenated stacks, upon penetration of a deuterated polyelectrolyte from solution, were held constant for all annealed samples, in fitting varying only the outermost layer's thickness, interfacial roughnesses, and SLD. In another design, films contained a dPMAA block within the middle region of the film, i.e., had $QPC_8/dPMAA_9/QPC_{14}^{4min}$, $QPC_8/dPMAA_9/QPC_{14}^{8min}$, $QPC_4/dPMAA_5/QPC_{10}^{16min}$, or $QPC_4/dPMAA_5/QPC_8^{24min}$ architecture.

NR measurements were performed at the Spallation Neutron Source Liquids Reflectometer (SNS-LR) at the Oak Ridge National Laboratory (ORNL). The reflectivity data were collected using a sequence of 3.4-Å-wide continuous wavelength bands (selected from 2.55 Å < λ < 16.7 Å) and incident angles (ranging over 0.6° < θ < 2.34°). The momentum transfer, $Q = (4\pi \sin\theta/\lambda)$, was varied over a range of 0.008 $Å^{-1}$ < Q < 0.193 $Å^{-1}$. Reflectivity curves were assembled by combining seven different wavelength and angle data sets together, maintaining a constant relative instrumental resolution of $\delta Q/Q = 0.023$ by varying the incident-beam apertures. Scattering densities within hydrogenated and deuterated stacks were averaged over the 12 constituent bilayers, with each stack exhibiting its characteristic thickness, scattering-length density, and interlayer roughness. Those characteristic parameters were adjusted until the reflectivity curve was best fitted (minimized χ^2).

3. DIFFUSIONAL RESPONSE OF LAYER-BY-LAYER ASSEMBLED POLYELECTROLYTE CHAINS TO SALT ANNEALING[1]

3.1. Introduction

Assembly of polyelectrolyte multilayer (PEM) films using the layer-by-layer (LbL) technique has emerged as a powerful means to create a variety of coatings and/or functional nanostructured materials useful in biomedical, sensing, photovoltaics, separation, and photonic applications.[13, 34-37] Many applications of LbL assemblies in photonics and for multistage drug delivery rely on film stratification. Yet layering of sequentially adsorbed polyelectrolytes is diffuse[1, 91] because of the propensity of polymer chains to increase their conformational entropy, and mixing is further enhanced by chain interdiffusion. Studies of the internal structure of LbL films composed of various polyelectrolyte types using neutron reflectometry (NR) have revealed correlations between the strength and type of polymer-polymer interactions and layer intermixing. While strongly ionically paired poly(allylamine hydrochloride)/poly(styrene sulfonate) (PSS/PAH) films consistently show the smallest degree of layer interpenetration,[1, 66, 73] weak polyelectrolyte and hydrogen bonded films are much more interdiffused.[61, 67] A further decrease in the inter-polyelectrolyte binding strength leads to complete loss of film structure and formation of strongly interdiffused, exponentially depositing films.[72] In contrast to the consistent picture showing the role of polyelectrolyte type (i.e. strength of

[1] Reprinted with permission from "Diffusional response of layer-by-layer assembled polyelectrolyte chains to salt annealing" by Victor Selin, John F. Ankner, and Svetlana A. Sukhishvili, **2015**. Macromolecules, 48, 3983–3990, Copyright 2015 by American Chemical Society.

polyelectrolyte "sticky" binding points) and charge density on stratification of LbL films,[61, 73-74] our understanding of the effect of other fundamental parameters of polyelectrolyte chains (such as polyelectrolyte molecular weight) on film structure is still in its infancy.[62,65]

Among many external factors that influence assembly and post-assembly behavior of LbL films (such as temperature, solvent, and pH, among others), the effect of salt is most closely related to the electrostatic nature of ionic pairing within PEM films. Stratified LbL films are built from kinetically frozen polyelectrolyte chains, which are stitched together by multiple ionic polymer-polymer associations. Atomic force microscopy (AFM) studies of film surface topography[55-56] and fluorescence recovery after photobleaching (FRAP)[57-58] studies of the diffusion of assembled PE chains reveals an absence of chain motion and rearrangement at low salt concentrations. Addition of salt promotes chain motion as the salt ions break "old" polymer-polymer contacts and allow new ones to form. Such mobility has been observed as AFM-measured film smoothing,[55-56] or as the center-of-mass diffusion of assembled polymer chains as demonstrated by FRAP.[57-59] Post-assembly exposure of PEMs to salt solutions also increases film fuzziness, *i.e.* the degree of interpenetration between individual film layers, as indicated by NR[60-62] and neutral impact collision ion scattering spectroscopy.[63] Yet salt-induced diffusion of PE chains within the bulk of PEM films remains poorly understood quantitatively, with the only experimental results on salt dependence being an AFM topography study of the film surface.[56] Molecular-level information on the structure and dynamics of LbL films has been derived from FRAP and NR experiments,[64-67] but these

studies did not explore the functional dependence of polymer chain dynamics and LbL film structure on salt concentration.

While multilayer films are closely related to polyelectrolyte complexes (PECs),[68-69] the layering and anisotropic dynamics of polymer chains[70] raises new questions about the directional dependence of polymer chain motions. However, even for PECs, the salt dependence of chain dynamics has scarcely been studied, with only one recent report of a stretched exponential dependence of the PEC apparent relaxation time on salt concentration in a rheological experiment.[71] For structured, anisotropic PEM films, McAloney *et al*. observed an exponential dependence of the characteristic time for film surface smoothing on salt concentration.[56] However, for the bulk of PEM films, such dependencies are not reported. Here, we quantitatively explore functional dependences of center-of-mass diffusion of LbL-assembled polyelectrolyte chains on salt concentration in directions parallel and perpendicular to the substrate, and an additionally study the molecular weight dependency of the salt-induced film layer intermixing.

3.2. Materials

Branched polyethylenimine (BPEI) with M_w = 25 kDa and PDI = 2.50 were purchased from Aldrich. Hydrogenated PMAA polymethacrylic acid (*h*PMAA, or PMAA) with M_w/M_n 1.02-1.05 with M_w 7 kDa, 35 kDa and 145 kDa, abbreviated as $PMAA_{7k}$, $PMAA_{35k}$ and $PMAA_{145k}$, as well as deuterated PMAA (*d*PMAA) with molecular weights 5 kDa, 40 kDa and 180 kDa ($dPMAA_{5k}$, $dPMAA_{40k}$ and $dPMAA_{180k}$, M_w/M_n < 1.1) were purchased from Polymer Source, Inc. Ultrapure Milli-Q water

(Millipore) with a resistivity of 18.2 MΩ/cm was used in all experiments. All other chemicals were purchased from Aldrich and used without further purification.

3.3. Effect of Molecular Weight of a Weak PE on Film Deposition, Internal Layering and Salt-induced Intermixing

Fig. 3-1 compares ellipsometry data (Fig. 3-1A, B) on total film thickness and NR results (Fig. 3-1C, D) on interfacial intermixing in films constructed using QPC and PMAA of different molecular weights. While only hydrogenated polymers were used in film deposition for the ellipsometry measurements (panels A and B), films for NR measurements were composed of two 10-12-bilayer stacks containing hydrogenated and deuterated polyacids, respectively. In all assemblies, QPC of the same molecular weight of 35 kDa was used, while the molecular weight of PMAA was varied. QPC/PMAA films for ellipsometry measurements were constructed using $hPMAA_{7k}$, $hPMAA_{35k}$ and $hPMAA_{145k}$, while the film architecture for NR was $(QPC/hPMAA_{7k})_{12}/(QPC/dPMAA_{5k})_{12}$, $(QPC/hPMAA_{35k})_{10}/(QPC/dPMAA_{40k})_{10}$, and $(QPC/hPMAA_{145k})_{10}/(QPC/dPMAA_{180k})_{10}$, abbreviated below as 12bl-12bl and 10bl-10-bl two-stack films, respectively. All films were deposited on Si wafers containing a BPEI/hPMAA precursor layer. Figs. 3-1A and 3-1B show that the average ellipsometric bilayer thickness of dry QPC/PMAA, 5.2± 0.2 nm, was similar for all of the films. In contrast, NR measurements of the internal film structure indicate dramatic differences in the degree of layer intermixing (Figs. 3-1C and 3-1D). The internal mixing in as-deposited films has been characterized by the film interfacial width $\sigma_{int,0}$, calculated as a Gaussian width of the boundary between hydrogenated and deuterated stacks. Note that the

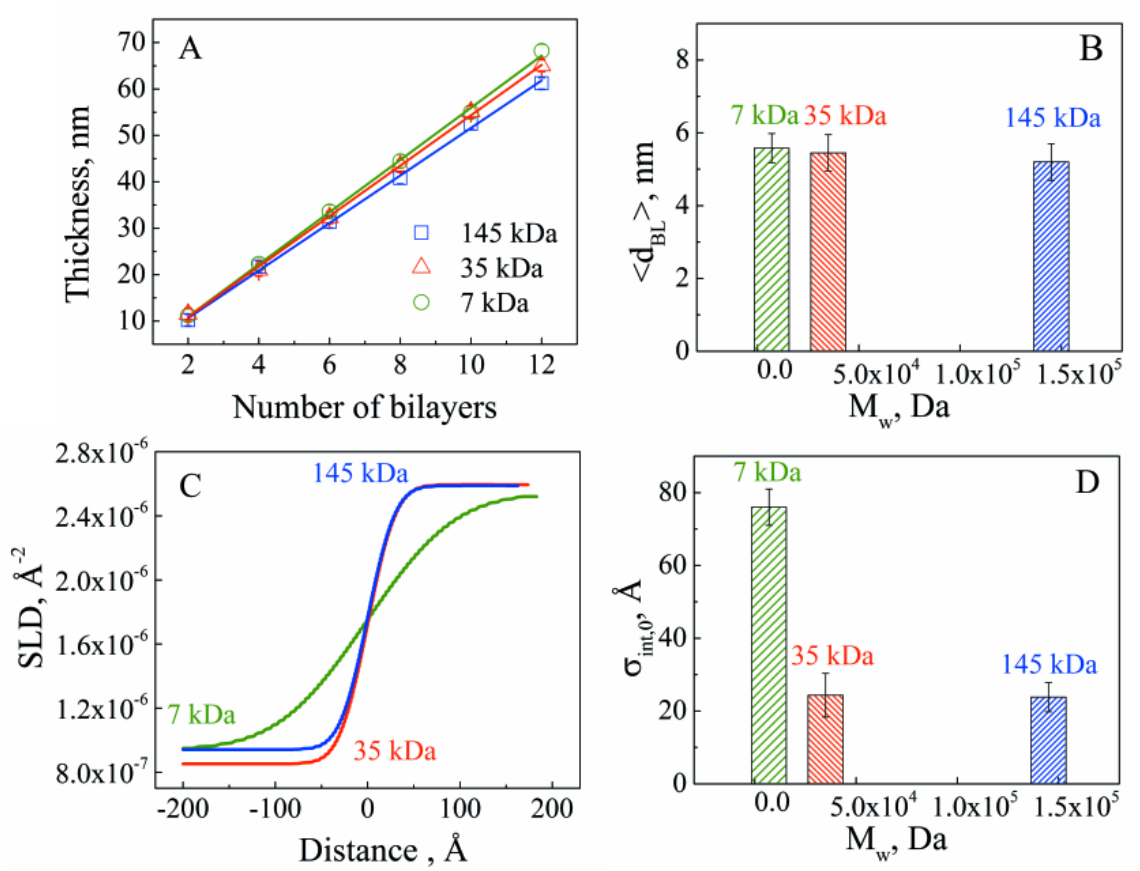

Fig. 3-1. The effect of PMAA molecular weight on QPC/PMAA LbL film growth and intermixing: (A, B) film growth and the average bilayer thickness of dry films as determined by ellipsometry. (C) neutron scattering density profiles for 12bl-12bl QPC/PMAA$_{7k}$, 10bl-10bl QPC/PMAA$_{35k}$ and QPC/PMAA$_{145k}$ two-stack films shown in the interfacial region, where distance equal to zero corresponds to the interface between hydrogenated and deuterated stacks; and (D) interfacial width between hydrogenated and deuterated stacks after film deposition. Reprinted from [114] with permission from American Chemical Society.

Gaussian width is a factor of 2.35 smaller than interfacial widths given as full-width-at-half-maximum (fwhm) as presented in our earlier reports.[59, 61] For the two higher molecular weight polymers (dPMAA$_{40k}$ and dPMAA$_{180k}$), the $\sigma_{int,0}$ value of 2 nm was significantly smaller than the dimensions of unbound PMAA chains, 5.5 and 12 nm for dPMAA$_{40k}$ and dPMAA$_{180k}$, respectively, estimated as $2R_G$ (where R_G is the radius of

gyration of a Gaussian coil, calculated using the monomer length and the persistence length of PMAA chains as 0.255 and 0.3 nm, respectively[92]). Therefore, long PMAA chains are largely constrained within the *xy* plane during adsorption to the surface, and are dramatically flattened due to cooperative binding of PMAA with highly charged QPC. In contrast, the internal layers of the shortest polymer $PMAA_{7k}$ are much more diffuse, with $\sigma_{int,0}$ of 7.8 nm (Figs. 3-1C and 3-1D) being 2.5-fold larger than the $PMAA_{7k}$ $2R_G$ of 3 nm. Therefore, there is a strong nonlinear dependence of internal chain intermixing on PMAA molecular weight. One possible contribution to such dependence might be variations in the PEM surface roughness for films assembled using PMAA of different lengths. However, the surface roughness was ~5 nm for films assembled with both the shortest $PMAA_{7k}$ and the longest $PMAA_{145k}$ (see Supporting Information). While the contribution of the film roughness to broadening the internal film interfaces cannot be excluded, layer intermixing can also occur when PE chains adsorb within the top layer of the film during immersion of substrates in PE-containing 0.01M buffer solutions. Within the outermost film layer, chains are more hydrated[93-94] and more mobile than within the bulk of the film[59] because of the asymmetric environment at the film-buffer interface. When films are exposed to PE solutions for extended periods of time (10 min per layer deposition), invading short chains can penetrate significant depths into neighboring layers. In our previous work, we studied the effect of PMAA molecular weight on the lateral diffusion of PMAA chains assembled within the bulk of a film consisting of another polycation (non-quaternized PDMAEMA), and found that the characteristic diffusion time scales linearly with molecular weight.[59] Here, NR data on PMAA interdiffusion in the direction

perpendicular to the substrate suggest a different type of behavior, with much higher mobility of short $PMAA_{7k}$ chains. If one assumes that layer intermixing occurs only during a single deposition cycle when $PMAA_{7k}$ was included within the top bilayer (total deposition time of 30 min, including rinsing steps), and that the interfacial broadening follows a simple Fickian diffusion law, then the diffusion coefficient in the direction perpendicular to the substrate, $D_{\perp}$, can be calculated from the equation $\sigma_{int,0}^2=2D_{\perp}t$.[62] Such a calculation is an extreme oversimplification of the complex diffusion process in layered films, and gives only a rough estimate of the upper bound of diffusional chain intermixing during film buildup. The estimate gave a value of $2x10^{-16}$ cm^2/s, which is about two orders of magnitude larger than the deposition-induced interdiffusion coefficient of longer (M_w 80 kDa) polystyrene sulfonate chains assembled with a long polycation in low-salt conditions. This difference can be accounted for by both weaker PMAA/QPC ionic pairing and by the lower molecular weight of the polyanion used in our work.

We next aim to explore whether a similarly strong effect of the PMAA chain length

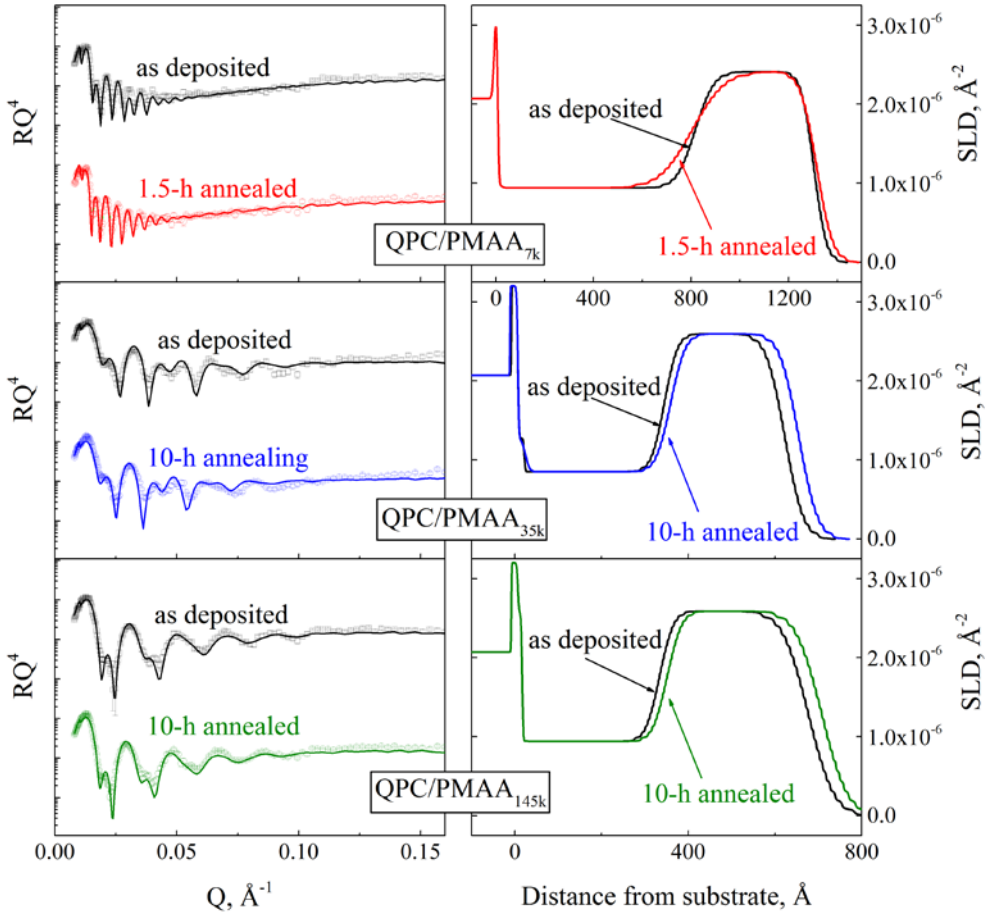

Fig. 3-2. The effect of annealing in 0.4 M NaCl solutions on the internal structure of PEMs. Neutron reflectivity data (left - plotted as RQ4 to enhance small features) and corresponding scattering length density profiles (right) for dry12bl-12bl QPC/PMAA$_{7k}$ and 10bl-10bl QPC/PMAA$_{35k}$ and QPC/PMAA$_{145k}$ films before and after annealing in 0.4 M NaCl at pH 4.5. Reprinted from [114] with permission from American Chemical Society.

on film intermixing is exhibited during post-assembly annealing of LbL films in salt solutions. Fig. 3-2 illustrates the impact of salt annealing in 0.4 M NaCl on the internal structure of 12bl-12bl films assembled using PMAA of different molecular weights. The

neutron scattering length density profiles in Fig. 3-2 indicate much stronger salt-induced layer intermixing in samples constructed using the shortest molecular weight of PMAA, $PMAA_{7k}$, and a dramatically smaller change in interfacial width for films assembled with longer PMAA chains. The change in internal interfacial width for the 7k data, our diffusion marker, is seen via a change in the modulation of the intensity of the total-film-thickness fringes. A 3-5% increase in the overall thickness of $PMAA_{35k}$- and $PMAA_{145k}$-containing films is likely due to inclusion of hydrated salt ions within the film. Such an increase comprised <1% of the film thickness for $PMAA_{7k}$-containing films, probably due to shorter exposure of these films to 45%-humidity ambient air prior to NR measurements (2-4 hours after drying with nitrogen gas *vs.* several days for films with longer PMAA). Since LbL films become glassy when dried,[95] slight variations in film hydration after drying did not affect the chain mobility measurements, which were triggered by exposure to salt solutions.

Because of the extremely small broadening ($\leq$ 3 Å, i.e. much smaller than chain dimensions) of the interfacial width in QPC/$PMAA_{35k}$ and QPC/$PMAA_{145k}$ films after 10-hr annealing in 0.4 M NaCl, we did not proceed with further annealing of these samples, and estimated only an upper-bound value of $D_{\perp}$ for dPMAA chain diffusion in these films. The estimated diffusion coefficients were extremely low, ~$2x10^{-19}$ cm^2/s and ~$1x10^{-19}$ cm^2/s for QPC/$PMAA_{35k}$ and QPC/$PMAA_{145k}$ films, respectively. An extremely sluggish salt-induced layer intermixing of polyelectrolytes in LbL films was also observed by Schlenoff and co-workers[60] and Helm and co-workers.[62] An increase in salt concentration was an obvious possibility to observe faster intermixing in QPC/$PMAA_{35k}$

and QPC/PMAA$_{145k}$ films, but in this study we were especially interested in PEM films which contained fast-diffusing short PMAA$_{7k}$ chains, which fall apart in solutions with salt concentrations higher than 0.5 M NaCl.

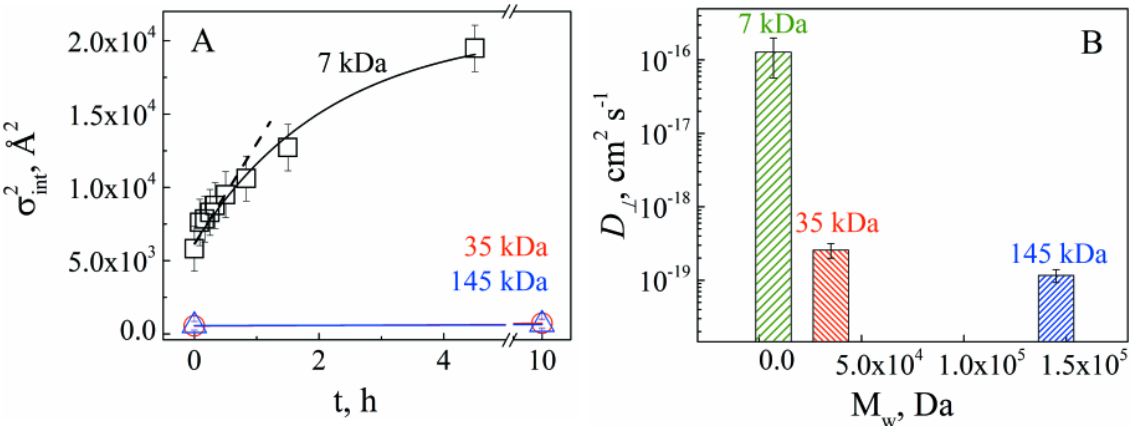

Fig. 3-3. NR data on time evolution of the square of the internal interfacial width (A) and the corresponding diffusion coefficients (B) for perpendicular-to-the substrate diffusion of PMAA chains of different molecular weights assembled within stacked multilayer films of the same architecture as in Fig. 3-2 during film annealing in 0.4 M NaCl at pH 4.5. Reprinted from [114] with permission from American Chemical Society.

The faster intermixing QPC/PMAA$_{7k}$ system allowed us to perform systematic measurements of the diffusional broadening its internal structure. Fig. 3-3 summarizes these results (A, B), and compares them with the layer intermixing rates in films containing longer PMAA chains (B, C). The dependence of σ_{int}^2 on time becomes nonlinear at long annealing times, probably due to thinning of the PEM supply stacks and consequent deviation of the diffusion conditions from the infinite reservoir model. From the initial slope of the $\sigma_{int}^2 - t$ for annealing times $\leq$ 0.5 hour, a diffusion coefficient of ~1x10^{-16} cm^2/s was calculated for QPC/PMAA$_{7k}$. This value is about 3 orders of magnitude larger than those found in the QPC/PMAA$_{35k}$ and QPC/PMAA$_{145k}$ systems.

Surprisingly, while for the two longer PMAAs ($PMAA_{35k}$ and $PMAA_{145k}$) the perpendicular-to-the-substrate diffusion coefficient $D_{\perp}$ is very weakly dependent on the PMAA molecular weight, as shown in Fig. 3-3. Such a difference might be due to significant barriers to out-of-plane chain motions due to chain flattening and stretching of long PE chains upon adsorption, which must be overcome upon salt annealing. Salt should break cooperative polymer-polymer ionic pairs and transform laterally stretched long PE chains into more relaxed 3D conformations prior to inducing their significant center of mass diffusion. In contrast, shorter $PMAA_{7k}$ chains are much more mobile and form highly interdiffused layers even before annealing in salt. More interdiffused layer boundaries within initially deposited QPC/$PMAA_{7k}$ films enable faster layer intermixing upon annealing the films in salt solutions.

3.4. Effect of Salt Concentration on Diffusion of LbL-assembled $PMAA_{7k}$ Polymer Chains

We next quantitatively explore the dependence of layer intermixing on the concentration of small ions. To that end, 12bl-12bl QPC/$PMAA_{7k}$ films were annealed for different time intervals in NaCl solutions with concentrations between 0.1 and 0.4 M NaCl. At concentrations lower than 0.1 M NaCl, the time required to observe significant layer intermixing was prohibitively long. In solutions with NaCl concentrations 0.5 M and higher, films quickly decomposed. Fig. 3-4 illustrates changes in layer intermixing during prolonged annealing of the films in salt solutions. Neutron reflectivity data together with the neutron scattering density profiles for different times of film annealing in 0.4M NaCl solution are given in Supporting Information and summarized in Fig. A-1.At times longer

than 0.5 h for annealing in 0.4M NaCl, and longer than 6-h exposure to 0.1 M NaCl solutions, diffusion eventually occurred over distances larger that the size of the unperturbed polymer ($2R_G$ for $PMAA_{7k}$ of 3 nm). Diffusion kinetics initially followed a linear dependence σ_{int}^2 *vs. t* (Fig. 3-4A), but slowed down at longer annealing times. Deviations from a single-slope behavior in the dependence of σ_{int}^2 on annealing time have been recently reported for PEM multilayers by Soltwedel *et al.*,[62] and explained by depletion of the supply of macromolecules in the reservoir stacks at long annealing times. Although in this work the supply regions of the film in hydrogenated and deuterated stacks were still partially preserved even after 10-hour film annealing in NaCl solutions of the highest concentration of 0.4 M (Fig. 3-4A), it is possible that gradual depletion of the supply of diffusing molecules within polymer stacks causes deviations from a simple infinite reservoir diffusion model as film layers become significantly interdiffused at long exposure times. In addition, re-establishment of entanglements of QPC chains in more interdiffused films may also contribute to long-time nonlinearity in Fig. 3-4A.

Fig. 3-4B shows the ionic strength dependence of the diffusion coefficients for layer intermixing, $D_\perp$, calculated from the initial slopes of σ_{int}^2 *vs. t* on salt concentration as $D_\perp = \sigma_{int}^2/2t$. Diffusion accelerated nearly an order of magnitude in response to a 4-fold increase in NaCl concentration (Fig. 3-4B). Among various possible functional dependences (power law[60], exponential[96] or stretched exponential[71]), the best fit for the data was an exponential function $D_\perp \propto e^{b[NaCl]}$, were b is the slope of the semi-logarithmic plot (Fig. 3-4B).

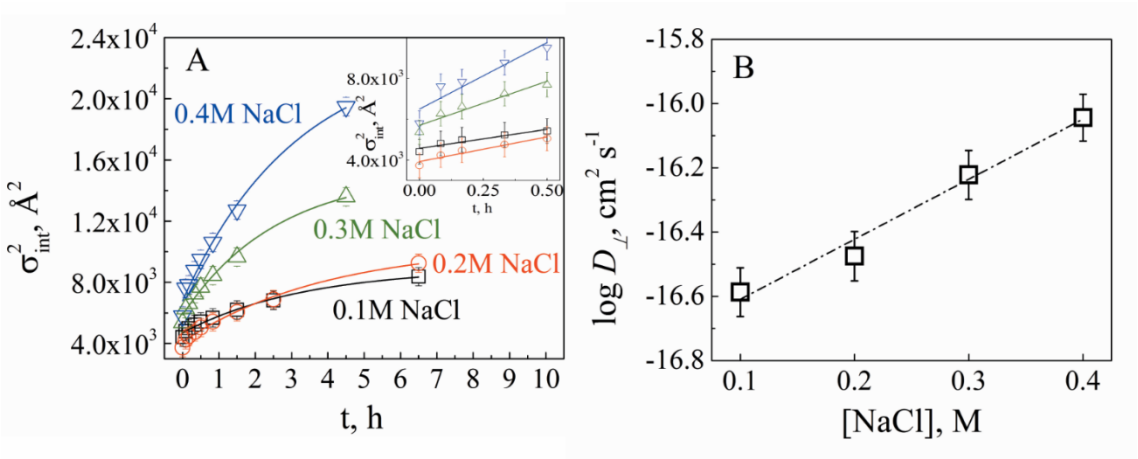

Fig. 3-4. The effect of salt concentration on time evolution of interfacial width (A) and diffusion coefficients (B) during annealing of 12bl-12bl QPC/PMAA$_{7k}$ films in salt solutions. The inset in panel A shows short-time linear regions of σ_{int}^2 *vs. t* dependences. Reprinted from [114] with permission from American Chemical Society.

To explore whether a similar dependence on salt concentration holds for PMAA chain diffusion in the direction parallel to the substrate, we have performed FRAP measurements. For these experiments, PEM films were constructed that contained PMAA$_{7k}$ with covalently attached Alexa-488 label (PMAA$_{7k}$*) molecules as a marker layer. Fluorescent PMAA$_{7k}$* was assembled within the center of the bulk of the film to avoid effects at the substrate or PEM/water interfaces.[70] After bleaching a spot using a focused high-power laser beam, fluorescence recovered to ~80% of the original value when exposed to salt solutions. Following the assumption that diffusion of polymer chains obeys a Gaussian distribution of chain displacement probability, lateral diffusion coefficients of LbL-assembled PMAA* were calculated as $D_{//}=\gamma R^2/4t_{1/2}$ (where the beam shape factor γ is 1.4 for the chosen bleaching depth, and R = 0.24 μm is the radius of the bleaching spot). The data again revealed an intuitive result that diffusion speeds up with

an increase in salt concentration, as is illustrated by representative recovery curves in Fig. 4-5A. Specifically, the characteristic recovery half-time (calculated as the time required for recovery of 50% of bleached fluorescence intensity, when the recovery curves were fitted as $y=y_0+Ae^{xt}$, (where y is normalized fluorescence intensity, $y_0=0.2$ is fluorescent intensity just after bleaching, t – time, and A and x - fitting parameters) was 43 and 6 min for 0.1 M and 0.4M NaCl solutions, respectively. Although the data could be satisfactorily fitted with a single exponential function, suggesting that within our experimental error there was only a single population of mobile PMAA* chains within the LbL films, fluorescence intensity consistently recovered to ~ 80%, independent of the solution ionic strength, indicating that a fraction of the PMAA* chains remained immobile. Control experiments (Fig. A-2) indicate that a change in the bleaching degree to 0.1, achieved by an increase in bleaching time, did not affect the plateau value of recovered fluorescence, suggesting that film photo-crosslinking probably has did not occur in experiments reported in Fig. 3-4. For each ionic strength, recovery curves were measured repeatedly at different points within the same multilayer films and with different samples (new cells, new QPC/PMAA films), and the data averaged over five bleaching experiments were used to calculate $D_{//}$ shown in Fig. 3-5B. Absolute values of $D_{//}$ in Fig. 3-5B are higher than those we previously reported in a similar multilayer system, which however contained non-quaternized PC rather than a quaternized polycation QPC.[59] For example, the $D_{//}$ of $8.3\pm0.2\times10^{-14}$ cm^2s^{-1} reported for $PC/PMAA_{7k}$ films exposed to 0.4 M NaCl solutions[59] is ~6-fold lower than the $5.1\pm0.2\times10^{-13}$ cm^2s^{-1} measured in this work for $QPC/PMAA_{7k}$ films. The faster diffusion found in this work can be explained by sterically weakened

ionic pairing between the polycation and PMAA after quaternization of polycation units. In our previous study, such an effect accounted for a two-fold difference in $PMAA_{110k}$* mobility assembled within similar LbL films.[70]

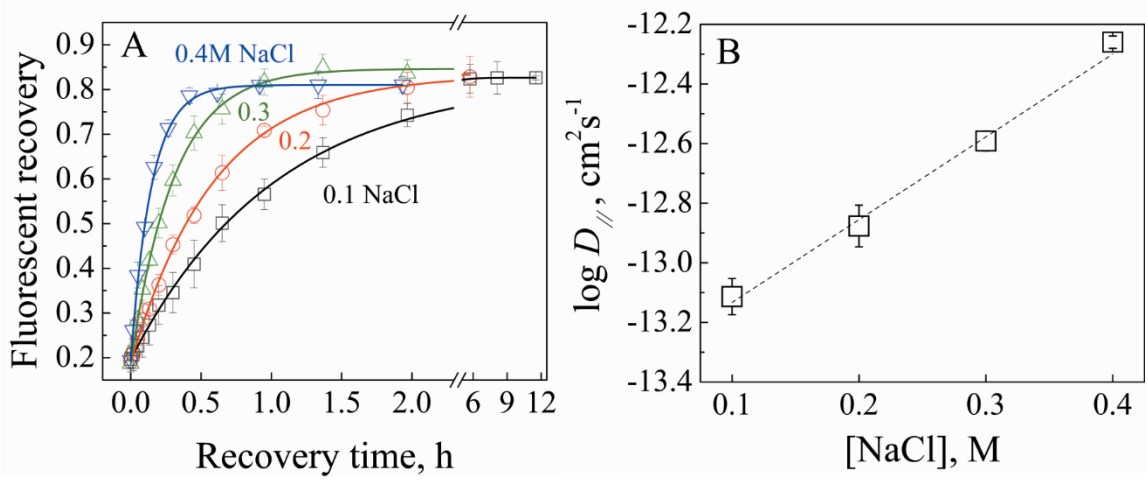

Fig. 3-5. Lateral diffusion of $PMAA_{7k}$* chains assembled within $(QPC/PMAA_{7k})_3/(QPC/PMAA_{7k}*)/(QPC/PMAA_{7k})_3$ films in NaCl solutions of different concentrations: FRAP recovery curves (A) and dependence of $D_{//}$ on ionic strength (B). Reprinted from [114] with permission from American Chemical Society.

Fig. 3-5B illustrates that the data on the ionic strength dependence of $D_{//}$ gave a straight line when plotted semi-logarithmically, suggesting an exponential dependence of lateral diffusion on salt concentration. Interestingly, a similarly simple exponential dependence on salt concentration has been reported for a very different system, in which chain mobility was inferred not from a direct measurement of center-of-mass molecular diffusion as done in this work, but from measurements of film topography, *i.e.* time evolution of surface roughness in salt solutions as studied by atomic force microscopy.[56] Annealing poly(diallyldimethylammonium chloride) (PDADMAC)/PSS films in salt solutions revealed that the half-life of the film morphology $t_{0.5}$ scaled as $t_{0.5} \sim \exp(-$

c_{salt}/c_0),[56] where c_{salt} is the concentration of NaCl in annealing solutions, and c_0 is concentration of polyelectrolyte repeating units in the assembled LbL films. This model is based on a probabilistic approach of finding an ion within the film, and suggests that salt ions enable breaking of old and formation of new polymer-polymer contacts, therefore facilitating morphology changes.[56]

Another approach also suggests that the breaking of inter-polyelectrolyte contacts by salt ions is central to the rearrangement and reorganization of bound polyelectrolyte chains, but considers this as an activated process governed by a free energy barrier related to the separation of ionic groups within polymer-polymer contacts and surrounding them with monovalent ions. If one assumes that separated ionic groups behave independently, then interactions between these ions via a screened electrostatic potential leads to a square root dependence of the activation barrier on salt concentration, and the resulting stretched exponential dependence of the relaxation time on salt concentration.[71] Such a dependence has been recently proposed by Spruijt *et al.* to describe the relaxation dynamics of electrostatically assembled polyelectrolyte complexes in rheological experiments.[71] Our data in Fig. 3-5A did not give a satisfactory fit to this model, however.

A different, more common line of argument considers that counterions are thermodynamically bound, or condensed on polyelectrolyte chains with a high linear charge density,[97] and therefore small ions cannot be considered "free" after disruption of polymer-polymer ionic pairs. Release of condensed counterions upon polyelectrolyte assembly, therefore, presents a significant entropic contribution to the free energy of polyelectrolyte binding. This approach, developed by Record *et al.*[98-99] to describe the

binding of biomolecules, has become a powerful tool to study a variety of biomolecular assembly events.[100-101] Similar physics drives the association of polyelectrolyte complexes composed of synthetic polymers.[102-103] For the case of layered polyelectrolyte complexes, *i.e.* PEM films, an approach based on consideration of ionic equilibrium upon inclusion of ions within LbL films was developed by Schlenoff and co-workers.[55, 60] The model considers that diffusion occurs through the motion of polyelectrolyte segments of several charged units, and that several polymer-polymer ionic pairs must break simultaneously before a segment moves. This line of argument leads to a power law dependence of the polyelectrolyte chain characteristic time and diffusion coefficient on salt concentration $D \sim D_0[\mathrm{NaCl}]^{\lambda}$, where D_0 is the bulk diffusion coefficient, and λ is the length of a diffusing segment, proportional to the number of adjacent charged moving polyelectrolyte units.[60] For PDADMAC/PSS LbL films, a λ of 4 units has been predicted. Although the fit of our experimental data to this model gave a low value of R^2=0.93 (data not shown), D_0 for vertical and lateral diffusion $D_{\perp 0}$ and $D_{// 0}$ of 2.54×10^{-16} cm^2/s and 3.50×10^{-12} cm^2/s, respectively, could be estimated. The estimated value of bulk diffusion coefficient for $D_{\perp 0}$ is comparable to the 7.1 x 10^{-17} cm^2/s value reported by Schlenoff, with an expected deviation because of the different polyelectrolytes used for LbL film construction.

The fact that our data could be best fitted by an exponential ($D_{\perp}= 1.6\times10^{-17}e^{1.87[\mathrm{NaCl}]}$ cm^2/s and $D_{//} = 4.0\times10^{-14}e^{2.56[\mathrm{NaCl}]}$ cm^2/s) rather than a power law function is somewhat surprising, as it is the power law model that takes into account ion condensation, polymer chain rigidity and cooperativity in inter-polyelectrolyte binding. There are many contributions, however, that this model does not consider, including the release of water

molecules (changes in multilayer hydration), any non-electrostatic contribution to segmental binding, and changes in the film dielectric environment at different levels of "doping" of LbL films with salt ions. Non-electrostatic contributions to the free energy of binding ΔG can be taken into account, for example, by an additional term which depends linearly rather than logarithmically on salt concentration C_{salt}: $\Delta G = a + b\ln C_{salt} + mC_{salt}$, where a is a fitting parameter, and b and m describe the magnitude of electrostatic and non-electrostatic interactions.[101] At the same time, the dielectric environment within LbL films (dielectric constants of 30 and <19 were reported for PAH/PSS) and PDADMAC/PSS films, respectively[104]) changes with the "doping" with salt. This latter effect depends on the relative hydration of multilayers and invading small ions, and varies with counterion type and concentration.[105] If the hydration of LbL films increases at higher concentrations of small ions, then electrostatic interactions within the film weaken, allowing for more efficient salt inclusion. All of these effects might lead to deviations from the predicted power law dependence of the diffusion coefficient, and even the occurrence of the seemingly simple exponential scaling observed in this work.

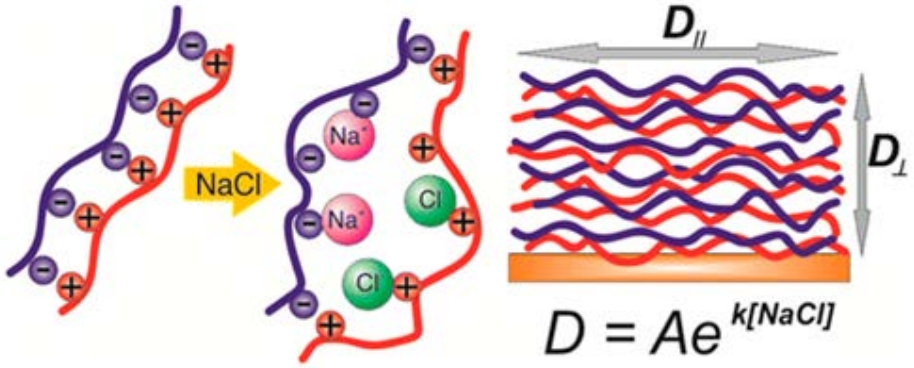

Fig. 3-6. Schematic representation of the main findings in the current chapter.

4. NONLINEAR LAYER-BY-LAYER FILMS: EFFECTS OF CHAIN DIFFUSIVITY ON FILM STRUCTURE AND SWELLING[2]

4.1. Introduction

The layer-by-layer (LbL) technique presents a versatile way to coat the surfaces of a diverse range of materials with nanoscopically structured films.[38] LbL-deposited polyelectrolyte multilayers (PEMs) have found a number of applications, showing particular promise for surface functionalization of biomedical devices to control cell adhesion, antibacterial properties and localized delivery of bioactive molecules.[37,39,40] For the use of LbL films as drug-delivery coatings, the overall capacity for loading bioactive molecules is especially important, and micron-thick rather than ultrathin films are optimal. At the same time, it is desirable to control film stratification to enable sequential delivery of multiple functional molecules.[88] Addressing this challenge requires detailed understanding of LbL films that grow non-nonlinearly and feature more mass deposited in fewer steps compared to films grown linearly.[20] The designation of PEMs as either linear or nonlinear (*l*PEMs and *nl*PEMs, respectively) refers to the shape of their growth curves, wherein total film thickness is plotted *vs*. deposition time or number of deposition steps. The rate of deposition and whether it increases with time is determined by the strength of binding between polyelectrolyte components.[18, 75] Linear film growth is typical for strongly bound polyelectrolytes, and exhibits a constant increment in mass increase

[2] Reprinted with permission from "Nonlinear layer-by-layer films: effects of chain diffusivity on film structure and swelling" by Victor Selin, John F. Ankner, and Svetlana A. Sukhishvili, **2017**. Macromolecules, 50, 6192–6201, Copyright 2017 by American Chemical Society.

per deposition step and fast saturation of mass at each deposition step. In contrast, accelerated, non-linear (also often called "exponential") film growth is mostly observed for systems with weak binding between polyelectrolyte chains.[19, 77-78] Thicker films are formed as mobile polymer chains do not just bind at the film surface, but penetrate deeper within films.[84, 106] Recently, differing growth kinetics for linear and nonlinear films was reported for a clay-containing system, with a strong increase in film thickness with deposition time observed for weakly bound polymer/clay pairs, and film thickness being almost independent of deposition time for strongly interacting polymer-clay pairs.[107] Chain mobility and film growth modes are dependent on polyelectrolyte type and chain rigidity, [108] and can be modulated by concentration and type of salt,[109,58, 110-111] temperature,[112-113] or solution pH. [22-23]

Films which grow nonlinearly (exponentially) were first seen in pairs of weakly associating biological polyelectrolytes. [19-20, 84, 106] Diffusion of at least one of polyelectrolytes within the film was established as a condition necessary to observe exponential film growth, and a model suggesting "in-and-out" free diffusion of polyelectrolyte chains between film and solution at alternating film deposition cycles was developed.[19, 84, 106] Diffusion of polyelectrolyte chains being limited to a zone close to the film-solution interface was also suggested, and used to explain a transition from exponential to linear film growth after a large number of deposition steps.[85] The "in-and-out" model is widely but not universally accepted; some groups propose an alternative "dendritic and island" explanation for exponential film growth.[86] Overall, in spite of an increasing number of experimental reports of nonlinear growth in LbL films, the structure

and dynamics of these films are still poorly understood. The only existing mathematical model of exponential film growth[21] assumes diffusion of polyelectrolytes throughout PEMs and consequent film swelling. To assess the validity of such assumptions, it is necessary to measure and quantify chain diffusion and layer intermixing in nonlinear PEMs.

In recent studies, we used neutron reflectometry to study the effect of ionic strength and film deposition techniques on the diffusivity of polyelectrolyte chains within linear PEMs.[14, 114] In this work, we focus on *nl*PEMs and study the correlation between chain diffusivity, polyelectrolyte deposition time and film internal structure at different stages of film growth for films of varying deposition history.

4.2. Materials

Branched polyethyleneimine (BPEI) with M_w=25 kDa and M_w/M_n = 2.50 was purchased from Aldrich. Hydrogenated polymethacrylic acid (*h*PMAA, or PMAA) with M_w 180 kDa and M_w/M_n=1.02 was purchased from Polymer Standard Services (PSS) GmbH, Germany. Deuterated poly(2-(dimethylamino)ethyl methacrylate) (*d*PDMAEMA, d15) with M_w 90 kDa and M_w/M_n 1.8, as well as deuterated PMAA (*d*PMAA) with molecular weight 180 kDa and M_w/M_n < 1.1 were purchased from Polymer Source, Inc. Hydrogenated 2-(dimethylamino)ethyl methacrylate monomer (DMAEMA), ethyl 2-bromoisobutyrate (EBiB), CuBr and 1,1,4,7,10,10-hexamethyltriethylenetetramine (HMTETA), hydrogenated and fully deuterated methyl sulfate (d6), as well as all solvents were purchased from Sigma-Aldrich. Ultrapure Milli-Q water (Millipore) with a

resistivity of 18.2 MΩ/cm was used in all experiments. All other chemicals were purchased from Aldrich and used without further purification.

4.3. Film Growth, Swelling and Polyelectrolyte Ionization

Fig. 4-1 illustrates the effect of the deposition time on the growth of PMAA/QPC films. Fig. 4-1A shows that the amount of material assembled within multilayer films increases with the deposition time, and switches from being constant per deposition cycle

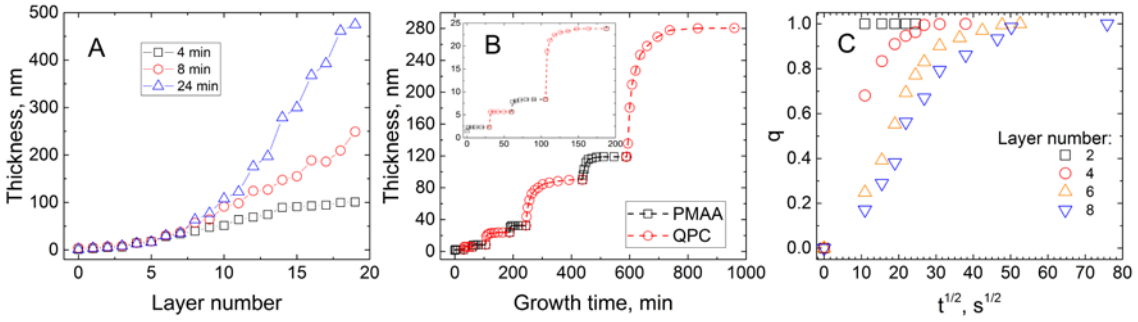

Fig. 4-1. (A) Thickness of dry PMAA/QPC films constructed using 0.1 mg/ml polymer solutions in 0.01 M phosphate buffer at pH 6 and 4, 8 or 24 min per-layer deposition times (squares, circles, and triangles, respectively). (B) Thicknesses of the dry PMAA/QPC film when the amount of polymer deposited was allowed to saturate at each deposition step. The inset presents an enlarged view of deposition within the first four layers. (C) The kinetics of QPC uptake by 1-, 3-, 5- and 7-layer films containing PMAA as the top layer (2nd, 4th, 6th and 8th layer deposition steps). Reprinted from [133] with permission from American Chemical Society.

to being thickness-dependent when layer deposition time increases from 4 and 24 minutes. This effect is strong and results in a 5-fold difference in film thickness after ten deposition cycles using 4 or 24 minutes per layer. Qualitatively, this result is similar to observations by Schlenoff and co-workers, which were made for a different polyelectrolyte system studied at high salt concentrations,[81] where an almost two-fold increase in film thickness

was reported when the polyelectrolyte deposition time increased from 8 to 20 min. Fig. 4-1B shows the growth of the film when the deposition time per layer was not fixed, but instead the mass of the deposited polymers was allowed to equilibrate and reach a plateau value at each deposition step. Twice as much QPC as PMAA was deposited, in agreement with the higher molecular weight of the QPC repeat units compared to PMAA (150 and 72 g/mol, respectively).

Importantly, both the masses of PMAA and QPC deposited at each film growth step and the kinetics of polyelectrolyte uptake were strikingly different between the first several layers and subsequent film deposition steps (Fig. 4-1B). The small mass deposited within the first layers (2-4 mg/m^2, calculated assuming a density of dry LbL films of 1 g/cm^3) is consistent with a monolayer coverage, indicating binding of polyelectrolytes only in the outermost film region. In contrast, during adsorption of the film's 8^{th} layer, QPC mass uptake was as large as ~160 mg/m^2, suggesting deposition of QPC within the interior of the film. Deposition of polyelectrolytes at the film surface or within the interior was kinetically distinct (Fig. 4-1B and C). While adsorption of polyelectrolytes within the first and second layers (PMAA and QPC, respectively) saturated within the first 2 minutes, equilibration of the QPC mass deposited within the 8^{th} layer of the film with an initial thickness of 120 nm continued for as long as 150 min. Rapid binding of polyelectrolytes within the first layers was limited by the diffusion flux from solution and persisted as the mode of polyelectrolyte adsorption till the 4^{th} layer (Fig. 4-1C). A similar trend was observed for uptake of PMAA (Fig. B-2). For films with a larger number of layers, fast polyelectrolyte binding and saturation at the film's surface was followed by the slow

diffusion of a large amount of material within the film interior. Fig. 1C highlights these differences by showing the kinetics of QPC uptake by the film plotted as a function of the normalized polymer mass uptake, q versus $\sqrt{t}$, where q is a normalized mass uptake, calculated from the dry film thickness as $(l_t - l_0)/(l_\infty - l_0)$, where l_0, l_t, l_∞ – initial, effective (at time t) and equilibrated thicknesses of the dry films, and t denotes the exposure time.[115] The maximum film thickness at which polyelectrolytes adsorbed at the film surface rather than penetrating into the interior (corresponding to a three-layer film, Figs. 4-1B and C) was about 8 nm. After subtraction of the thickness of the precursor BPEI layer of 1.5 nm, the remaining 6.5 nm can be taken as an estimate of a dense, near-substrate zone in which chains are immobilized as a result of adsorption and pinning to a solid surface and hence are inhibited from rearranging and allowing penetration of newly binding chains.

While the data in Fig. 4-1 are presented for dry films, dynamic interpolymer binding and uptake of polyelectrolytes within the film bulk are expected to cause significant film swelling. Fig. 4-2A shows changes in the degree of swelling as PMAA/QPC film was built up when saturated with polyelectrolytes at each deposition step. The swelling ratio was determined as the ratio of wet film thickness, measured by in situ ellipsometry in the presence of buffer above the growing film, to the thickness of the dry films. For measurements of wet film thicknesses, polyelectrolyte solutions were replaced with a buffer at desired time points in order to inhibit the uptake of polyelectrolytes within the film and avoid the interference of an increased refractive index of the backing solutions. For measurements of dry film thicknesses, films were taken out

of the polyelectrolyte solutions, repeatedly rinsed with 0.01 M phosphate buffer.

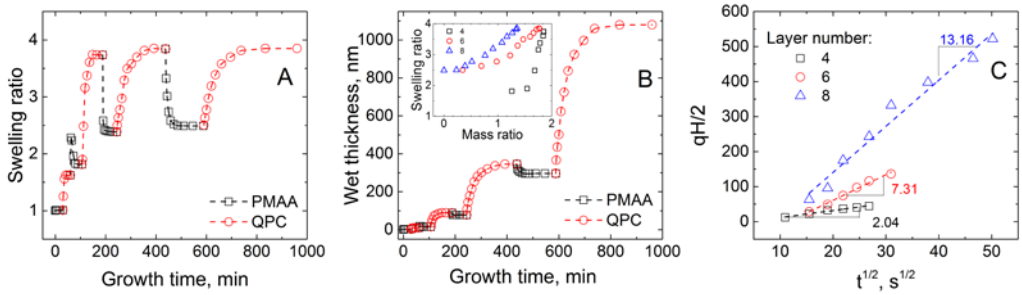

Fig. 4-2. (A) The swelling ratio of a PMAA/QPC film monitored during deposition of the first 8 layers. Red circles and black squares correspond to exposure of the film to QPC and PMAA solutions, respectively. (B) *In situ* thicknesses of PMAA/QPC film when deposited polymer amounts were allowed to saturate at each deposition step. (C) qH/2 versus $t^{1/2}$ dependence plotted for the construction of 4th, 6th and 8th layers of the PMAA/QPC film. Reprinted from [133] with permission from American Chemical Society.

The swelling data correlate well with the uptake of polyelectrolytes within the films. While films composed of up to three polyelectrolyte layers contained less than 100% of water (calculated by deriving water fraction from the swelling thickness, assuming a constant density), consecutive film construction steps caused a dramatically larger uptake of water, and the swelling ratio oscillated between the limiting values of 3.8 and 2.4 for deposition of QPC and PMAA, respectively. Based on these ratios, *nl*PEMs swell much more than linear PEMs, whose water content is usually about 40-60%.[116-118] Fig. 4-2B shows *in situ* thicknesses during PMAA/QPC film growth, and the inset in Fig. 4-2B – the correlation between the polyelectrolyte mass deposited and film swelling. Note that the data for film swelling as a function of QPC deposited within the 6th and 8th deposition cycles collapses onto almost the same curve when plotted as a function of the relative amount of QPC

bound to the film (the ratio of the mass of QPC to the initial mass of the film at the beginning of polycation deposition), again suggesting penetration of QPC throughout the entire film. The uptake of QPC (which carries permanent charge) results in a strong increase in film swelling, caused by the excess charge brought in by QPC charged loops, *i.e*. QPC units that do not participate in formation of ionic pairs with PMAA. The addition of a weak polyelectrolyte – PMAA – on the contrary, resulted in film de-swelling as charge in the PMAA loops was suppressed as larger amounts of the polyacid accommodated within the film.[119] As polyelectrolytes were allowed enough time to diffuse through the entire film, the limiting swelling ratios oscillated between those characteristic of QPC and of PMAA, depending on which was being added.

To quantitatively assess diffusion of the polyelectrolyte with a permanent charge, QPC, within the film, we used a Fickian diffusion model. The diffusion coefficients for QPC chains can be determined from the slopes of the initial linear region of qH/2 plotted against square root of time (Fig. 4-2C) following the equation $Dt = \frac{q^2 H^2}{4}$, where D is the diffusion coefficient, q is the normalized mass uptake, calculated from measurements of dry film thicknesses as $(l_t - l_0)/(l_\infty - l_0)$, where l_0, l_t, l_∞ – initial, effective (at time t) and equilibrium thicknesses of dry films, t – exposure time to a polyelectrolyte solution, and H − film thickness at time t. In this simplistic model, the choice of film thickness presents the biggest uncertainty.[120] We have chosen H to be the wet film thickness as measured with spectroscopic ellipsometry. The value of H increases with time with the uptake of polymer chains. While a reliable determination of the diffusion constant was not feasible

based on our data when chains diffused in solution and bound to the film surface (the deposition of the 2nd layer), diffusion coefficients determined from the slopes in Fig. 4-2C for layer numbers 4, 6 and 8 reflected penetration of QPC chains into the multilayer film. The diffusion coefficients for transport of QPC chains within the film were $1.3\pm0.5\times10^{-13}$ cm^2/s, $1.7\pm0.8\times10^{-12}$ cm^2/s and $5.4\pm1.2\times10^{-12}$ cm^2/s for deposition of the 4th, 6th and 8th layers, respectively, i.e. values of D increased with a lower rate as the films grew thicker, indicating 'fading' memory of the attachment to the hard substrate. These values are five orders of magnitude smaller than those found for diffusion of free polyelectrolyte chains of similar molecular weight in solution[23, 89], and similar to those observed for the mobility of QPC chains within linearly deposited LbL films in the presence of high concentrations of salts.[120]

As for the mechanism of polyelectrolyte diffusion, it is likely that QPC diffuses within the films while remaining bound to PMAA chains rather than in its "free" state (diffusion of "free" polyelectrolyte chains was earlier found in a different LbL system composed of natural macromolecules and/or synthetic polypeptides[121]). In the PMAA/QPC system, while chains remain bound to the film matrix during polymer uptake from solution, propagation of the invading chains within the bulk of the film is likely to occur though the exchange of polyelectrolyte 'sticky' binding points in the electrostatic network. The large number of invading QPC chains diffusing within the film introduce a large charge excess that is accommodated by loops of polymer chains bound within a network of electrostatically associated chains. The multilayer is reminiscent of surface-immobilized non-stoichiometric polyelectrolyte complexes, which are significantly

swollen by excess charge accumulated in polymer loops and the osmotic pressure originating from the inclusion of charge-compensating small counter-ions.

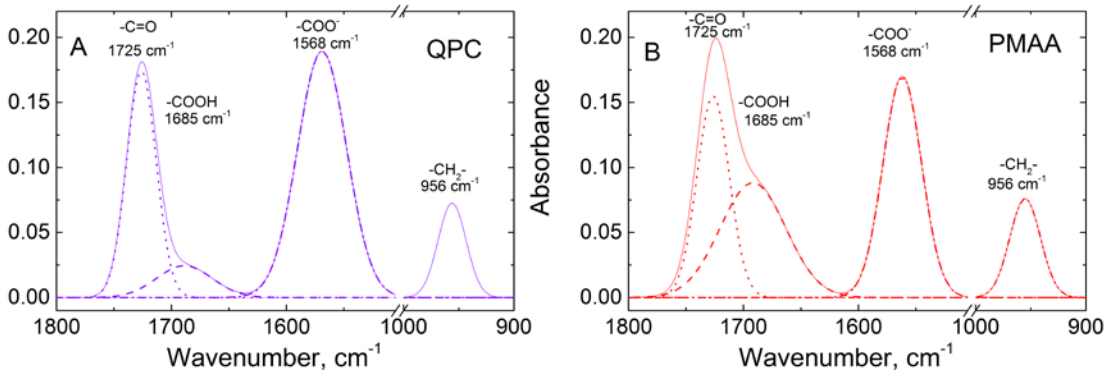

Fig. 4-3. FTIR spectra of dry PMAA/QPC films containing either QPC (A, 10-layer film) or PMAA (B, 11-layer film) as and outermost layer. The data illustrate reduced ionization of PMAA in the films containing PMAA as the outermost layer. Reprinted with permission from "Nonlinear layer-by-layer films: effects of chain diffusivity on film structure and swelling" by Victor Selin, John F. Ankner, and Svetlana A. Sukhishvili, **2017**. Macromolecules, 50, 6192–6201, Copyright 2017 by American Chemical Society.

As shown in Fig. 4-2, binding a weak polyelectrolyte (PMAA) rather than QPC has an opposite effect on film swelling, *i.e.* the film deswelled as more polyelectrolyte was bound. We hypothesize that this is due to the adjustment of charge in the PMAA chains to the total charge in the *nl*PEM film, and have directly detected charge renormalization using FTIR spectroscopy. While in earlier studies, this technique was used by several groups, including ours, to study ionization of weak polyelectrolytes assembled within linear PEMs,[119,122] here we apply FTIR spectroscopy to study the ionization of PMAA within *nl*PEMs. Fig. 4-3 shows FTIR spectra of a 10-layer PMAA/QPC film deposited in saturation conditions and terminated with QPC, as well as the same film after deposition

of PMAA as the 11th layer in the film. Both spectra show vibrational bands at 1725 cm^{-1} and 1568 cm^{-1} associated with stretching vibrations of uncharged carboxylic groups (ν, −C═O) and asymmetric stretching vibrations of the carboxylate groups (ν_{as}, $-COO^-$), respectively, as well as a small peak at 1685 cm^{-1} associated with hydrogen-bonded dimers (−COOH) of protonated carboxylic groups. The ionization degree of PMAA within the assembled multilayers was calculated as the ratio of the area of $-COO^-$ to the sum of −COOH and $-COO^-$ absorbances, assuming equal extinction coefficients for vibrations associated with these bands.[123] This quantification gave the ionization degrees of PMAA as 60±2% and 38±2% for films terminated with QPC and PMAA, respectively. These data clearly show that uptake of QPC causes an increase in the average ionization of assembled PMAA chains due to formation of ion pairs between QPC and previously uncharged PMAA units, while the addition of PMAA causes suppression of the ionization of PMAA in the adsorbed polymer loops, likely as a result of accumulation of an excess of negative charge within the film. Also note that the integrated intensity of the 956 cm^{-1} band characteristic of QPC and probably associated with CH_2 wagging vibrations of methylene group,[124] remained unchanged after PMAA addition (Fig. 4-3), suggesting that polyacid binds to the electrostatically associated network without causing desorption of QPC chains.

4.4. Film Internal Structure: Neutron Reflectometry Studies

In earlier studies, neutron reflectometry has been applied to establish correlations between the strength of intermolecular binding and film intermixing for linear PEMs of electrostatically assembled films, [23, 61, 114,73,66,] and films stabilized by hydrogen bonding.[67]

In this work, neutron reflectometry is used to study the effect of a new parameter important for *nl*PEMs– layer deposition time – on internal film structure and to quantitatively measure the diffusion of invading polyelectrolytes into the film.

Table 4-1. Fitted parameters of the thickness and interfacial roughness of a deuterated stack incorporated within the hydrogenated matrix of different PMAA/QPC films (Design I).

	*d*PMAA stack		*d*QPC stack	
Deposition time, min	d, nm	σ_{int}, nm	d, nm	σ_{int}, nm
4	14.4	6.7	16.7	12.8
8	26.0	12.0	26.7	15.8
24	35.2	12.0	90.6	16.0

To that end, we have designed two different types of experiments. In the first scenario (Design I), films were constructed in which deuterated polyelectrolytes (either *d*PMAA or *d*QPC) were included as 'marker' layers in the middle of PEMs constructed using hydrogenated polymers, wherein each layer was assembled using a specific deposition time (Figs. 4-4 and 4-5). In the second scenario (Design II, shown below in Fig. 4-6), films were first constructed using hydrogenated polymers, and then the kinetics of penetration of deuterated QPC chains into the film was studied as a function of exposure time to a *d*QPC solution. The reflectivity model for Design I consisted of the BPEI priming layer and three hydrogenated/deuterated/hydrogenated stacks. The *SLD* of the hydrogenated stacks was constrained to the value for the hydrogenated matrix determined

in an independent measurement of hydrogenated films. The *SLD* of the deuterated block was found by fitting the reflectivity data. The model for Design II initially consisted of only two stacks – a priming layer and a hydrogenated matrix. Upon absorption of deuterated chains, an additional stack representing the hydrogenated matrix enriched with deuterated polymers was introduced into the model.

Fig. 4-4 shows neutron reflectivity data and the calculated *SLD* profiles of *nl*PEMs constructed using per-layer deposition times which were constant for each individual film, but varied between different *nl*PEMs. Because the amount of material deposited was strongly time-dependent and, due to instrumental resolution, the total film thickness in NR should not exceed ~350 nm, films constructed using longer deposition times by design had fewer polyelectrolyte layers. Fig.4-4 shows the dramatic effect of layer deposition

time on internal film structure. Films constructed using 4, 8, and 24 min deposition times demonstrated increasingly larger and more diffuse deuterated stacks. For 4-min, 8-min-

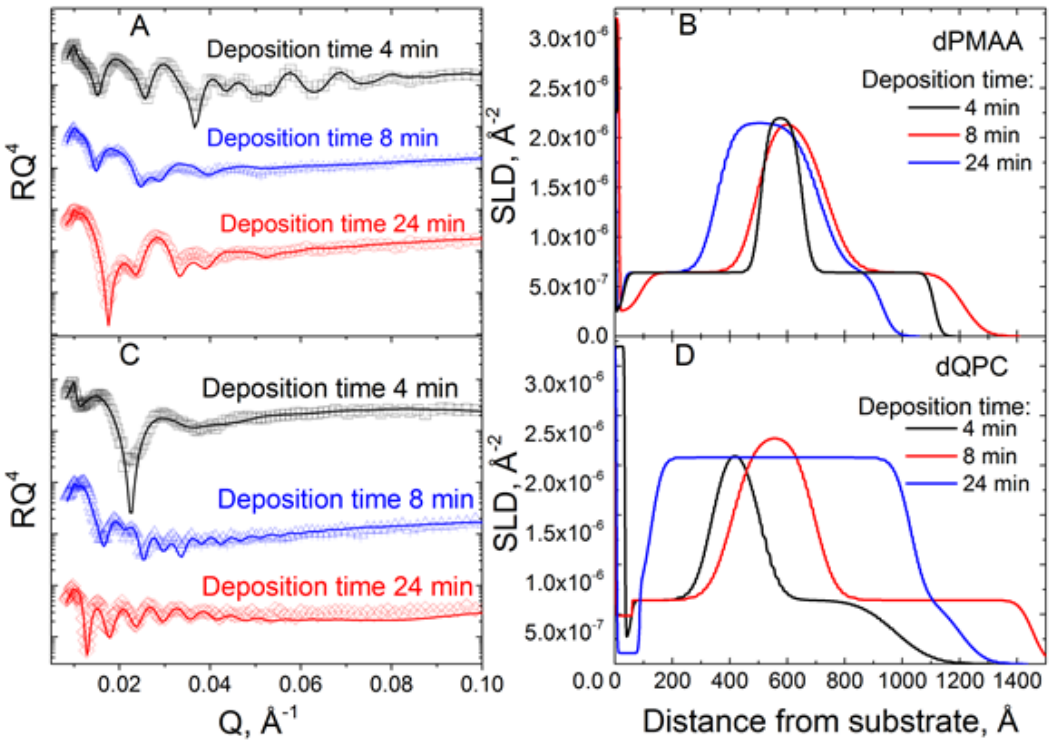

Fig. 4-4. Reflectometry data (A, C) and scattering length density profiles for PMAA/QPC films formed using hydrogenated and deuterated components. (B) SLD profiles of films assembled using dPMAA as a marker layer with design $(hPMAA/hQPC)_x$ / (dPMAA/hQPC) / $(hPMAA/ hQPC)_y$ using 4, 8 and 24 min deposition times (black, red and blue lines, respectively) where x and y indicate the number of bilayers (for 4 and 8 min deposition times x and y were 4; for the 24 min deposition time, x and y are 3 and 2 respectively. (D) SLD profiles of films assembled using dQPC as a marker layer with design $(hPMAA/hQPC)_x$ / (hPMAA/dQPC) / $(hPMAA /hQPC)_y$ for samples with 4, 8 and 24 min deposition times (black, red and blue lines, respectively) where x and y reflect the number of bilayers (for 4 and 8 min deposition times x and y were 4; for the 24 min deposition time x and y are 3 and 2, respectively). Reprinted from [133] with permission from American Chemical Society.

and 24-min film assemblies, the integrated area under the stacks of *d*PMAA and *d*QPC increased as 1 : 1.8 : 2 and 1 :1.7 : 3.4, respectively. This is in agreement with an increase

of the total mass of polymers bound within *nl*PEM films for different deposition times. This ratio, derived from ellipsometric data, yields values of 1 : 1.7 : 2.6 and 1 : 1.8 : 2.5 for films of comparable thickness (Fig. 4-1A). Tracking the increase in deposited polymer mass, the interfacial full width, σ_{int}, between hydrogenated and deuterated blocks increased from 6.7 to 12.0 nm for *d*PMAA, indicating greater intermixing between hydrogenated and deuterated stacks. Interestingly, the maximum SLD of *d*PMAA and *d*QP is independent of the layer deposition time, indicating there is a constant ratio between hydrogenated and deuterated chains as they mix within the multilayer (Tables B-1 - B-6). At the same time, the kinetics of the increase in the deuterated stack width was strikingly different for *d*PMAA- and *d*QP-containing films (Fig. 4-4). An increase in either the width or the integrated SLD of the deuterated stacks indicates both an increased spreading and a larger amount of deuterated polymer adsorbed at each deposition step. Diffusion of polymer already within the films is coupled with the diffusion of arriving polyelectrolyte chains into the multilayer matrix, and so more polymer can be bound at the film surface from solution as deposition progresses. Therefore, the amount of additional adsorbed material is limited by the interdiffusion/penetration rate of polyelectrolyte into the existing film. The faster intermixing of QPC into the film and the larger amount of QPC adsorbed within each layer compared to *d*PMAA can be explained by the different degrees of polymerization (DP) of PMAA and QPC (DPs 2090 and 570 for PMAA and QPC, respectively), which leads to more sluggish dynamics of PMAA chains in the film. Diffusion coefficients for *d*PMAA and *d*QPC penetration estimated from d^2 vs. t dependences using the data in Table 4-1 yield estimated values of 3.9×10^{-15}

cm^2/s and 3.5×10^{-14} cm^2/s, respectively. These values, estimated from measurements of

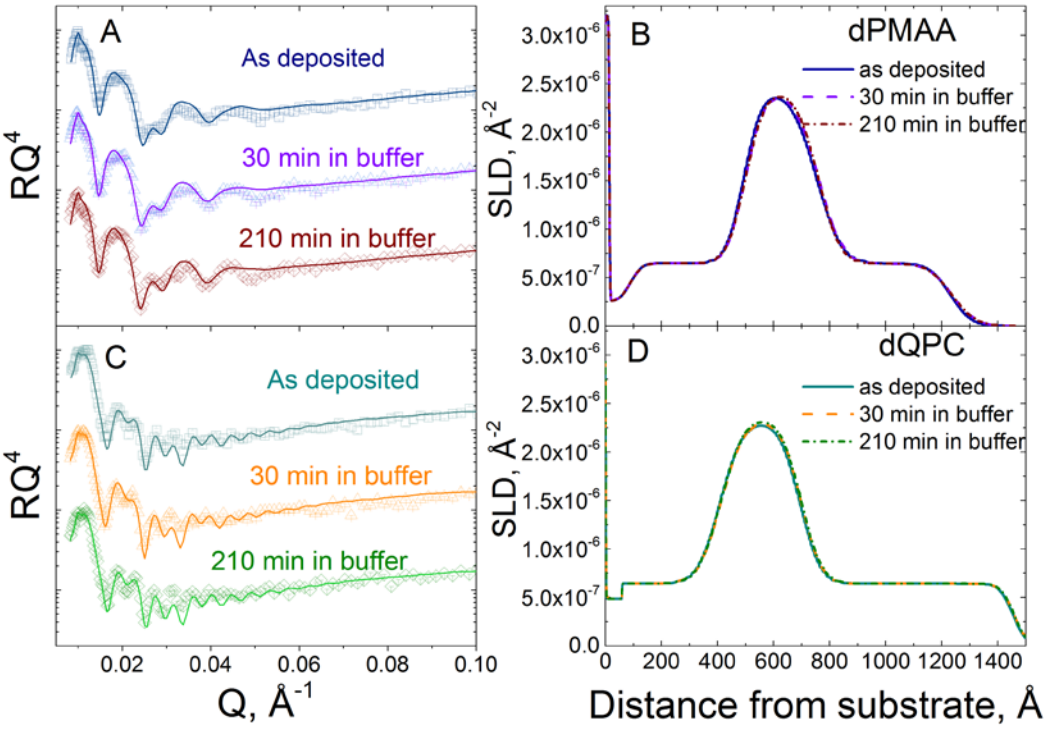

Fig. 4-5. Reflectometry data (A, C) and scattering length density profiles (B, D) for PMAA/QPC films formed using hydrogenated and deuterated components. (B) Film assembled using *d*PMAA as a marker layer with design (*h*PMAA/*h*QPC)$_4$ / (*d*PMAA/*h*QPC) / (*h*PMAA/*h*QPC)$_4$ prepared using an 8 min deposition time after 30 and 210 min exposure to 0.01 M phosphate buffer at pH 6.0. (D) Film assembled using *d*PMAA as a marker layer with design (*h*PMAA /*h*QPC)$_4$ / (*h*PMAA/*d*QPC) / (*h*PMAA/*h*QPC)$_4$ using an 8 min deposition time after 30 and 210 min exposure to 0.01 M phosphate buffer at pH 6.0. Reprinted from [133] with permission from American Chemical Society.

dry *nl*PEMs, are two orders of magnitude lower than those measured for the intrusion of polyelectrolyte molecules into wet films. Penetration of polyelectrolyte chains into the films is also determined by the presence of a 'supply' of polyelectrolyte chains in solution, and did not occur when films were immersed in polyelectrolyte-free buffer solutions. Fig.

4-5 shows that *nl*PEMs, featuring deuterated marker layers in the middle region of the film, using 8 min deposition time did not show any changes in internal structure upon exposure to a 0.01 M phosphate buffer solution for as long as two hours (Tables B-7 - B10).

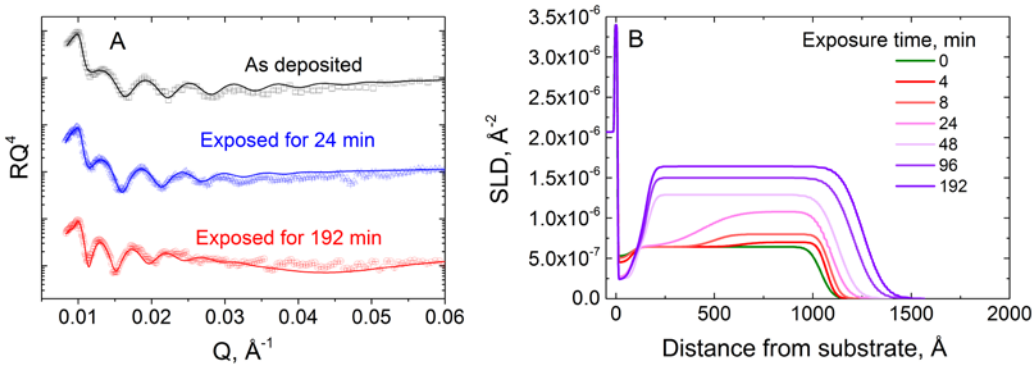

Fig. 4-6. The effect on the film internal structure of the exposure of a 6-bilayer hydrogenated PMAA/QPC film to a 0.2 mg/ml dQPC solution, as illustrated by neutron reflectometry data (plotted as RQ^4 to enhance small features) (left) and the corresponding fitted scattering length density profiles (right). Reprinted from [133] with permission from American Chemical Society.

We next aimed to directly observe the diffusion of deuterated polyelectrolyte chains *as they* invade the film. In this experiment, a hydrogenated 6-bilayer *nl*PEM assembled using the 8-min per layer protocol containing PMAA as the outermost layer was immersed in a 0.2 mg/ml solution of *d*QPC; the film was taken out of solution, rinsed with buffer and dried prior to the NR measurement. Fig. 4-6 summarizes the NR data for various times of exposure to *d*QPC solutions (Tables B-11 – B-17).

Upon exposure to the deuterated polymer solution, the oscillation minima shift to lower Q values indicating an increase in total film thickness. The reflectivity data for the

initially hydrogenated matrix have been fitted using a precursor film plus a single stack. After exposure to the deuterated polymer, we use a two-stack model, with the bottom stack corresponding to the hydrogenated material, and the upper stack associated with the addition of deuterated polymer. The fitted neutron reflectometry profiles are shown in Fig. 4-6, right. The addition of *d*QPC to the film is observed from an increase in *SLD* values, which at shorter times occurred only within the upper part of the film. As exposure time increased, an enhanced *SLD* zone propagated deeper in the film until the deposited polymer was distributed throughout the film. A zone impermeable to *d*QPC penetration even at longer times is seen in the fitted *SLD* profiles in Fig. 4-6. The total thickness of this zone of hydrogenated polyelectrolytes (Table B-16) was ~150 Å, which included a 75-Å layer of lower *SLD* incorporating the BPEI layer. The remaining 75 Å of the PMAA/QPC film, approximately corresponding to a single bilayer, is strongly bound to the substrate and cannot be replaced by deuterated chains. This is in good agreement with the 6.5 nm thickness of the dense near-substrate zone estimated from ellipsometry experiments (see above). Fig. 4-7A shows the kinetics of *d*QPC penetration into the film as represented by changes in the width of the deuterated stack *d*. The diffusion coefficient was determined to be $1.1\pm0.1\times10^{-14}$ cm^2/s from the d^2 *vs*. *t* graph shown as an inset in Fig. 4-7A. This value is one to two orders of magnitude smaller than that of QPC chains

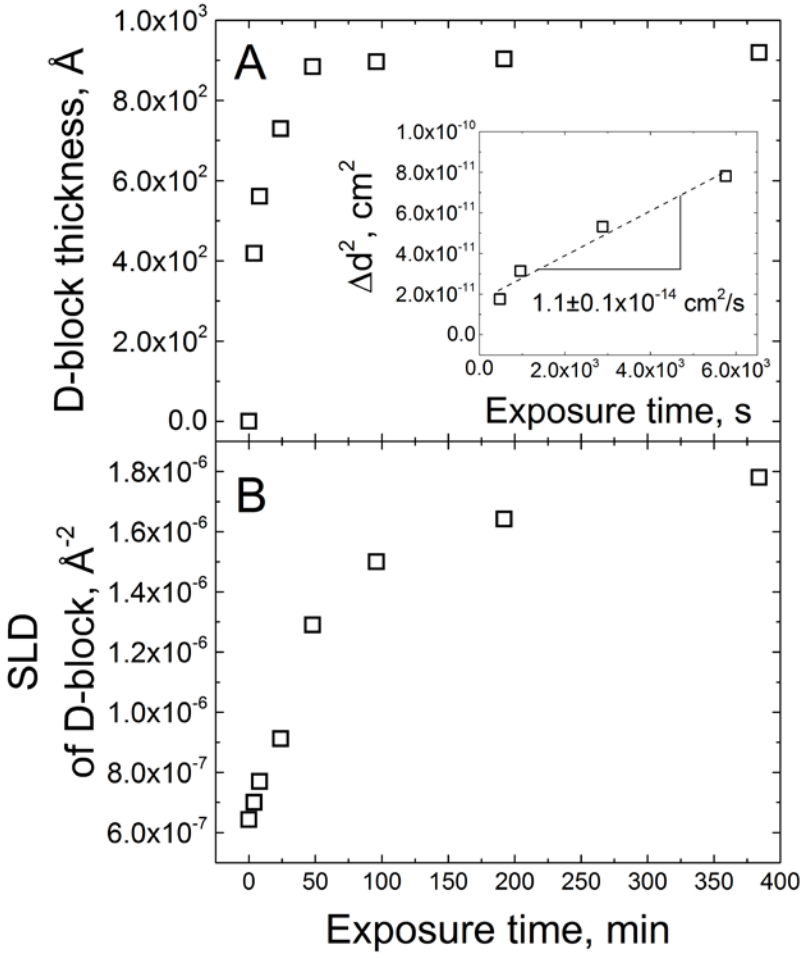

Fig. 4-7. Time dependence of the polyelectrolyte penetration depth, *d* (A) and the plateau SLD value (B) during the invasion of *d*QPC chains into a hydrogenated 6-bilayer PMAA/QPC film assembled using the 8 minutes per layer deposition procedure. Reprinted from [133] with permission from American Chemical Society.

determined using the thicknesses of swollen films in Fig. 4-2, since the diffusion coefficient will be underestimated if the diffusion distances are taken from dry film measurements. Fig. 4-7B shows the plateau values of *SLD* of *d*QPC-containing films, which are largely composed of hydrogenated PMAA and deuterated QPC chains, as a

function of time. By comparing the data in Figs. 4-7A and B, two regimes for *d*QPC penetration into *nl*PEM can be distinguished. The first regime is caused by diffusion of the initial *d*QPC, which occurs with the diffusion coefficient estimated above. The second process involves a slower enrichment of PMAA/QPC complexes with deuterated chains. This slower addition of deuterated chains is rate limited by the sluggish chain rearrangements of earlier formed *h*PMAA/QPC contacts to accommodate excess *d*QPC within the film. The arriving polyelectrolyte chains bring in excess charge that causes the film to swell as shown in Fig. 4-2 above.

The fitted plateau values of *SLD* also enable us to estimate the relative amounts of hydrogenated and deuterated polymers, as well as the content of water in the LbL film. We first analyzed the initial, as deposited PEM which contained only hydrogenated polyelectrolytes. The total SLD_H of this matrix was found by fitting the reflectivity data to be 6.43×10^{-7} Å^{-2}. One can express the total SLD_H of the hydrogenated matrix as follows:

$$SLD_H = \omega_{hPMAA} SLD_{hPMAA} + \omega_{hQPC} SLD_{hQPC} + \omega_{H_2O} SLD_{H_2O}, \quad \textbf{(4-1)}$$

where the ω values represent the mass fractions of the different film components. *SLD* values of each component were calculated using known atomic densities and polymer atomic compositions (Table B-18). The values of ω were fitted simultaneously with the boundary conditions set for ω for PMAA and QPC not to exceed 0.6, and for ω for H_2O not to exceed 0.2, and the sum of the ω components adds up to 1. Only one solution for film composition was found, i.e. ω_{hQPC} = 0.46, ω_{hPMAA} = 0.439 and ω_{H2O} = 0.101. The

water content of 10.1% is in a good agreement with previously reported values found using neutron reflectometry for linear PEMs.[125]

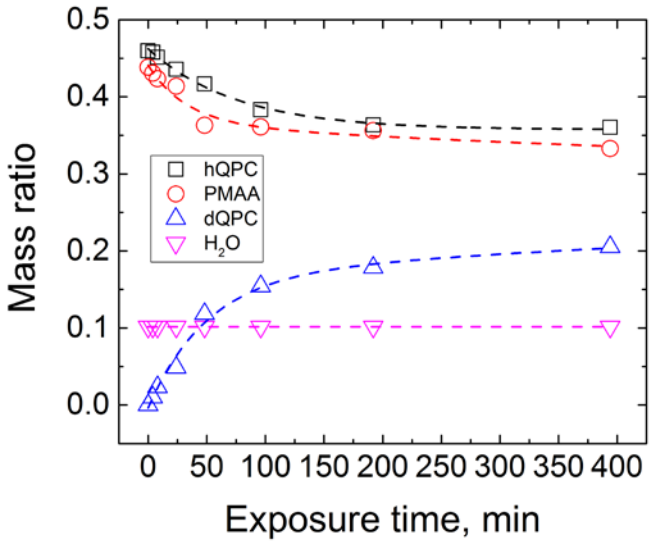

Fig. 4-8. Effect of the exposure time of a hydrogenated PMAA/QPC film to a 0.2 mg/ml dQPC solution on the mass ratios of all components within the 6-bilayer nlPEM film. Reprinted from [133] with permission from American Chemical Society.

The fitted values of ω_{hQPC} and $\omega_{h\text{PMAA}}$ were taken as initial values for further calculations, performed for films after the addition of *d*QPC. The water content in the films was assumed to be constant for all film compositions, because samples were dried with the same procedure. Also, the amount of deuterated polyelectrolyte was allowed to increase assuming no loss of hydrogenated polymer. Then, after exposure of the film to *d*QPC, the *SLD* of the top block can be calculated as follows:

$$SLD_D = \omega_{hPMAA} SLD_{hPMAA} + \omega_{hQPC} SLD_{hQPC} + \omega_{H_2O} SLD_{H_2O} + \omega_{dQPC} SLD_{dQPC}, \quad \textbf{(4-2)}$$

where two additional parameters, *i.e.* $\omega_{d\text{QPC}}$ and the *SLD* of *d*QPC, with $\omega_{d\text{QPC}}$ set to be less than $\omega_{h\text{QPC}}$. With the fitted values of the parameters set to be less than initial values of the hydrogenated matrix, the equation was fitted to find $\omega_{d\text{QPC}}$. The calculated mass ratios (ω) of each component in the stack enriched with the deuterated material are provided in Table B-19. The calculations indicate that the content of *d*QPC in the film increases from zero to ~20% with time, while the fractional content of hydrogenated PMAA and QPC decreases to below 40% of the total mass. These results show that even after long-term (192 min) exposure of *nl*PEMs to *d*QPC, films contain both hydrogenated and deuterated polycation chains, *i.e.* enrichment with polycations is likely to occur as co-adsorption of additional *d*QPC chains rather than *via* replacement of the original *h*QPC (Fig 4-9).

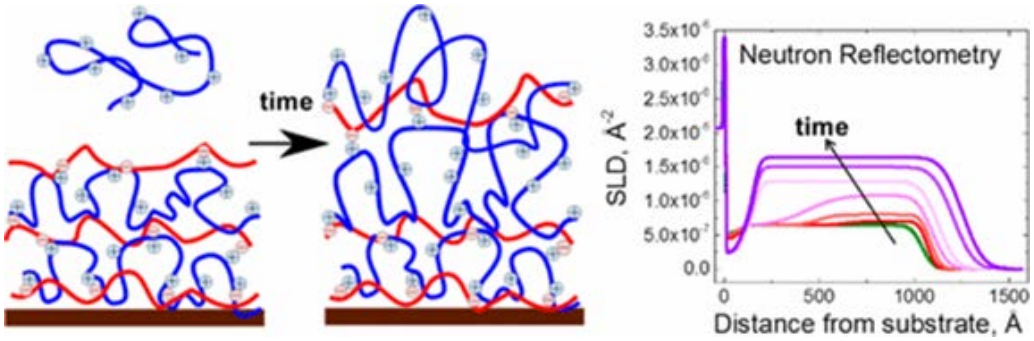

Fig. 4-9. Schematic representation of main findings for the current chapter.

5. IONICALLY PAIRED LAYER-BY-LAYER HYDROGELS: WATER AND POLYELECTROLYTE UPTAKE CONTROLLED BY DEPOSITION TIME[3]

5.1. Introduction

Polyelectrolyte multilayers (PEMs) are traditionally made by sequential deposition of oppositely charged polymers at a surface using the layer-by-layer (LbL) technique[38]. In addition to ionically pairs, cooperative interactions that lie at the heart of many LbL systems—secondary interactions such as hydrogen bonding, van der Waals forces, and hydrophobic interactions—can also play important role in LbL assembly[50-52]. The cooperative type of intermolecular interactions is quite universal and can be applied to metal-protein[53] and hydrogen bonding systems[54]. The applicability of the LbL technique to a wide range of polymers and substrates, and the ease of incorporation of highly functional molecules within these films, have excited interest in a wide range of applications including tissue engineering[126], in which LbL assemblies can be used to enhance tissue regeneration[127-128]. Moreover, PEMs show particular promise for surface functionalization of biomedical devices to create hemocompatible, antibacterial, and antioxidant surfaces[129], or to control cell adhesion-localized delivery of bioactive molecules[18, 37, 39]. Future proposed applications of PEMs as bioactive matrices or drug molecule carriers dictate certain requirements for film capacity and functionality, defined by the overall film thickness and controllable swelling. In particular, it becomes

[3] Reprinted with permission from "Ionically paired layer-by-layer hydrogels: water and polyelectrolyte uptake controlled by deposition Time" by Victor Selin, John F. Ankner, and Svetlana A. Sukhishvili, **2018**. Gels, 4, 7, Copyright 2018 by MDPI.

increasingly desirable to achieve a film thickness on the order of microns upon the deposition of a small number of bilayers. In addition, well-controlled interaction with water, *i.e.*, swelling, can enable controlling the dosage of an active component released from the film.

Depending on the binding strength between the components[18, 75], and therefore the mobility of polymer chains during LbL film deposition, two main types of film growth can be distinguished. Namely, linear LbL growth describes those systems that exhibit a constant increment in thickness with deposition of successive bilayers and is usually a characteristic of strongly paired polyelectrolytes and/or nanoparticles[20, 76]. On the other hand, nonlinear films demonstrate an increase in deposited film mass per deposition step, reflecting the high mobility of chains during deposition and the resulting penetration of the invading component into the film[19, 77-78]. This growth mode has been predominantly reported for more weakly bound systems, and can be additionally controlled by several parameters. One of these parameters is polymer molecular weight—a parameter that is directly related to mobility of polymer chains within the films[59, 79]. For ionically paired PEMs, the mobility of chains also can be regulated by the introduction of small ions[80-81]. Moreover, in the case of weak polyelectrolytes, ionization of polymer chains, determined by solution pH and assembly conditions, can also affect chain mobility and film growth[82-83].

The literature fundamentally agrees that the main factor causing exponential growth is enhanced diffusivity of polymer chains[86, 106, 130]. For more strongly bound films, the invading component is kinetically frozen at the outermost PEM layer and does not

diffuse deeply, resulting in linear film growth with a small incremental mass increase that corresponds to monolayer coverage. The original mechanism of exponential growth was attributed to an "in-and-out" diffusion of polymer chains throughout the entire film thickness[86]. This mechanism was later modified to include chain diffusivity in systems that do not exhibit diffusion throughout the whole film[20, 130-132]. Very recently, another mechanism of exponential growth has been proposed by Schlenoff that describes nonlinear deposition as a consequence of the diffusion of ionic binding sites rather than mass diffusion of the polymers[87].

Our group recently conducted a study of nonlinear growth where the deposition time used for adsorption of each individual layer was not fixed, but instead polymer adsorption and absorption was followed up to complete saturation of the film with the incoming polyelectrolyte[133]. At saturation, nonlinear films exhibited high (up to 4-fold of dry thickness) swelling ratios and were reminiscent of substrate-bound ionically crosslinked gels. We have demonstrated that as more time was allowed for an incoming polyelectrolyte to penetrate the film, film swelling continuously increased, and more time was required to reach saturation for larger layer numbers. In this work, we studied a more practical scenario, in which deposition times were fixed for all layers within the film, but varied between different films. While previously, by applying the neutron reflectometry (NR) technique[23, 61, 66-67, 73, 114] to dry LbL films, we demonstrated that layer deposition time controlled film internal structure[133]; here, we study swelling of LbL films constructed using fixed deposition time and explore how the internal film structure affects kinetics of polyelectrolyte chain invasion. Moreover, we explore the effect of layer deposition time

on film stability in salt solutions. This study further contributes to the understanding of the relationship between growth conditions of non-linear PEMs and the behavior of these films in aqueous solutions containing small ions and/or polyelectrolytes.

5.2. Materials

Branched polyethyleneimine (BPEI) with M_w = 25 kDa and M_w/M_n = 2.50 was purchased from Sigma-Aldrich (St. Louis, MO, USA). Hydrogenated polymethacrylic acid (*h*PMAA, or PMAA) with M_w 180 kDa and M_w/M_n = 1.02 was purchased from Polymer Standard Services (PSS) GmbH (Mainz, Germany). Deuterated poly(2-(dimethylamino)ethyl methacrylate) (*d*PDMAEMA, d15) with M_w 90 kDa and M_w/M_n 1.8, as well as deuterated PMAA (*d*PMAA) with molecular weight 180 kDa and $M_w/M_n < 1.1$, were purchased from Polymer Source, Inc (Dorval, Québec, Canada). Hydrogenated 2-(dimethylamino)ethyl methacrylate monomer (DMAEMA), ethyl 2-bromoisobutyrate (EBiB), CuBr and 1,1,4,7,10,10-hexamethyltriethylenetetramine (HMTETA), hydrogenated and fully deuterated methyl sulfate (d6), as well as all solvents, were purchased from Sigma-Aldrich (St. Louis, MO, USA). Ultrapure Milli-Q water (Merck Millipore, Burlington, MA, USA) with a resistivity of 18.2 MΩ/cm was used in all experiments. All other chemicals were purchased from Aldrich and used without further purification.

5.3. Multilayer Buildup and Polyelectrolyte Uptake Experiments

LbL films were deposited on silicon wafer substrates (111 orientation, Institute of Electronic Materials Technology, Warsaw, Poland). Prior to film deposition, silicon wafers were cleaned as described elsewhere [81] and primed with a monolayer of BPEI

adsorbed from 0.2 mg/mL solution at pH 9 for 15 min. PEM film was then deposited by sequential dipping in 0.2 mg/mL PMAA and QPC solutions in 0.01 M phosphate buffer at pH 6.0 for 4, 8, 16, or 24 min. In between polymer deposition steps, the wafers were rinsed by immersing twice in 0.01 M phosphate buffer solutions at pH 6.0 for 2 min. The procedure was repeated until the required number of layers was reached. Deposition time per cycle during PEM assembly is denoted as a superscript with the number of minutes used for deposition written next to the layer name. The number of layers in the PEM films is denoted by a subscript. Thus, $PMAA_7^{16min}$ denotes a PEM film assembled using 16 min per step and terminated at layer number 7, which is PMAA.

For the polyelectrolyte uptake studies using neutron reflectometry (NR), hydrogenated films $PMAA_{11}^{8min}$ and $PMAA_7^{24min}$ were exposed to 0.2 mg/L solutions of *d*QPC in 0.01 M phosphate buffer at pH 6.0 for different time intervals. After rinsing with 18.2 MΩ/cm Milli-Q water and drying under nitrogen flow for 5 min, NR measurements were performed, and then the films were returned to the polymer solution for continued polymer uptake. Samples for internal structure studies were assembled using 4 and 8 min deposition times per immersion cycle having the design $QPC_8/dPMAA_9/QPC_{14}$ or 16 and 24 min deposition times with design $QPC_4/dPMAA_5/QPC_{10}$ and $QPC_4/dPMAA_5/QPC_8$, respectively. The difference in sample architectures was dictated by the resolution requirements for thickness determination using NR.

5.4. Film Swelling, Stability in Salt, and Poly(Methacrylic Acid) (PMAA) Ionization as a Function of Layer Deposition Time

Fig. 5-1 shows the total dry film thickness as a function of deposition time per layer. To compare the increment in thickness during film growth for each deposition time,

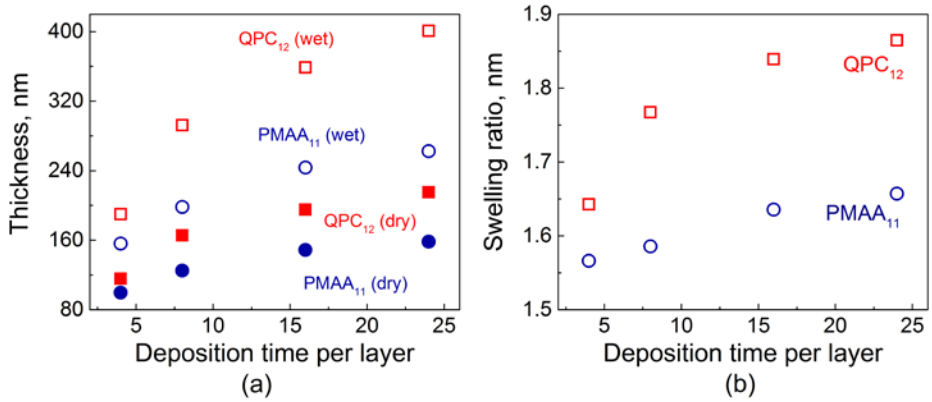

Fig. 5-1. (a) Dry and in situ thicknesses of $PMAA_{11}$ (poly(methacrylic acid),red symbols) and QPC_{12} (quaternized poly-2-(dimethylamino)ethyl methacrylate, blue symbols) films as a function of deposition time per layer; (b) Calculated swelling ratio of $PMAA_{11}$ (red symbols) and QPC_{12} (blue symbols) films as a function of deposition time per layer. Reprinted with permission from "Ionically paired layer-by-layer hydrogels: water and polyelectrolyte uptake controlled by deposition Time" by Victor Selin, John F. Ankner, and Svetlana A. Sukhishvili, **2018**. Gels, 4, 7, Copyright 2018 by MDPI.

two samples were deposited simultaneously, terminated with either poly(methacrylic acid) (PMAA) or quaternized poly-2-(dimethylamino)ethyl methacrylate (QPC). Fig. 5-1a illustrates that the total amount of material absorbed increases with deposition time per layer. The dry thickness of both $PMAA_{11}^{24min}$ and QPC_{12}^{24min} films was more than 1.5× greater than that for the films made using an 8 min deposition time. Similar observations by Schlenoff and co-workers were made for a different polyelectrolyte system studied at high salt concentrations: when the polyelectrolyte deposition time increased from 3 to 20

min, a 1.5-fold increase in film thickness was observed[81]. The thicknesses of QPC-terminated films were greater in all cases, with a tendency to increase with time. Moreover, comparison of the thickness ratios $QPC_{12}^{4min}/PMAA_{11}^{4min}$ and $QPC_{12}^{24min}/PMAA_{11}^{24min}$ gives 1.1 and 1.35, respectively, reflecting a strong dependence of mass absorbed on exposure time and therefore confirming the diffusive nature of growth in non-linear PEMs, also described in our previous work[133].

Fig. 5-1b shows that not only the amount of polymers uptaken by the film at each deposition step but also the degree of film swelling was strongly affected by the deposition time per layer. The swelling ratio was determined as the ratio of wet film thickness, measured by in situ ellipsometry in the presence of buffer above the growing film, to the thickness of the dry films. Longer layer deposition times allowed for greater film intermixing, charge overcompensation, and enhanced creation of QPC loops, which are formed by QPC units that do not participate in the formation of ionic pairs with PMAA and carry a permanent charge[133]. The osmotic pressure created by the counterions, electrostatic and steric repulsion between excess charge in the loops, as well as the film hydration all contribute to an uptake of large amounts of water into the films. In addition, film swelling was higher for QPC-capped films. On the contrary, the penetration during deposition of PMAA, which is a weak polyelectrolyte, resulted in lower swelling, as a charge in the PMAA loops was suppressed by the greater amount of the polyacid accommodated within the films[119, 133].

The amount of water penetrating into the films intuitively should be related to binding strength between assembled polyelectrolytes. One way to characterize the polyelectrolyte binding strength is to compare the stability of LbL films in different salt solutions, where small ions compete with electrostatic pairs formed by polymer association. Exposure of PEMs to salt concentrations lower than those of film dissolution promotes polymer diffusion and causes film smoothening as shown and quantified by atomic force microscopy for systems formed by strong and weak polyelectrolytes[55, 134]. Notably, prior work on PEM films of strong polyelectrolytes, often composed of strongly electrostatically pairing polystyrene sulfonate (PSS), has shown that these films can sustain relatively high salt concentrations, up to 3.5 M NaCl[55-56]. Such concentrations of salt can disassemble PEM films if they are formed by weak polyelectrolytes, such as PAA[26] or the PMAA used in this work. To avoid film dissolution, much lower salt concentrations (0.1–0.4 M) were used to study enhanced polyelectrolyte chain dynamics within QPC/PMAA films[114]. Fig. 5-2 shows that higher salt concentrations (such as a 0.54 M NaCl solution) lead to disassembly of QPC/PMAA films. The dry thickness of LbL films assembled using various deposition times per layer was measured after overnight exposure to a 0.54 M NaCl solution. The decrease in thickness results from binding site disruption and subsequent loss of material. The rate of desorption of polyelectrolytes from the film was not affected by the film deposition time, thickness, and/or internal structure and was approximately the same (~3–4 nm/min, data not shown) for all films. However, the equilibrated mass loss was larger for thicker $PMAA_{11}^{24min}$ films when compared to thinner $PMAA_{11}^{4min}$ films (~90% and ~75% of the original thickness, respectively) after

exposure to 0.54 M NaCl for 24 h (Fig. 5-2a). This effect demonstrates that increased

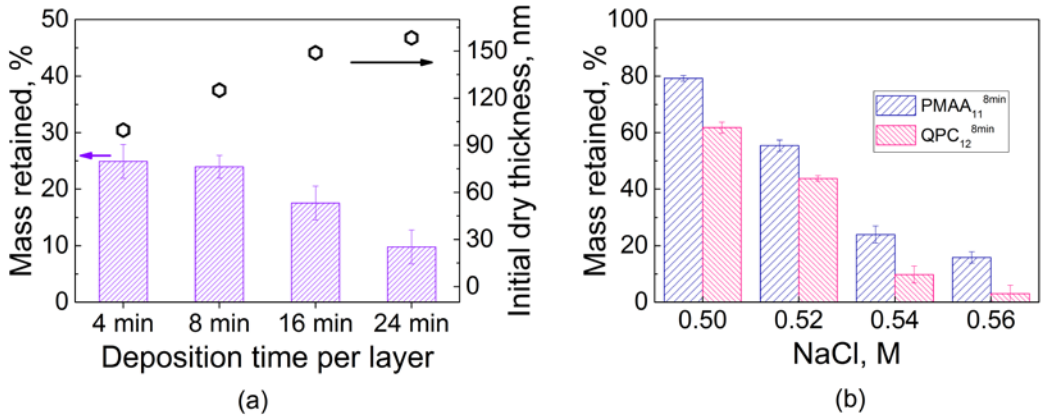

Fig. 5-2. (a) Total film thicknesses and stability of $PMAA_{11}$ films assembled using different deposition times per layer upon post assembly overnight exposure to 0.54 M NaCl; (b) stability of $PMAA_{11}^{8min}$ and QPC_{12}^{8min} films within NaCl solutions of various concentrations after overnight exposure. Reprinted with permission from "Ionically paired layer-by-layer hydrogels: water and polyelectrolyte uptake controlled by deposition Time" by Victor Selin, John F. Ankner, and Svetlana A. Sukhishvili, **2018**. Gels, 4, 7, Copyright 2018 by MDPI.

deposition time per layer results in a decrease in film stability in salt solutions. Shorter deposition times produce better-layered structures, with fewer polymer units included in loops and a larger number of ionic pairs per single polymer chain, which can withstand salt ion assaults better. In contrast, longer deposition times produce highly intermixed nonlinear PEMs that are more prone to disassembly in salt solutions. Fig. 5-2b compares mass retained after an overnight immersion of PMAA-capped and QPC-capped films in solutions with different salt concentrations. Both films showed the same expected trend of decreasing stability with increasing salt concentration, but films capped with QPC in all

salt concentrations were less stable than PMAA-capped assemblies. This observation shows that it might be possible to control film stability via QPC immersion.

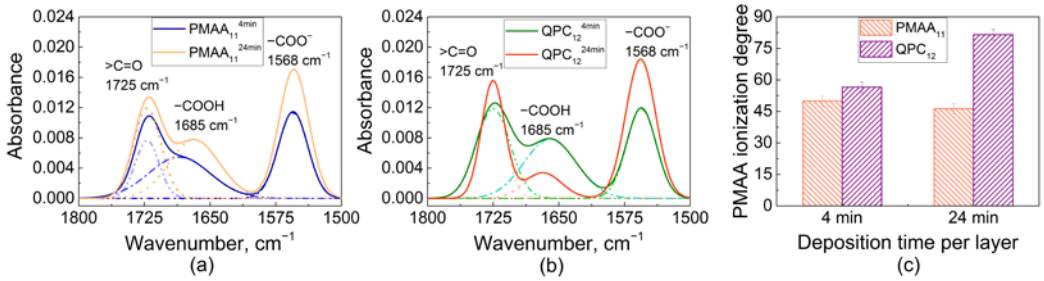

Fig. 5-3. Fourier-transform infrared spectroscopy (FTIR) spectra of dry $PMAA_{11}{}^{4min}$ and $PMAA_{11}{}^{24min}$ (a); FTIR spectra of dry $QPC_{12}{}^{4min}$ and $QPC_{12}{}^{24min}$ (b); calculated values of PMAA ionization degree within $QPC_{12}{}^{4min}$, $QPC_{12}{}^{24min}$, $PMAA_{11}{}^{4min}$ and $PMAA_{11}{}^{24min}$ films (c). Reprinted with permission from "Ionically paired layer-by-layer hydrogels: water and polyelectrolyte uptake controlled by deposition Time" by Victor Selin, John F. Ankner, and Svetlana A. Sukhishvili, **2018**. Gels, 4, 7, Copyright 2018 by MDPI.

An explanation for this effect was then sought in the higher swelling of QPC-capped films (Fig. 5-1b), and ionization of assembled PMAA was determined using FTIR. Earlier, FTIR was used by several groups, including ours, to study the ionization of weak polyelectrolytes assembled within linear PEMs[14, 119, 122, 133]. Fig. 5-3a shows FTIR spectra of $PMAA_{11}{}^{4min}$ and $PMAA_{11}{}^{24min}$ films. Both spectra show vibrational bands at 1725 cm^{-1} and 1568 cm^{-1} associated with the stretching vibrations of carbonyl vibrations of QPC (ν, >C=O) and asymmetric stretching vibrations of the carboxylate groups (ν_{as}, $-COO^-$), respectively, as well as a peak at 1685 cm^{-1} associated with the vibrations of protonated carboxylic groups (−COOH). The ionization degree of PMAA within the assembled multilayers was calculated as the ratio of the area of $-COO^-$ to the sum of −COOH and $-COO^-$ absorbances, assuming equal extinction coefficients for vibrations associated with these bands[123]. The ionization degrees of PMAA were 50 ± 2% and 46 ± 2% for

$PMAA_{11}^{4min}$ and $PMAA_{11}^{24min}$ films, respectively. A layer of QPC was then deposited on these films and the resulting QPC_{12}^{4min} and QPC_{12}^{24min} films were measured again (Fig. 5-3b), yielding PMAA ionization of 57 ± 2% and 82 ± 2%, respectively. QPC taken up by the film causes an increase in the average ionization of assembled PMAA chains due to the formation of ion pairs between QPC and previously uncharged PMAA units, while the addition of PMAA suppresses the ionization of PMAA in the adsorbed polymer loops, likely because of the accumulation of an excess of negative polymer charge within the film. Previously, it was shown by several groups that complexation of weak polyelectrolytes in PEMs lowers the pKa and alters the ionization of carboxylic groups[135],[136]. The effect of capping layer on ionization of assembled weak polyelectrolytes was previously reported for PEMs that demonstrate linear growth[137-138]. Here, we show that the capping layer also impacts ionization of weak polyelectrolytes in non-linear LbL films.

It is also clearly seen that ionization of PMAA is strongly dependent on deposition time (Fig. 5-3c), and larger amounts of uptaken QPC lead to higher charge in assembled PMAA chains. As shown in Fig. 5-2, however, larger deposition time per layer decreases the stability of LbL films in salt solutions, suggesting that ionization of PMAA within the films is inversely correlated to films stability. We suggest that a key to lower salt stability of the films constructing using longer deposition times is their larger swelling, caused by more loopy conformations of QPC. In highly swollen films, loopy QPC chains have fewer binding points with PMAA and accumulate excess charge, increasing osmotic pressure

within the film. As a result, the net interaction energy between polyelectrolytes decreases, leading to faster chain dynamics.

5.5. Effect of Film Internal Structure on Polyelectrolyte Uptake: Neutron Reflectometry Studies

A central point of this work is an exploration of how assembly conditions of non-linear LbL films, and therefore internal film structure, affect invasion of polyelectrolyte chains. To that end, we assembled films with different internal structures, using deposition times that were fixed for all layers within the same film, and varied between various films. In the first set of experiments, which sought to quantify the internal structure of the films using NR, a layer of *d*PMAA was incorporated within the film for contrast (Fig. 5-4). After establishing the required film thicknesses, a number of layers, and quantifying layer intermixing, *d*PMAA was substituted with hydrogenated PMAA for film construction, and fully hydrogenated films, assembled with different deposition time per layer, were exposed to a solution of *d*PMAA to study the effect of internal film layering on the uptake of invading chains. The results of the latter 'chain invasion' experiments are shown in Fig. 5-5 and 5-6. In both cases, the sample design was dictated by the requirements of the NR technique. Thus, knowing that the thickness of deposited films is a function of deposition time, the number of bilayers was altered for 4, 8, 16, and 24 min films. Because the amount of material deposited depended strongly on immersion time and, due to instrumental resolution, the total film thickness in NR should not exceed ~350 nm, films constructed using longer deposition times by design had fewer polyelectrolyte layers. Upstream collimation determines the angular divergence of the incident beam ($\delta\theta$) which, in turn, is

the dominant term in the instrumental resolution of the SNS-LR ($\delta Q/Q = \delta\theta/\theta$, where θ is the angle of incidence onto the sample). The maximum resolvable film thickness is given by $d_{max} = 2\pi/\delta Q$, which is about 350 nm for these measurements.

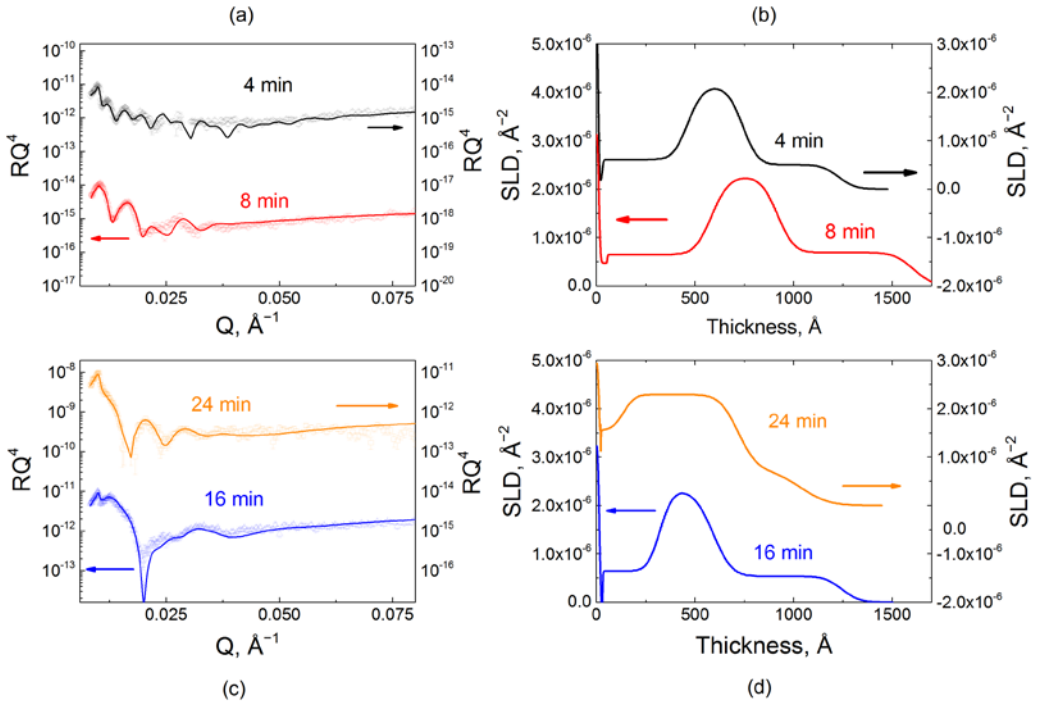

Fig. 5-4. Reflectometry data (a,c) and scattering length density profiles for PMAA/QPC films formed using hydrogenated and deuterated components; (b) *SLD* profiles of films assembled using *d*PMAA as a marker layer with layer sequences $QPC_8/dPMAA_9/QPC_{14}^{4min}$ and $QPC_8/dPMAA_9/QPC_{14}^{8min}$, (black and red lines, respectively); (d) *SLD* profiles of films assembled using *d*PMAA as a marker layer with layer sequences $QPC_4/dPMAA_5/QPC_{10}^{16min}$ and $QPC_4/dPMAA_5/QPC_8^{24min}$ for samples with 16 and 24 min deposition times (blue and orange lines, respectively). Reprinted with permission from "Ionically paired layer-by-layer hydrogels: water and polyelectrolyte uptake controlled by deposition Time" by Victor Selin, John F. Ankner, and Svetlana A. Sukhishvili, **2018**. Gels, 4, 7, Copyright 2018 by MDPI.

Fig. 5-4 shows reflectivity data and fitted profiles for a series of samples containing incorporated *d*PMAA marker layers (*i.e.*, $QPC_8/dPMAA_9/QPC_{14}^{4min}$, $QPC_8/dPMAA_9/QPC_{14}^{8min}$, $QPC_4/dPMAA_5/QPC_{10}^{16min}$ and $QPC_4/dPMAA_5/QPC_8^{24min}$ films) with designed varied internal structure controlled by layer deposition time. The polymer layers included in the reflectivity model consisted of the BPEI priming layer and three hydrogenated/deuterated/hydrogenated stacks. The SLD of the hydrogenated stacks was constrained to be the value for the hydrogenated matrix determined in an independent measurement. The SLD of the deuterated block was found by fitting the reflectivity data (Tables C-1 – C-4). Fig. 5-4 highlights the dramatic effect of layer deposition time on internal film structure. As seen from the SLD profiles, the deuterated marker layers appear as peaks in SLD, whose shape indicates the amount of material deposited, its position, and its spatial extent within the layer. Importantly, the value of the SLD of the deuterated block has almost the same value, 2.33×10^{-6} Å^{-2}, for all four samples and is independent of the deposition time per layer and sample design.

Based on *d*PMAA chain diffusivity, allowing more time per layer deposition encouraged penetration of PMAA chains into neighboring layers. This effect is revealed by a change in interfacial width and deuterated block thickness as a function of deposition time. Thus, based on chain diffusivity, 4 and 8 min deposition times do not allow chains to penetrate much into the hydrogenated bulk. However, increasing deposition time to 16 and 24 min causes a noticeable change in chain intermixing. Tracking the increase in deposited polymer mass, the interfacial full width, σ_{int}, between hydrogenated and deuterated blocks increased from 6.7 to 16.7 nm for *d*PMAA, indicating a greater

intermixing between hydrogenated and deuterated stacks. Continuing this trend, 24 min immersion allows enough time for *d*PMAA to penetrate completely through the film, down to a dense layer (entangled with BPEI) near the substrate, as described in our previous work [133].

Fig. 5-5 illustrates penetration of deuterated *d*QPC chains into the hydrogenated matrix constructed using different deposition times per layer. Specifically, hydrogenated matrices were assembled using 8 and 24 min immersions per layer ($PMAA_{11}^{8min}$ and $PMAA_{7}^{24min}$). These films were immersed in a 0.2 mg/mL solution of *d*QPC, then taken out of solution, rinsed with buffer, and dried prior to the NR measurement. The model used to fit the NR data initially consisted of only two stacks—a priming layer and a hydrogenated matrix. Upon absorption of deuterated chains, an additional stack representing the hydrogenated matrix enriched with deuterated polymers was introduced into the model. Fig. 5-5 shows NR data and the calculated *SLD* profiles of PEMs constructed using per-layer deposition times that were constant for each individual film but varied between different PEMs, specifically 8 and 24 min (Tables C-5 – C-12). For both deposition times ($PMAA_{11}^{8min}$ and $PMAA_{7}^{24min}$), upon exposure to the deuterated polymer solution, the reflectivity oscillation minima shifted to lower *Q* values indicating an increase in total film thickness. The fitted NR profiles are shown in Fig. 5-5b,d.

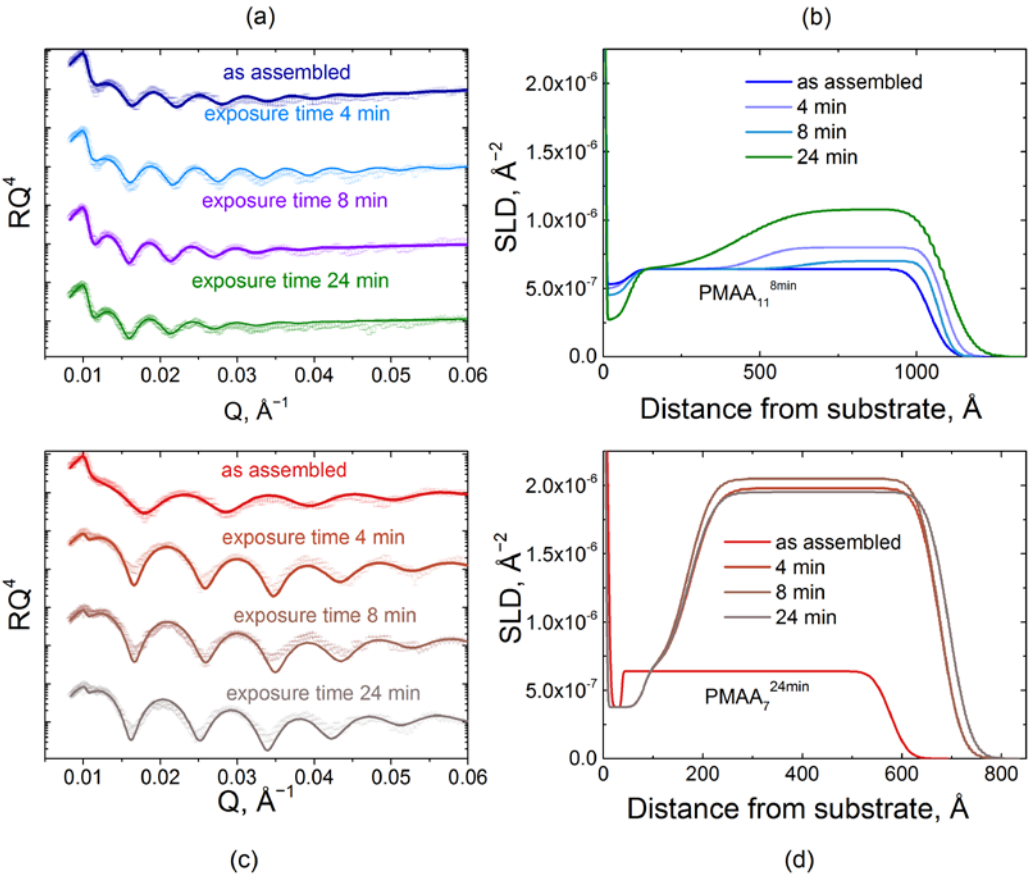

Fig. 5-5. The effect on the film internal structure of the exposure of hydrogenated $PMAA_{11}^{8min}$ and $PMAA_{7}^{24min}$ films to a 0.2 mg/mL *d*QPC solution, as illustrated by neutron reflectometry. Reflectometry data (plotted as RQ^4 to enhance small features) (a,c) and scattering length density profiles (b,d) for $PMAA_{11}^{8min}$ and $PMAA_{7}^{24min}$ films exposed to *d*QPC solution for 4, 8, and 24 min in phosphate buffer at pH 6.0. Reprinted with permission from "Ionically paired layer-by-layer hydrogels: water and polyelectrolyte uptake controlled by deposition Time" by Victor Selin, John F. Ankner, and Svetlana A. Sukhishvili, **2018**. Gels, 4, 7, Copyright 2018 by MDPI.

Polycation penetration into the two films was strikingly different. The addition of *d*QPC to the films is observed by the increase in *SLD* values, which, at shorter times, occurred only within the near-surface region of the $PMAA_{11}^{8min}$ film. The more tightly

bound and structured $PMAA_{11}^{8min}$ matrix demonstrated only a gradual increase of *SLD* for the second block at short exposure times. As exposure time increased, an enhanced *SLD* zone propagated deeper into the film until the deposited polymer was distributed

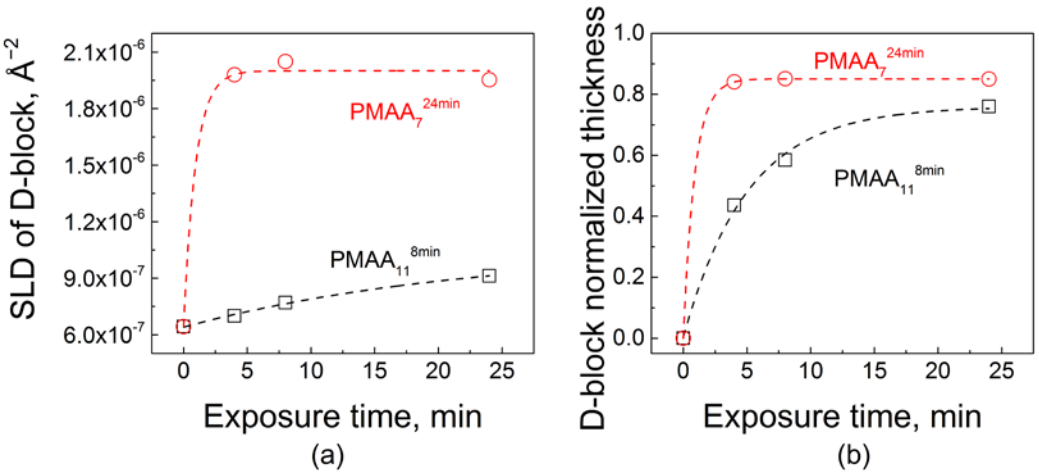

Fig. 5-6. A comparison of the effect on film internal structure of the exposure of hydrogenated $PMAA_{11}^{8min}$ and $PMAA_7^{24min}$ films to a 0.2 mg/mL *d*QPC solution, as illustrated by fitted scattering length density (a) and the fitted thicknesses of deuterated block (b). Reprinted with permission from "Ionically paired layer-by-layer hydrogels: water and polyelectrolyte uptake controlled by deposition Time" by Victor Selin, John F. Ankner, and Svetlana A. Sukhishvili, **2018**. Gels, 4, 7, Copyright 2018 by MDPI.

throughout the film. A thin layer impermeable to *d*QPC was present at the substrate in both systems. The presence of a ~8 nm-thick impermeable zone was previously observed and rationalized as a single bilayer that is strongly bound to the substrate and could not be replaced by deuterated chains[133]. Fig. 5-6a shows a quantitative analysis of NR data upon *d*QPC penetration. The initial values of *SLD* correspond to zero time of exposure and are equal to the *SLD* of the hydrogenated block. Quantitatively, after 4 min of exposure to *d*QPC solution, the *SLD* of the block enriched with deuterated material increased by 8% and 68% for $PMAA_{11}^{8min}$ and $PMAA_7^{24min}$ films, respectively. Adsorption of the

deuterated polycation was also accompanied by an increase in the overall film thicknesses, as seen in the NR profiles. Relatively slow dynamics of penetration of polymer chains within $PMAA_{11}^{8min}$ films can be explained by the higher degree of layering and higher density of barriers in the *d*QPC penetration path. In drastic contrast, penetration into the $PMAA_{7}^{24min}$ matrix was enhanced in comparison with penetration into the $PMAA_{11}^{8min}$ films. As seen in Fig. 5-6, even for the shortest *d*QPC exposure time of 4 min, the polymer permeated the entire film, and a waiting time of 24 min was sufficient for the film to become saturated with the polycation. Note that the time scale of polycation invasion within $PMAA_{7}^{24min}$ film was comparable to that of penetration of QPC into nonlinear films assembled using times required to reach saturation at each deposition step [133]. Both the high degrees of swelling hydrogenated films assembled with longer deposition times (Fig. 5-1b), as well as differences in film layering (Fig. 5-4), might have contributed to faster penetration kinetics of *d*QPC within $PMAA_{7}^{24min}$ films. The difference in the degree of swelling of $PMAA_{11}^{8min}$ and $PMAA_{7}^{24min}$ films is not large (swelling rations 1.6 and 1.7, respectively), however. It is likely that the strikingly different internal structure and layering of $PMAA_{11}^{8min}$ and $PMAA_{7}^{24min}$ films seen in Fig. 5-4 determined the large

differences in the kinetics of uptake of polyelectrolyte chains within LbL films (Fig. 5-6). Schematically, this process represented on Fig. 5-7.

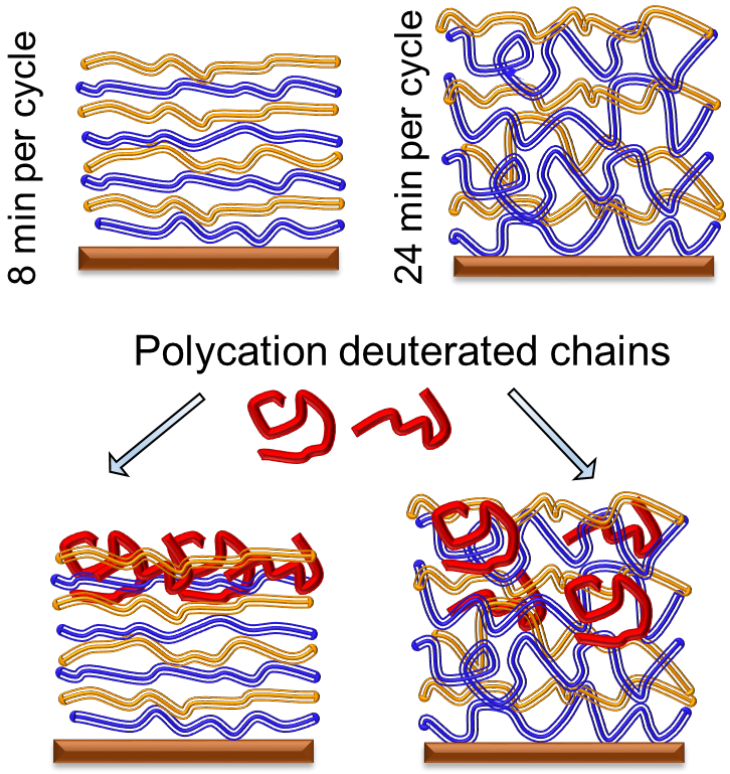

Fig. 5-7. Schematic representation of polycation (dQPC, red lines) penetration into matrices assembled at different conditions. PMAA and QPC chains represented as orange and blue lines, respectively.

6. CONCLUSIONS

Quantitative studies of the diffusion of polyelectrolytes within linear PEMs revealed several features. First, the propensity of films to layer intermixing in salt solutions was strongly dependent on polyelectrolyte molecular weight (barrier-like). Films assembled with the shortest polyelectrolyte chains demonstrated significant center-of-mass diffusion of assembled polyelectrolyte chains in the direction perpendicular to the substrate when these films were annealed in solutions with moderate salt concentrations. Measurements of diffusion coefficients of assembled chains in directions perpendicular and parallel to the substrate as a function of salt concentration demonstrated that both diffusion coefficients rose exponentially with increased salt content.

We also performed quantitative studies of the dynamic of polyelectrolyte chains within non-linear PEMs. The growth of electrostatically assembled films was strongly time-dependent, with the amount of material deposited at each deposition step increasing with the number of deposition steps. Diffusion of polyelectrolytes during film deposition was directly correlated with this thickness increase when diffusion coefficients of the penetrating polymer chains were estimated from ellipsometry and neutron reflectometry measurements. While diffusion coefficients of polyelectrolyte chains were drastically slower than those in solution for both dry and solvent-swollen films, significant chain diffusivity occurred within highly swollen non-linear PEMs. Swelling of the film was correlated with penetration of polyelectrolytes and accumulation of excess charge throughout the entire film thickness. Interestingly, binding of permanently charged and weak polyelectrolytes had opposite effects on film swelling, resulting in periodic

oscillations of film swelling with layer number. Furthermore, we demonstrated that deposition time can be effectively used to control the internal structure of non-linear PEMs as shown by neutron reflectometry and that polyelectrolyte layers can be localized within the film by reducing the deposition time allowed for layer assembly. The estimated values of diffusion coefficients argue for diffusion of polyelectrolytes within the film in their bound rather than “free” state.

REFERENCES

1. Decher, G., Fuzzy Nanoassemblies: Toward Layered Polymeric Multicomposites. *Science* **1997,** *277* (5330), 1232-1237.

2. Zhang, X.; Chen, H.; Zhang, H., Layer-by-layer assembly: from conventional to unconventional methods. *Chem. Commun.* **2007,** (14), 1395-1405.

3. Shutava, T. G.; Kommireddy, D. S.; Lvov, Y. M., Layer-by-Layer Enzyme/Polyelectrolyte Films as a Functional Protective Barrier in Oxidizing Media. *J. Am. Chem. Soc.* **2006,** *128* (30), 9926-9934.

4. Ma, N.; Zhang, H.; Song, B.; Wang, Z.; Zhang, X., Polymer Micelles as Building Blocks for Layer-by-Layer Assembly: An Approach for Incorporation and Controlled Release of Water-Insoluble Dyes. *Chem. Mater.* **2005,** *17* (20), 5065-5069.

5. An, H.; Habib, T.; Shah, S.; Gao, H.; Radovic, M.; Green, M. J.; Lutkenhaus, J. L., Surface-agnostic highly stretchable and bendable conductive MXene multilayers. *Science Advances* **2018,** *4* (3).

6. Richardson, J. J.; Björnmalm, M.; Caruso, F., Technology-driven layer-by-layer assembly of nanofilms. *Science* **2015,** *348* (6233).

7. Chua, P.-H.; Neoh, K.-G.; Kang, E.-T.; Wang, W., Surface functionalization of titanium with hyaluronic acid/chitosan polyelectrolyte multilayers and RGD for promoting osteoblast functions and inhibiting bacterial adhesion. *Biomaterials* **2008,** *29* (10), 1412-1421.

8. Tuong, S. D.; Lee, H.; Kim, H., Chemical fixation of polyelectrolyte multilayers on polymer substrates. *Macromolecular Research* **2008,** *16* (4), 373-378.

9. Chen, W.; McCarthy, T. J., Layer-by-Layer Deposition: A Tool for Polymer Surface Modification. *Macromolecules* **1997,** *30* (1), 78-86.

10. Larocca, N. M.; Filho, R. B.; Pessan, L. A., Influence of layer-by-layer deposition techniques and incorporation of layered double hydroxides (LDH) on the morphology and gas barrier properties of polyelectrolytes multilayer thin films. *Surf. Coat. Technol.* **2018,** *349*, 1-12.

11. Gu, B.; Aung, C. Y.; Chong, P. H. J.; Guan, Y. L.; Yong, K., Reversible and Fast Responsive Optical Fiber Relative Humidity Sensor Based on Polyelectrolyte Self-Assembly Multilayer Film. *IEEE Sens. J.* **2018,** *18* (3), 1081-1086.

12. Goryacheva, O. A.; Gao, H.; Sukhorukov, G. B. In *Modification of polyelectrolyte microcapsules into a container for the low molecular weight compounds*, Saratov Fall Meeting 2017, SPIE: 2018; p 7.

13. Decher, G.; Schlenoff, J. B., *Multilayer Thin Films: Sequential Assembly of Nanocomposite Materials*. 2nd ed.; Wiley-VCH Verlag GmbH & Co. KGaA: Weinheim, Germany, 2012.

14. Zhuk, A.; Selin, V.; Zhuk, I.; Belov, B.; Ankner, J. F.; Sukhishvili, S. A., Chain conformation and dynamics in spin-assisted weak polyelectrolyte multilayers. *Langmuir* **2015,** *31* (13), 3889-96.

15. Seo, J.; Lutkenhaus, J. L.; Kim, J.; Hammond, P. T.; Char, K., Effect of the Layer-by-Layer (LbL) Deposition Method on the Surface Morphology and Wetting Behavior of Hydrophobically Modified PEO and PAA LbL Films. *Langmuir* **2008,** *24* (15), 7995-8000.

16. Kolasinska, M.; Krastev, R.; Gutberlet, T.; Warszynski, P., Layer-by-Layer Deposition of Polyelectrolytes. Dipping versus Spraying. *Langmuir* **2009,** *25* (2), 1224-1232.

17. Caruso, F.; Niikura, K.; Furlong, D. N.; Okahata, Y., 2. Assembly of Alternating Polyelectrolyte and Protein Multilayer Films for Immunosensing. *Langmuir* **1997,** *13* (13), 3427-3433.

18. Schoeler, B.; Kumaraswamy, G.; Caruso, F., Investigation of the Influence of Polyelectrolyte Charge Density on the Growth of Multilayer Thin Films Prepared by the Layer-by-Layer Technique. *Macromolecules* **2002,** *35* (3), 889-897.

19. Picart, C.; Lavalle, P.; Hubert, P.; Cuisinier, F. J. G.; Decher, G.; Schaaf, P.; Voegel, J. C., Buildup Mechanism for Poly(l-lysine)/Hyaluronic Acid Films onto a Solid Surface. *Langmuir* **2001,** *17* (23), 7414-7424.

20. Lavalle, P.; Gergely, C.; Cuisinier, F. J. G.; Decher, G.; Schaaf, P.; Voegel, J. C.; Picart, C., Comparison of the Structure of Polyelectrolyte Multilayer Films Exhibiting a Linear and an Exponential Growth Regime: An in Situ Atomic Force Microscopy Study. *Macromolecules* **2002,** *35* (11), 4458-4465.

21. Hoda, N.; Larson, R. G., Modeling the Buildup of Exponentially Growing Polyelectrolyte Multilayer Films. *J. Phys. Chem. B* **2009,** *113* (13), 4232-4241.

22. Bieker, P.; Schönhoff, M., Linear and Exponential Growth Regimes of Multilayers of Weak Polyelectrolytes in Dependence on pH. *Macromolecules* **2010,** *43* (11), 5052-5059.

23. Xu, L.; Pristinski, D.; Zhuk, A.; Stoddart, C.; Ankner, J. F.; Sukhishvili, S. A., Linear versus Exponential Growth of Weak Polyelectrolyte Multilayers: Correlation with Polyelectrolyte Complexes. *Macromolecules* **2012,** *45* (9), 3892-3901.

24. Michel, M.; Toniazzo, V.; Ruch, D.; Ball, V., Deposition Mechanisms in Layer-by-Layer or Step-by-Step Deposition Methods: From Elastic and Impermeable Films to Soft Membranes with Ion Exchange Properties. *ISRN Materials Science* **2012,** *2012*, 13.

25. Tang, K.; Besseling, N. A. M., Formation of polyelectrolyte multilayers: ionic strengths and growth regimes. *Soft Matter* **2016,** *12* (4), 1032-1040.

26. Dubas, S. T.; Schlenoff, J. B., Polyelectrolyte Multilayers Containing a Weak Polyacid: Construction and Deconstruction. *Macromolecules* **2001,** *34* (11), 3736-3740.

27. Salomäki, M.; Vinokurov, I. A.; Kankare, J., Effect of Temperature on the Buildup of Polyelectrolyte Multilayers. *Langmuir* **2005,** *21* (24), 11232-11240.

28. Cornelsen, M.; Helm, C. A.; Block, S., Destabilization of Polyelectrolyte Multilayers Formed at Different Temperatures and Ion Concentrations. *Macromolecules* **2010,** *43* (9), 4300-4309.

29. Nestler, P.; Block, S.; Helm, C. A., Temperature-Induced Transition from Odd–Even to Even–Odd Effect in Polyelectrolyte Multilayers Due to Interpolyelectrolyte Interactions. *J. Phys. Chem. B* **2012,** *116* (4), 1234-1243.

30. Kujawa, P.; Moraille, P.; Sanchez, J.; Badia, A.; Winnik, F. M., Effect of Molecular Weight on the Exponential Growth and Morphology of Hyaluronan/Chitosan Multilayers: A Surface Plasmon Resonance Spectroscopy and Atomic Force Microscopy Investigation. *J. Am. Chem. Soc.* **2005,** *127* (25), 9224-9234.

31. Sun, B.; Jewell, C. M.; Fredin, N. J.; Lynn, D. M., Assembly of Multilayered Films Using Well-Defined, End-Labeled Poly(acrylic acid): Influence of Molecular Weight on Exponential Growth in a Synthetic Weak Polyelectrolyte System. *Langmuir* **2007,** *23* (16), 8452-8459.

32. Houska, M.; Brynda, E.; Bohatá, K., The effect of polyelectrolyte chain length on layer-by-layer protein/polyelectrolyte assembly—an experimental study. *J. Colloid Interface Sci.* **2004,** *273* (1), 140-147.

33. Chen, F.; Liu, G.; Zhang, G., Formation of Multilayers by Star Polyelectrolytes: Effect of Number of Arms on Chain Interpenetration. *J. Phys. Chem. B* **2012,** *116* (35), 10941-10950.

34. Ariga, K.; Hill, J. P.; Ji, Q., Layer-by-layer assembly as a versatile bottom-up nanofabrication technique for exploratory research and realistic application. *Phys. Chem. Chem. Phys.* **2007,** *9*, 2319-40.

35. Iost, R. M.; Crespilho, F. N., Layer-by-layer self-assembly and electrochemistry: Applications in biosensing and bioelectronics. *Biosens. Bioelectron.* **2012,** *31* (1), 1-10.

36. Krogman, K. C.; Cohen, R. E.; Hammond, P. T.; Rubner, M. F.; Wang, B. N., Industrial-scale spray layer-by-layer assembly for production of biomimetic photonic systems. *Bioinspir. Biomim.* **2013,** *8* (4), 045005.

37. Pavlukhina, S.; Sukhishvili, S., Polymer assemblies for controlled delivery of bioactive molecules from surfaces. *Adv. Drug Del. Rev.* **2011,** *63* (9), 822-836.

38. Decher, G., Layer-by-Layer Assembly (Putting Molecules to Work). In *Multilayer Thin Films*, Wiley-VCH Verlag GmbH & Co. KGaA: 2012; pp 1-21.

39. Liu, X.; Han, F.; Zhao, P.; Lin, C.; Wen, X.; Ye, X., Layer-by-layer self-assembled multilayers on PEEK implants improve osseointegration in an osteoporosis rabbit model. *Nanomed. Nanotechnol. Biol. Med.* **2017,** *13* (4), 1423-1433.

40. Min, J.; Choi, K. Y.; Dreaden, E. C.; Padera, R. F.; Braatz, R. D.; Spector, M.; Hammond, P. T., Designer Dual Therapy Nanolayered Implant Coatings Eradicate Biofilms and Accelerate Bone Tissue Repair. *ACS Nano* **2016,** *10* (4), 4441-4450.

41. Garg, S.; Serruys, P. W., Coronary Stents: Current Status. *J. Am. Coll. Cardiol.* **2010,** *56* (10, Supplement), S1-S42.

42. Mani, G.; Feldman, M. D.; Patel, D.; Agrawal, C. M., Coronary stents: A materials perspective. *Biomaterials* **2007,** *28* (9), 1689-1710.

43. Zilberman, M.; Eberhart, R. C., Drug-eluting bioresorbable stents for various applications. *Annu. Rev. Biomed. Eng.* **2006,** *8*, 153-180.

44. Holmes, D. R.; Kereiakes, D. J.; Garg, S.; Serruys, P. W.; Dehmer, G. J.; Ellis, S. G.; Williams, D. O.; Kimura, T.; Moliterno, D. J., Stent Thrombosis. *J. Am. Coll. Cardiol.* **2010,** *56* (17), 1357-1365.

45. Langer, R., Biomaterials for drug delivery and tissue engineering. *MRS Bull.* **2006,** *31* (6), 477-485.

46. Welle, A.; Grunze, M.; Tur, D., Plasma Protein Adsorption and Platelet Adhesion on Poly[bis(trifluoroethoxy)phosphazene] and Reference Material Surfaces. *J. Colloid Interface Sci.* **1998,** *197* (2), 263-274.

47. Lanzer, P.; Sternberg, K.; Schmitz, K.-P.; Kolodgie, F.; Nakazawa, G.; Virmani, R., Drug-Eluting Coronary Stent Very Late Thrombosis Revisited. *Herz Kardiovaskuläre Erkrankungen* **2008,** *33* (5), 334-342.

48. Lei, L.; Guo, S.-R.; Chen, W.-L.; Rong, H.-J.; Lu, F., Stents as a platform for drug delivery. *Expert Opinion on Drug Delivery* **2011,** *8* (6), 813-831.

49. Saylor, D. M.; Guyer, J. E.; Wheeler, D.; Warren, J. A., Predicting microstructure development during casting of drug-eluting coatings. *Acta Biomater.* **2011,** *7* (2), 604-613.

50. Kharlampieva, E.; Kozlovskaya, V.; Sukhishvili, S. A., Layer-by-Layer Hydrogen-Bonded Polymer Films: From Fundamentals to Applications. *Adv. Mater.* **2009,** *21* (30), 3053-3065.

51. Borges, J.; Mano, J. F., Molecular Interactions Driving the Layer-by-Layer Assembly of Multilayers. *Chem. Rev.* **2014,** *114* (18), 8883-8942.

52. Quinn, J. F.; Johnston, A. P. R.; Such, G. K.; Zelikin, A. N.; Caruso, F., Next generation, sequentially assembled ultrathin films: beyond electrostatics. *Chem. Soc. Rev.* **2007,** *36* (5), 707-718.

53. Liljestrom, V.; Ora, A.; Hassinen, J.; Rekola, H. T.; Nonappa; Heilala, M.; Hynninen, V.; Joensuu, J. J.; Ras, R. H. A.; Torma, P.; Ikkala, O.; Kostiainen, M. A., Cooperative colloidal self-assembly of metal-protein superlattice wires. *Nat Commun* **2017,** *8*.

54. Su, C.; Sun, J. X.; Zhang, X. J.; Shen, D.; Yang, S. G., Hydrogen-Bonded Polymer Complex Thin Film of Poly(2-oxazoline) and Poly(acrylic acid). *Polymers-Basel* **2017,** *9* (8).

55. Dubas, S. T.; Schlenoff, J. B., Swelling and Smoothing of Polyelectrolyte Multilayers by Salt. *Langmuir* **2001,** *17* (25), 7725-7727.

56. McAloney, R. A.; Dudnik, V.; Goh, M. C., Kinetics of Salt-Induced Annealing of a Polyelectrolyte Multilayer Film Morphology. *Langmuir* **2003,** *19* (9), 3947-3952.

57. Nazaran, P.; Bosio, V.; Jaeger, W.; Anghel, D. F.; von Klitzing, R., Lateral Mobility of Polyelectrolyte Chains in Multilayers. .*J Phys. Chem. B* **2007,** *111* (29), 8572-8581.

58. Wong, J. E.; Zastrow, H.; Jaeger, W.; von Klitzing, R., Specific Ion versus Electrostatic Effects on the Construction of Polyelectrolyte Multilayers. *Langmuir* **2009,** *25* (24), 14061-14070.

59. Xu, L.; Selin, V.; Zhuk, A.; Ankner, J. F.; Sukhishvili, S. A., Molecular Weight Dependence of Polymer Chain Mobility within Multilayer Films. *ACS Macro Lett.* **2013,** *2* (10), 865-868.

60. Jomaa, H. W.; Schlenoff, J. B., Salt-Induced Polyelectrolyte Interdiffusion in Multilayered Films: A Neutron Reflectivity Study. *Macromolecules* **2005,** *38* (20), 8473-8480.

61. Xu, L.; Ankner, J. F.; Sukhishvili, S. A., Steric Effects in Ionic Pairing and Polyelectrolyte Interdiffusion within Multilayered Films: A Neutron Reflectometry Study. *Macromolecules* **2011,** *44* (16), 6518-6524.

62. Soltwedel, O.; Nestler, P.; Neumann, H.-G.; Paßvogel, M.; Köhler, R.; Helm, C. A., Influence of Polycation (PDADMAC) Weight on Vertical Diffusion within

Polyelectrolyte Multilayers during Film Formation and Postpreparation Treatment. *Macromolecules* **2012,** *45* (19), 7995-8004.

63. Krebs, T.; Tan, H. L.; Andersson, G.; Morgner, H.; Gregory Van Patten, P., Increased layer interdiffusion in polyelectrolyte films upon annealing in water and aqueous salt solutions. *Phys. Chem. Chem. Phys.* **2006,** *8* (46), 5462-5468.

64. Jourdainne, L.; Lecuyer, S.; Arntz, Y.; Picart, C.; Schaaf, P.; Senger, B.; Voegel, J.-C.; Lavalle, P.; Charitat, T., Dynamics of Poly(l-lysine) in Hyaluronic Acid/Poly(l-lysine) Multilayer Films Studied by Fluorescence Recovery after Pattern Photobleaching. *Langmuir* **2008,** *24* (15), 7842-7847.

65. Jang, Y.; Seo, J.; Akgun, B.; Satija, S.; Char, K., Molecular Weight Dependence on the Disintegration of Spin-Assisted Weak Polyelectrolyte Multilayer Films. *Macromolecules* **2013,** *46* (11), 4580-4588.

66. Lösche, M.; Schmitt, J.; Decher, G.; Bouwman, W. G.; Kjaer, K., Detailed Structure of Molecularly Thin Polyelectrolyte Multilayer Films on Solid Substrates as Revealed by Neutron Reflectometry. *Macromolecules* **1998,** *31* (25), 8893-8906.

67. Kharlampieva, E.; Kozlovskaya, V.; Ankner, J. F.; Sukhishvili, S. A., Hydrogen-Bonded Polymer Multilayers Probed by Neutron Reflectivity. *Langmuir* **2008,** *24* (20), 11346-11349.

68. Kovacevic, D.; van der Burgh, S.; de Keizer, A.; Cohen Stuart, M. A., Kinetics of Formation and Dissolution of Weak Polyelectrolyte Multilayers: Role of Salt and Free Polyions. *Langmuir* **2002,** *18* (14), 5607-5612.

69. Sukhishvili, S. A.; Kharlampieva, E.; Izumrudov, V., Where Polyelectrolyte Multilayers and Polyelectrolyte Complexes Meet. *Macromolecules* **2006,** *39* (26), 8873-8881.

70. Xu, L.; Kozlovskaya, V.; Kharlampieva, E.; Ankner, J. F.; Sukhishvili, S. A., Anisotropic Diffusion of Polyelectrolyte Chains within Multilayer Films. *ACS Macro Lett.* **2011,** *1* (1), 127-130.

71. Spruijt, E.; Sprakel, J.; Lemmers, M.; Stuart, M. A. C.; van der Gucht, J., Relaxation Dynamics at Different Time Scales in Electrostatic Complexes: Time-Salt Superposition. *Physi. Rev. Lett.* **2010,** *105* (20), 208301.

72. Picart, C.; Mutterer, J.; Richert, L.; Luo, Y.; Prestwich, G. D.; Schaaf, P.; Voegel, J. C.; Lavalle, P., Molecular basis for the explanation of the exponential growth of polyelectrolyte multilayers. *Proc. Natl. Acad. Sci. USA* **2002,** *99* (20), 12531-12535.

73. Korneev, D.; Lvov, Y.; Decher, G.; Schmitt, J.; Yaradaikin, S., Neutron Reflectivity Analysis of Self-Assembled Film Superlattices with Alternate Layers of Deuterated and Hydrogenated Polysterenesulfonate and Polyallylamine. *Physica B* **1995,** *213,* 954-956.

74. Soltwedel, O.; Ivanova, O.; Nestler, P.; Müller, M.; Köhler, R.; Helm, C. A., Interdiffusion in Polyelectrolyte Multilayers. *Macromolecules* **2010,** *43* (17), 7288-7293.

75. Ramsden, J. J.; Lvov, Y. M.; Decher, G., Determination of optical constants of molecular films assembled via alternate polyion adsorption. *Thin Solid Films* **1995,** *254* (1-2), 246-251.

76. Kwon, S. R.; Elinski, M. B.; Batteas, J. D.; Lutkenhaus, J. L., Robust and Flexible Aramid Nanofiber/Graphene Layer-by-Layer Electrodes. *ACS Appl. Mater. Interfaces* **2017,** *9* (20), 17125-17135.

77. Elbert, D. L.; Herbert, C. B.; Hubbell, J. A., Thin Polymer Layers Formed by Polyelectrolyte Multilayer Techniques on Biological Surfaces. *Langmuir* **1999,** *15* (16), 5355-5362.

78. Ruths, J.; Essler, F.; Decher, G.; Riegler, H., Polyelectrolytes I: Polyanion/Polycation Multilayers at the Air/Monolayer/Water Interface as Elements for Quantitative Polymer Adsorption Studies and Preparation of Hetero-superlattices on Solid Surfaces. *Langmuir* **2000,** *16* (23), 8871-8878.

79. Nestler, P.; Paßvogel, M.; Helm, C. A., Influence of Polymer Molecular Weight on the Parabolic and Linear Growth Regime of PDADMAC/PSS Multilayers. *Macromolecules* **2013,** *46* (14), 5622-5629.

80. Guzman, E.; Ritacco, H.; Rubio, J. E. F.; Rubio, R. G.; Ortega, F., Salt-induced changes in the growth of polyelectrolyte layers of poly(diallyl-dimethylammonium chloride) and poly(4-styrene sulfonate of sodium). *Soft Matter* **2009,** *5* (10), 2130-2142.

81. Dubas, S. T.; Schlenoff, J. B., Factors controlling the growth of polyelectrolyte multilayers. *Macromolecules* **1999,** *32* (24), 8153-8160.

82. Butergerds, D.; Kateloe, C.; Cramer, C.; Schonhoff, M., Influence of the Degree of Ionization on the Growth Mechanism of Poly(Diallyldimethylammonium)/Poly(Acrylic Acid) Multilayers. *J. Polym. Sci. B Polym. Phys.* **2017,** *55* (5), 425-434.

83. Alonso, T.; Irigoyen, J.; Iturri, J. J.; larena, I. L.; Moya, S. E., Study of the multilayer assembly and complex formation of poly(diallyldimethylammonium chloride) (PDADMAC) and poly(acrylic acid) (PAA) as a function of pH. *Soft Matter* **2013,** *9* (6), 1920-1928.

84. Richert, L.; Lavalle, P.; Payan, E.; Shu, X. Z.; Prestwich, G. D.; Stoltz, J.-F.; Schaaf, P.; Voegel, J.-C.; Picart, C., Layer by Layer Buildup of Polysaccharide Films: Physical Chemistry and Cellular Adhesion Aspects. *Langmuir* **2004,** *20* (2), 448-458.

85. Hübsch, E.; Ball, V.; Senger, B.; Decher, G.; Voegel, J.-C.; Schaaf, P., Controlling the Growth Regime of Polyelectrolyte Multilayer Films: Changing from Exponential to Linear Growth by Adjusting the Composition of Polyelectrolyte Mixtures. *Langmuir* **2004,** *20* (5), 1980-1985.

86. Haynie, D. T.; Cho, E.; Waduge, P., "In and out diffusion" hypothesis of exponential multilayer film buildup revisited. *Langmuir* **2011,** *27* (9), 5700-4.

87. Fares, H. M.; Schlenoff, J. B., Diffusion of Sites versus Polymers in Polyelectrolyte Complexes and Multilayers. *J. Am. Chem. Soc.* **2017,** *139* (41), 14656-14667.

88. Hsu, B. B.; Hagerman, S. R.; Hammond, P. T., Rapid and efficient sprayed multilayer films for controlled drug delivery. *J. Appl. Polym. Sci.* **2016,** *133* (25), n/a-n/a.

89. Pristinski, D.; Kozlovskaya, V.; Sukhishvili, S. A., Fluorescence correlation spectroscopy studies of diffusion of a weak polyelectrolyte in aqueous solutions. *The Journal of Chemical Physics* **2005,** *122* (1), 014907.

90. Zhang, X.; Xia, J. H.; Gaynor, S. G.; Matyjaszewski, K., Atom transfer radical polymerization using functional initiators containing carboxylic acid group. *Abstr. Pap. Am. Chem. S.* **1998,** *216*, U872-U872.

91. Kellogg, G. J.; Mayes, A. M.; Stockton, W. B.; Ferreira, M.; Rubner, M. F.; Satija, S. K., Neutron Reflectivity Investigations of Self-Assembled Conjugated Polyion Multilayers. *Langmuir* **1996,** *12* (21), 5109-5113.

92. Ortiz, C.; Hadziioannou, G., Entropic Elasticity of Single Polymer Chains of Poly(methacrylic acid) Measured by Atomic Force Microscopy. *Macromolecules* **1999,** *32* (3), 780-787.

93. Koehler, R.; Steitz, R.; von Klitzing, R., About different types of water in swollen polyelectrolyte multilayers. *Adv. Colloid Interface Sci.* **2014,** *207* (0), 325-331.

94. Tanchak, O. M.; Yager, K. G.; Fritzsche, H.; Harroun, T.; Katsaras, J.; Barrett, C. J., Ion distribution in multilayers of weak polyelectrolytes: A neutron reflectometry study. *J. Chem. Phys.* **2008,** *129* (8), 084901.

95. Vidyasagar, A.; Sung, C.; Gamble, R.; Lutkenhaus, J. L., Thermal Transitions in Dry and Hydrated Layer-by-Layer Assemblies Exhibiting Linear and Exponential Growth. *ACS Nano* **2012,** *6* (7), 6174-6184.

96. Du, W.; Yuan, G.; Wang, M.; Han, C. C.; Satija, S. K.; Akgun, B., Initial Stages of Interdiffusion between Asymmetrical Polymeric Layers: Glassy Polycarbonate and Melt Poly(methyl methacrylate) Interface Studied by Neutron Reflectometry. *Macromolecules* **2014,** *47* (2), 713-720.

97. Manning, G. S., Limiting Laws and Counterion Condensation in Polyelectrolyte Solutions I. Colligative Properties. *J. Chem. Phys* . **1969,** *51* (3), 924-933.

98. DeHaseth, P. L.; Lohman, T. M.; Record, M. T., Nonspecific interaction of lac repressor with DNA: an association reaction driven by counterion release. *Biochemistry-Us* **1977,** *16* (22), 4783-4790.

99. Record, M. T., Jr.; Anderson, C. F.; Lohman, T. M., Thermodynamic analysis of ion effects on the binding and conformational equilibria of proteins and nucleic acids: the roles of ion association or release, screening, and ion effects on water activity. *Q. Rev. Biophys.* **1978,** *11* (2), 103-178.

100. Barkley, M. D.; Lewis, P. A.; Sullivan, G. E., Ion effects on the lac repressor-operator equilibrium. *Biochemistry-Us* **1981,** *20* (13), 3842-3851.

101. Sukenik, S.; Boyarski, Y.; Harries, D., Effect of salt on the formation of salt-bridges in [small beta]-hairpin peptides. *Chem. Commun.* **2014,** *50* (60), 8193-8196.

102. Kabanov, V. A. Z., A.B., Soluble interpolymeric complexes as a new class of synthetic polyelectrolytes. *Pure Appl. Chem.* **1984,** *56* (3), 343-354.

103. Karibyants, N.; Dautzenberg, H., Preferential Binding with Regard to Chain Length and Chemical Structure in the Reactions of Formation of Quasi-Soluble Polyelectrolyte Complexes. *Langmuir* **1998,** *14* (16), 4427-4434.

104. Schönhoff, M.; Ball, V.; Bausch, A. R.; Dejugnat, C.; Delorme, N.; Glinel, K.; Klitzing, R. v.; Steitz, R., Hydration and internal properties of polyelectrolyte multilayers. *Colloid Surf. A* **2007,** *303* (1–2), 14-29.

105. Jaber, J. A.; Schlenoff, J. B., Counterions and Water in Polyelectrolyte Multilayers: A Tale of Two Polycations. *Langmuir* **2006,** *23* (2), 896-901.

106. Picart, C.; Mutterer, J.; Richert, L.; Luo, Y.; Prestwich, G. D.; Schaaf, P.; Voegel, J.-C.; Lavalle, P., Molecular basis for the explanation of the exponential growth of polyelectrolyte multilayers. *Proc. Natl. Acad. Sci. U.S.A* **2002,** *99* (20), 12531-12535.

107. Yang, Y.-H.; Malek, F. A.; Grunlan, J. C., Influence of Deposition Time on Layer-by-Layer Growth of Clay-Based Thin Films. *Industrial & Engineering Chemistry Research* **2010,** *49* (18), 8501-8509.

108. Wu, B.; Li, C.; Yang, H.; Liu, G.; Zhang, G., Formation of Polyelectrolyte Multilayers by Flexible and Semiflexible Chains. *J. Phys. Chem. B* **2012,** *116* (10), 3106-3114.

109. Liu, G.; Zou, S.; Fu, L.; Zhang, G., Roles of Chain Conformation and Interpenetration in the Growth of a Polyelectrolyte Multilayer. *J. Phys. Chem. B* **2008,** *112* (14), 4167-4171.

110. Schlenoff, J. B.; Dubas, S. T., Mechanism of Polyelectrolyte Multilayer Growth: Charge Overcompensation and Distribution. *Macromolecules* **2001,** *34* (3), 592-598.

111. Liu, G.; Hou, Y.; Xiao, X.; Zhang, G., Specific Anion Effects on the Growth of a Polyelectrolyte Multilayer in Single and Mixed Electrolyte Solutions Investigated with Quartz Crystal Microbalance. *J. Phys. Chem. B* **2010,** *114* (31), 9987-9993.

112. Büscher, K.; Graf, K.; Ahrens, H.; Helm, C. A., Influence of Adsorption Conditions on the Structure of Polyelectrolyte Multilayers. *Langmuir* **2002,** *18* (9), 3585-3591.

113. Vikulina, A. S.; Anissimov, Y. G.; Singh, P.; Prokopovic, V. Z.; Uhlig, K.; Jaeger, M. S.; von Klitzing, R.; Duschl, C.; Volodkin, D., Temperature effect on the build-up of exponentially growing polyelectrolyte multilayers. An exponential-to-linear transition point. *PCCP* **2016,** *18* (11), 7866-7874.

114. Selin, V.; Ankner, J. F.; Sukhishvili, S. A., Diffusional Response of Layer-by-Layer Assembled Polyelectrolyte Chains to Salt Annealing. *Macromolecules* **2015,** *48* (12), 3983-3990.

115. Comyn, J., Introduction to Polymer Permeability and the Mathematics of Diffusion. In *Polymer Permeability*, Comyn, J., Ed. Springer Netherlands: Dordrecht, 1985; pp 1-10.

116. Dodoo, S.; Steitz, R.; Laschewsky, A.; von Klitzing, R., Effect of ionic strength and type of ions on the structure of water swollen polyelectrolyte multilayers. *PCCP* **2011,** *13* (21), 10318-10325.

117. Zerball, M.; Laschewsky, A.; von Klitzing, R., Swelling of Polyelectrolyte Multilayers: The Relation Between, Surface and Bulk Characteristics. *J. Phys. Chem. B* **2015,** *119* (35), 11879-11886.

118. Kolasińska, M.; Krastev, R.; Gutberlet, T.; Warszyński, P., Swelling and Water Uptake of PAH/PSS Polyelectrolyte Multilayers. In *Surface and Interfacial Forces – From Fundamentals to Applications*, Auernhammer, G. K.; Butt, H.-J.; Vollmer, D., Eds. Springer Berlin Heidelberg: Berlin, Heidelberg, 2008; pp 30-38.

119. Kharlampieva, E.; Sukhishvili, S. A., Ionization and pH stability of multilayers formed by self-assembly of weak polyelectrolytes. *Langmuir* **2003,** *19* (4), 1235-1243.

120. Zan, X.; Peng, B.; Hoagland, D. A.; Su, Z., Polyelectrolyte uptake by PEMs: Impact of salt concentration. *Polymer Chemistry* **2011,** *2* (11), 2581-2589.

121. Jourdainne, L.; Lecuyer, S.; Arntz, Y.; Picart, C.; Schaaf, P.; Senger, B.; Voegel, J. C.; Lavalle, P.; Charitat, T., Dynamics of poly(L-lysine) in hyaluronic acid/poly(L-lysine)multilayer films studied by fluorescence recovery after pattern photobleaching. *Langmuir* **2008,** *24* (15), 7842-7847.

122. Owusu-Nkwantabisah, S.; Gammana, M.; Tripp, C. P., Dynamics of Layer-by-Layer Growth of a Polyelectrolyte Multilayer Studied in Situ Using Attenuated Total Reflectance Infrared Spectroscopy. *Langmuir* **2014,** *30* (39), 11696-11703.

123. Sukhishvili, S. A.; Granick, S., Layered, Erasable Polymer Multilayers Formed by Hydrogen-Bonded Sequential Self-Assembly. *Macromolecules* **2002,** *35* (1), 301-310.

124. Rishard, M. Z. M.; Irwin, R. M.; Laane, J., Vibrational Spectra, DFT Calculations, Unusual Structure, Anomalous CH2 Wagging and Twisting Modes, and Phase-Dependent Conformation of 1,3-Disilacyclobutane. *The Journal of Physical Chemistry A* **2007,** *111* (5), 825-831.

125. Köhler, R.; Dönch, I.; Ott, P.; Laschewsky, A.; Fery, A.; Krastev, R., Neutron Reflectometry Study of Swelling of Polyelectrolyte Multilayers in Water Vapors: Influence of Charge Density of the Polycation. *Langmuir* **2009,** *25* (19), 11576-11585.

126. Shukla, A.; Almeida, B., Advances in cellular and tissue engineering using layer-by-layer assembly. *Wiley Interdiscip Rev Nanomed Nanobiotechnol* **2014,** *6* (5), 411-21.

127. Gentile, P.; Ferreira, A. M.; Callaghan, J. T.; Miller, C. A.; Atkinson, J.; Freeman, C.; Hatton, P. V., Multilayer Nanoscale Encapsulation of Biofunctional Peptides to

Enhance Bone Tissue Regeneration In Vivo. *Advanced Healthcare Materials* **2017,** *6* (8), 1601182-n/a.

128. Gentile, P.; Ghione, C.; Ferreira, A. M.; Crawford, A.; Hatton, P. V., Alginate-based hydrogels functionalised at the nanoscale using layer-by-layer assembly for potential cartilage repair. *Biomaterials Science* **2017,** *5* (9), 1922-1931.

129. Peng, L.; Li, H.; Meng, Y., Layer-by-layer structured polysaccharides-based multilayers on cellulose acetate membrane: Towards better hemocompatibility, antibacterial and antioxidant activities. *Appl. Surf. Sci.* **2017,** *401* (Supplement C), 25-39.

130. Lavalle, P.; Picart, C.; Mutterer, J.; Gergely, C.; Reiss, H.; Voegel, J.-C.; Senger, B.; Schaaf, P., Modeling the Buildup of Polyelectrolyte Multilayer Films Having Exponential Growth. *J. Phys. Chem. B* **2004,** *108* (2), 635-648.

131. Porcel, C.; Lavalle, P.; Decher, G.; Senger, B.; Voegel, J. C.; Schaaf, P., Influence of the Polyelectrolyte Molecular Weight on Exponentially Growing Multilayer Films in the Linear Regime. *Langmuir* **2007,** *23* (4), 1898-1904.

132. Porcel, C.; Lavalle, P.; Ball, V.; Decher, G.; Senger, B.; Voegel, J.-C.; Schaaf, P., From Exponential to Linear Growth in Polyelectrolyte Multilayers. *Langmuir* **2006,** *22* (9), 4376-4383.

133. Selin, V.; Ankner, J. F.; Sukhishvili, S. A., Nonlinear Layer-by-Layer Films: Effects of Chain Diffusivity on Film Structure and Swelling. *Macromolecules* **2017,** *50* (16), 6192-6201.

134. Xu, L.; Kozlovskaya, V.; Kharlampieva, E.; Ankner, J. F.; Sukhishvili, S. A., Anisotropic Diffusion of Polyelectrolyte Chains within Multilayer Films. *ACS Macro Lett.* **2012,** *1* (1), 127-130.

135. Choi, J.; Rubner, M. F., Influence of the degree of ionization on weak polyelectrolyte multilayer assembly. *Macromolecules* **2005,** *38* (1), 116-124.

136. Burke, S. E.; Barrett, C. J., Acid−Base Equilibria of Weak Polyelectrolytes in Multilayer Thin Films. *Langmuir* **2003,** *19* (8), 3297-3303.

137. Müller, M.; Rieser, T.; Lunkwitz, K.; Berwald, S.; Meier-Haack, J.; Jehnichen, D., An in-situ ATR-FTIR study on polyelectrolyte multilayer assemblies on solid surfaces and their susceptibility to fouling. *Macromol. Rapid Commun.* **1998,** *19* (7), 333-336.

138. Müller, M.; Briššová, M.; Rieser, T.; Powers, A. C.; Lunkwitz, K., Deposition and properties of polyelectrolyte multilayers studied by ATR-FTIR spectroscopy. *Mater. Sci. Eng. C.* **1999,** *8-9* (Supplement C), 163-169.

APPENDIX A

SUPPORTING MATERIAL FOR CHAPTER 3

Table A-1. Average values and standard deviations for dry ellipsometric thicknesses of bilayers within QPC/PMAA films.

Multilayer films	QPC/PMAA		
M_w of PMAA	7,000	35,000	145,000
$d_{bilayer}$ (nm)	5.6 ± 0.4	5.5 ± 0.5	5.2 ± 0.5

Table A-2. Average vertical diffusion coefficients $D_\perp$ and standard deviations for PMAAs within QPC/PMAA PEMs obtained from NR results in Fig. 3-4.

	[NaCl]			
	0.1 M	0.2 M	0.3 M	0.4 M
$D_\perp$ of PMAA ($\times 10^{-17}$ cm^2/s)	2.59 ± 0.46	3.35 ± 0.55	6.00 ± 0.97	9.04 ± 0.19

Table A-3. Average lateral diffusion coefficients $D_{//}$ and standard deviations for $PMAA_{7k}^*$ within QPC/PMAA PEMs obtained from FRAP results in Fig. 3-5.

	[NaCl]			
	0.1 M	0.2 M	0.3 M	0.4 M
$D_{//}$ of PMAA* ($\times 10^{-13}$ cm^2/s)	0.77 ± 0.16	1.33 ± 0.21	2.56 ± 0.20	5.50 ± 0.26

Table A-4. Model parameters for a 10bl-10bl QPC/$PMAA_{145k}$ film.

Layer	Nb (Å^{-2})	d (Å)	$\sigma_{int,0}$ (Å)
(QPC/dPMAA)$_{10}$	2.59E-06	342.7	47.5
(QPC/hPMAA)$_{10}$	9.40E-07	317.3	23.8
BPEI	2.57E-06	8.0	0.9
SiO_2	3.20E-06	15.0	2.1
Si	2.07E-06	100.0	0.9

Table A-5. Model parameters for a 10bl-10bl QPC/$PMAA_{145k}$ film annealed in 0.4M NaCl for 10 hours.

Layer	Nb (Å^{-2})	d (Å)	σ_{int} (Å)
(QPC/dPMAA)$_{10}$	2.59E-06	356.0	47.7
(QPC/hPMAA)$_{10}$	9.40E-07	335.0	25.5
BPEI	2.57E-06	8.0	0.9
SiO_2	3.20E-06	15.0	0.9
Si	2.07E-06	100.0	0.9

Table A-6. Model parameters for a 10bl-10bl QPC/$PMAA_{35k}$ film.

Layer	Nb (Å^{-2})	d (Å)	$\sigma_{int,0}$ (Å)
(QPC/dPMAA)$_{10}$	2.59E-06	277.5	34.6
(QPC/hPMAA)$_{10}$	8.52E-07	323.5	24.3
BPEI	1.28E-06	15.0	2.1
SiO_2	3.20E-06	15.0	2.1
Si	2.07E-06	100.0	0.9

Table A-7. Model parameters for a 10bl-10bl QPC/PMAA$_{35k}$ film annealed in 0.4M NaCl for 10 hours.

Layer	Nb (Å^{-2})	d (Å)	σ_{int} (Å)
(QPC/dPMAA)$_{10}$	2.59E-06	295.1	34.9
(QPC/hPMAA)$_{10}$	8.52E-07	335.0	27.0
BPEI	1.28E-06	18.0	7.7
SiO$_2$	3.20E-06	18.0	2.1
Si	2.07E-06	100.0	0.9

Table A-8. Model parameters for a 12bl-12bl QPC/PMAA$_{7k}$ film.

Layer	Nb (Å^{-2})	d (Å)	$\sigma_{int,0}$ (Å)
(QPC/dPMAA)$_{12}$	2.540E-06	480.0	49.8
(QPC/hPMAA)$_{12}$	9.415E-07	810.0	76.2
BPEI	9.750E-07	18.0	7.7
SiO$_2$	3.400E-06	15.0	4.3
Si	2.070E-06	100.0	6.4

Table A-9. Model parameters for a 12bl-12bl QPC/PMAA$_{7k}$ film annealed in 0.4M NaCl for 5 minutes.

Layer	Nb (Å^{-2})	d (Å)	σ_{int} (Å)
(QPC/dPMAA)$_{12}$	2.540E-06	480.0	71.5
(QPC/hPMAA)$_{12}$	9.415E-07	810.0	81.2
BPEI	9.750E-07	18.0	7.7
SiO$_2$	3.200E-06	15.0	4.3
Si	2.070E-06	100.0	6.4

Table A-10. Model parameters for a 12bl-12bl QPC/$PMAA_{7k}$ film annealed in 0.4M NaCl for 10 minutes.

Layer	*Nb* (Å^{-2})	*d* (Å)	σ_{int} (Å)
(QPC/dPMAA)$_{12}$	2.540E-06	472.0	68.3
(QPC/hPMAA)$_{12}$	9.415E-07	818.0	88.5
BPEI	9.750E-07	18.0	7.7
SiO_2	3.200E-06	15.0	4.3
Si	2.070E-06	100.0	6.4

Table A-11. Model parameters for a 12bl-12bl QPC/$PMAA_{7k}$ film annealed in 0.4M NaCl for 15 minutes.

Layer	*Nb* (Å^{-2})	*d* (Å)	σ_{int} (Å)
(QPC/dPMAA)$_{12}$	2.540E-06	472.0	55.3
(QPC/hPMAA)$_{12}$	9.415E-07	820.0	91.0
BPEI	9.750E-07	18.0	7.7
SiO_2	3.200E-06	15.0	4.3
Si	2.070E-06	100.0	6.4

Table A-12. Model parameters for a 12bl-12bl QPC/PMAA$_{7k}$ film annealed in 0.4M NaCl for 20 minutes.

Layer	Nb (Å^{-2})	d (Å)	σ_{int} (Å)
(QPC/dPMAA)$_{12}$	2.540E-06	472.0	73.2
(QPC/hPMAA)$_{12}$	9.415E-07	820.0	93.6
BPEI	9.750E-07	18.0	7.7
SiO$_2$	3.200E-06	15.0	4.3
Si	2.070E-06	100.0	6.4

Table A-13. Model parameters for a 12bl-12bl QPC/PMAA$_{7k}$ film annealed in 0.4M NaCl for 30 minutes.

Layer	Nb (Å^{-2})	d (Å)	σ_{int} (Å)
(QPC/dPMAA)$_{12}$	2.540E-06	470.0	70.6
(QPC/hPMAA)$_{12}$	9.415E-07	811.0	97.4
BPEI	9.750E-07	18.0	7.7
SiO$_2$	3.200E-06	15.0	4.3
Si	2.070E-06	100.0	6.4

Table A-14. Model parameters for a 12bl-12bl QPC/$PMAA_{7k}$ film annealed in 0.4M NaCl for 50 minutes.

Layer	*Nb* (Å^{-2})	*d* (Å)	σ_{int} (Å)
$(QPC/dPMAA)_{12}$	2.540E-06	480.0	51.0
$(QPC/hPMAA)_{12}$	9.415E-07	812.0	103
BPEI	9.750E-07	18.0	7.7
SiO_2	3.200E-06	15.0	4.3
Si	2.070E-06	100.0	6.4

Table A-15. Model parameters for a 12bl-12bl QPC/$PMAA_{7k}$ film annealed in 0.4M NaCl for 90 minutes.

Layer	*Nb* (Å^{-2})	*d* (Å)	σ_{int} (Å)
$(QPC/dPMAA)_{12}$	2.540E-06	480.0	52.3
$(QPC/hPMAA)_{12}$	9.415E-07	810.0	112.8
BPEI	9.750E-07	18.0	7.7
SiO_2	3.200E-06	15.0	4.3
Si	2.070E-06	100.0	6.4

Table A-16. Model parameters for a 12bl-12bl QPC/PMAA$_{7k}$ film annealed in 0.4M NaCl for 150 minutes.

Layer	*Nb* (Å^{-2})	*d* (Å)	σ_{int} (Å)
(QPC/dPMAA)$_{12}$	2.540E-06	480.0	56.2
(QPC/hPMAA)$_{12}$	9.415E-07	810.0	106.4
BPEI	9.750E-07	18.0	7.7
SiO$_2$	3.200E-06	15.0	4.3
Si	2.070E-06	100.0	6.4

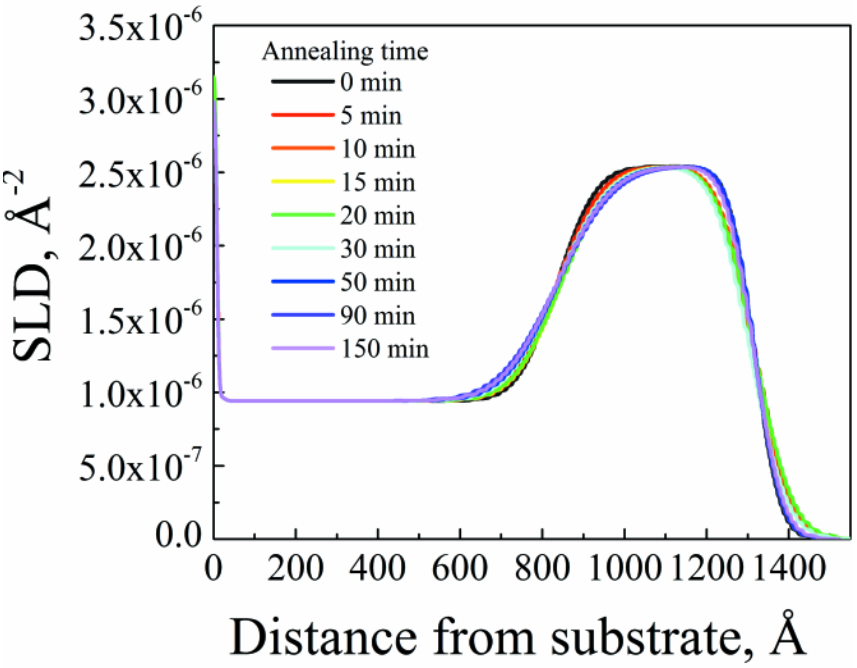

Fig. A-1. The neutron scattering density profiles for various times of annealing a 12bl-12bl QPC/PMAA$_{7k}$ film in 0.4M NaCl.

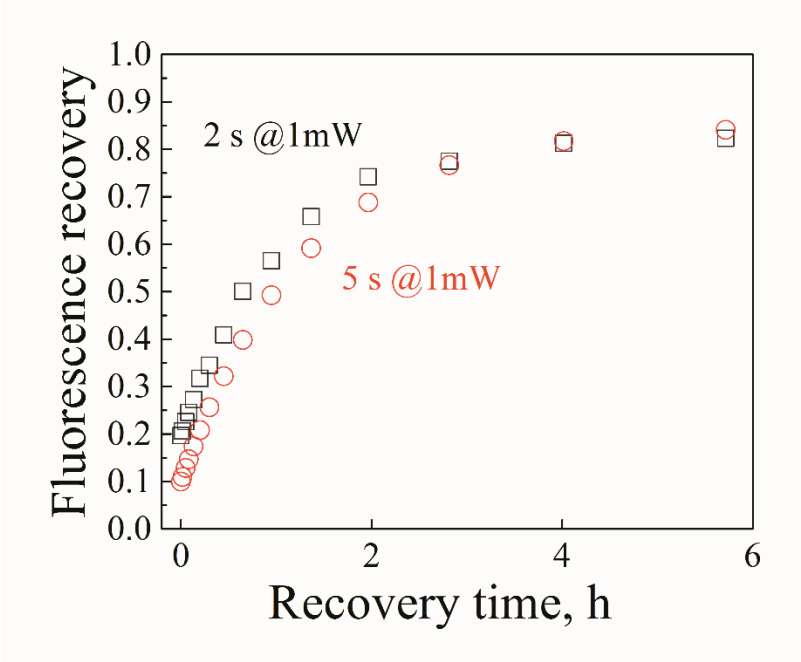

Fig. A-2. Fluorescence recovery monitored with a 1-μW laser beam for $(QPC/PMAA_{7k})_3/(QPC/PMAA_{7k}*)/(QPC/PMAA_{7k})_3$ films exposed to 0.1M NaCl solutions. Films were bleached to 20% and 10% of initial fluorescence for 2 and 5 s, respectively, using a 1mW laser beam.

APPENDIX B

SUPPORTING MATERIAL FOR CHAPTER 4

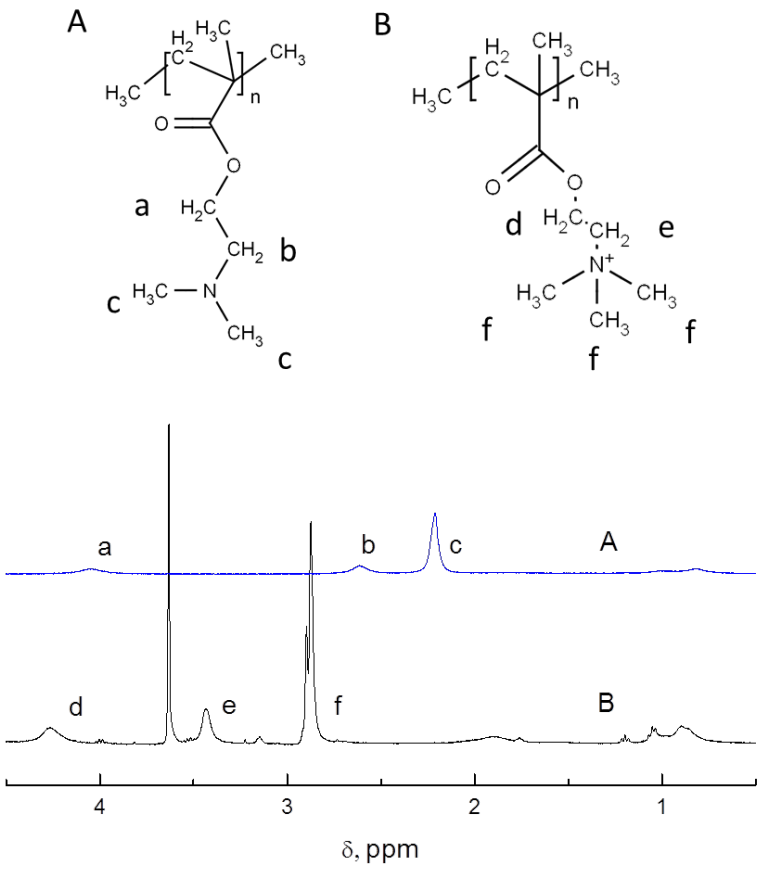

Fig. B-1. ^{1}H-NMR spectra of *h*PDMAEMA before quaternization (A) and after complete quaternization and conversion to *h*QPC (B) measured in D_2O at pH 9.

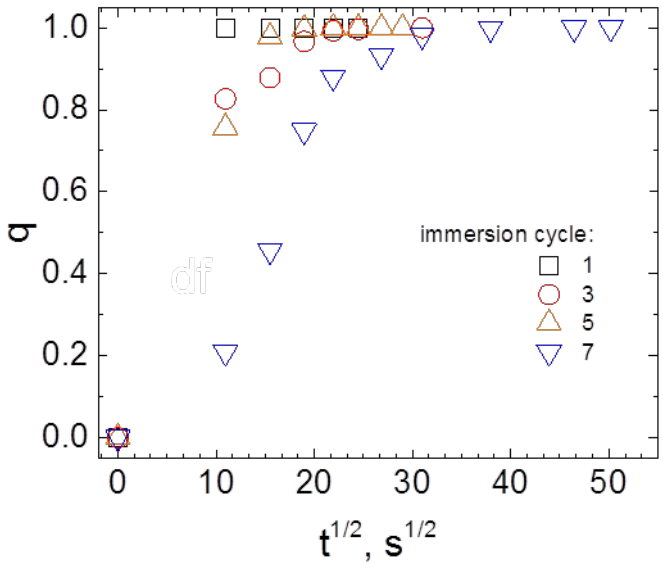

Fig B-2. The kinetics of PMAA uptake by the film during 1st, 3rd, 5th and 7th layer deposition steps.

Table B-1. Model parameters for $(PMAA/QPC)_4(dPMAA/QPC)(PMAA/QPC)_4$ film constructed using a 4 min per layer deposition time.

Layer	***Nb* (Å^{-2})**	***d* (Å)**	**σ_{int} (Å)**
H-stack	6.430E-07	457.0	47.6
d-stack	2.330E-06	143.4	66.8
H-stack	6.430E-07	478.3	57.2
BPEI	2.500E-07	29.8	29.8
SiO2	3.200E-06	18.0	5.0
Si	2.070E-06	100.0	5.0

Table B-2. Model parameters for $(PMAA/QPC)_4(QPC/dPMAA)(PMAA/QPC)_4$ film constructed using a 8 min per layer deposition time.

Layer	***Nb* (Å^{-2})**	***d* (Å)**	**σ_{int} (Å)**
H-stack	6.430E-07	477.4	139.0
D-stack	2.405E-06	260.0	166.0
H-stack	6.443E-07	404.0	118.8
BPEI	2.500E-07	75.0	75.0
SiO2	3.200E-06	18.0	5.0
Si	2.070E-06	100.0	5.0

Table B-3. Model parameters for $(PMAA/QPC)_3$ $(dPMAA/QPC)(PMAA/QPC)_2$ film constructed using a 24 min per layer deposition time.

Layer	***Nb* (Å^{-2})**	***d* (Å)**	**σ_{int} (Å)**
H-stack	6.430E-07	206.8	89.9
D-stack	2.136E-06	351.9	119.9
H-stack	6.430E-07	328.2	93.7
BPEI	2.500E-07	24.1	24.1
SiO2	3.200E-06	19.5	5.0
Si	2.070E-06	100.0	5.0

Table B-4. Model parameters for $(PMAA/QPC)_4(PMAA/dQPC)(PMAA/QPC)_4$ film constructed using a 4 min per layer deposition time.

.

Layer	***Nb* (Å^{-2})**	***d* (Å)**	σ_{int} **(Å)**
H-stack	6.430E-07	471.5	241.4
d-stack	2.260E-06	167.4	127.9
H-stack	6.430E-07	281.7	113.5
BPEI	2.500E-07	20.7	20.7
SiO2	3.200E-06	39.9	5.0
Si	2.070E-06	100.0	8.0

Table B-5. Model parameters for $(PMAA/QPC)_4(PMAA/dQPC)(PMAA/QPC)_4$ film constructed using a 8 min per layer deposition time.

Layer	***Nb* (Å^{-2})**	***d* (Å)**	σ_{int} **(Å)**
H-stack	6.430E-07	753.3	80.8
d-stack	2.522E-06	266.1	158.0
H-stack	6.430E-07	368.6	165.3
BPEI	4.850E-07	48.0	17.6
SiO2	3.200E-06	19.0	3.0
Si	2.070E-06	100.0	3.0

Table B-6. Model parameters for $(PMAA/QPC)_3(PMAA/dQPC)(PMAA/QPC)_2$ film constructed using a 24 min per layer deposition time.

Layer	*Nb* (Å^{-2})	*d* (Å)	σ_{int} (Å)
H-stack	6.430E-07	162.9	162.9
d-stack	2.080E-06	905.9	160.0
H-stack	6.430E-07	25.5	25.5
BPEI	1.100E-07	85.4	85
SiO2	3.200E-06	33.6	3.0
Si	2.070E-06	100.0	3.0

Table B-7. Model parameters for $(PMAA/QPC)_4(PMAA/dQPC)(PMAA/QPC)_4$ film constructed using a 8 min per layer deposition time after 30 min exposure to a 0.01 M phosphate buffer.

Layer	*Nb* (Å^{-2})	*d* (Å)	σ_{int} (Å)
H-stack	6.430E-07	753.3	80.8
d-stack	2.522E-06	266.0	148.4
H-stack	6.430E-07	382.4	165.3
BPEI	4.850E-07	48.0	17.6
SiO2	3.200E-06	19.0	3.0
Si	2.070E-06	100.0	3.0

Table B-8. Model parameters for $(PMAA/QPC)_4(dPMAA/QPC)(PMAA/QPC)_4$ film constructed using a 8 min per layer deposition time after 30 min exposure to a 0.01 M phosphate buffer.

Layer	*Nb* (Å^{-2})	*d* (Å)	σ_{int} (Å)
H-stack	6.430E-07	477.0	159.0
d-stack	2.405E-06	260.0	160.0
H-stack	6.443E-07	410.0	125.0
BPEI	2.500E-07	75.0	75.0
SiO2	3.200E-06	18.0	5.0
Si	2.070E-06	100.0	5.0

Table B-9. Model parameters for $(PMAA/QPC)_4(PMAA/dQPC)(PMAA/QPC)_4$ film constructed using a 8 min per layer deposition time after 210 min exposure to a 0.01 M phosphate buffer.

Layer	*Nb* (Å^{-2})	*d* (Å)	σ_{int} (Å)
H-stack	6.430E-07	753.3	78.0
d-stack	2.522E-06	266.0	167.0
H-stack	6.430E-07	366.7	165.3
BPEI	4.850E-07	48.0	17.6
SiO2	3.200E-06	19.0	3.0
Si	2.070E-06	100.0	3.0

Table B-10. Model parameters for $(PMAA/QPC)_4(dPMAA/QPC)(PMAA/QPC)_4$ film constructed using a 8 min per layer deposition time after 210 min exposure to a 0.01 M phosphate buffer.

Layer	*Nb* (Å^{-2})	*d* (Å)	σ_{int} (Å)
H-stack	6.430E-07	477.0	159.0
d-stack	2.405E-06	260.0	145.0
H-stack	6.443E-07	410.0	125.0
BPEI	2.500E-07	75.0	75.0
SiO2	3.200E-06	18.0	5.0
Si	2.070E-06	100.0	5.0

Table B-11. Model parameters for hydrogenated $(PMAA/QPC)_6$ film constructed using a 8 min per layer deposition time.

Layer	*Nb* (Å^{-2})	*d* (Å)	σ_{int} (Å)
H-Block	6.430E-07	1002.0	120.0
BPEI	3.790E-07	28.0	5.0
SiO2	3.200E-06	19.0	10.0
Si	2.070E-06	100.0	19.0

Table B-12. Model parameters for hydrogenated $(PMAA/QPC)_6$ film constructed using a 8 min per layer deposition time after 4 min exposure to a 0.2 mg/ml dQPC solution.

Layer	***Nb* (Å^{-2})**	***d* (Å)**	**σ_{int} (Å)**
D-block	7.000E-07	430.5	85.0
H-block	6.430E-07	556.6	180.0
BPEI	4.500E-07	73.5	62.5
SiO2	3.400E-06	16.0	5.0
Si	2.070E-06	100.0	5.0

Table B-13. Model parameters for hydrogenated $(PMAA/QPC)_6$ film constructed using a 8 min per layer deposition time after 8 min exposure to a 0.2 mg/ml dQPC solution.

Layer	***Nb* (Å^{-2})**	***d* (Å)**	**σ_{int} (Å)**
D-block	8.000E-07	589.7	100.8
H-block	6.430E-07	419.7	177.7
BPEI	5.000E-07	67.9	67.0
SiO2	3.400E-06	16.0	5.0
Si	2.070E-06	100.0	5.0

Table B-14. Model parameters for hydrogenated $(PMAA/QPC)_6$ film constructed using a 8 min per layer deposition time after 24 min exposure to a 0.2 mg/ml dQPC solution.

Layer	***Nb* (Å^{-2})**	***d* (Å)**	**σ_{int} (Å)**
D-block	1.080E-06	660.0	155.0
H-block	6.430E-07	352.0	325.9
BPEI	2.700E-07	75.0	62.5
SiO2	3.400E-06	16.0	5.0
Si	2.070E-06	100.0	5.0

Table B-15. Model parameters for hydrogenated $(PMAA/QPC)_6$ film constructed using a 8 min per layer deposition time after 48 min exposure to a 0.2 mg/ml dQPC solution.

Layer	***Nb* (Å^{-2})**	***d* (Å)**	**σ_{int} (Å)**
D-block	1.490E-06	1027.0	192.4
H-block	6.430E-07	68.8	88.6
BPEI	2.700E-07	75.0	62.5
SiO2	3.400E-06	16.0	5.0
Si	2.070E-06	100.0	5.0

Table B-16. Model parameters for hydrogenated $(PMAA/QPC)_6$ film constructed using a 8 min per layer deposition time after 96 min exposure to a 0.2 mg/ml dQPC solution.

Layer	***Nb* (Å^{-2})**	***d* (Å)**	**σ_{int} (Å)**
D-block	1.500E-06	1048.0	201.4
H-block	6.430E-07	75.0	64.2
BPEI	2.390E-07	75.0	62.5
SiO2	3.400E-06	16.0	5.0
Si	2.070E-06	100.0	5.0

Table B-17. Model parameters for hydrogenated $(PMAA/QPC)_6$ film constructed using a 8 min per layer deposition time after 192 min exposure to a 0.2 mg/ml dQPC solution.

Layer	***Nb* (Å^{-2})**	***d* (Å)**	σ_{int} **(Å)**
D-block	1.642E-06	1102.0	202.0
H-block	6.430E-07	69.4	69.4
BPEI	2.390E-07	75.0	62.5
SiO2	3.400E-06	16.0	5.0
Si	2.070E-06	100.0	5.0

Table B-18. SLD values calculated for the PEM components.

	QPC	PMAA	QPC	dPMAA	dQPC	PMAA	H_2O
SLD, Å^{-2}	4.71E-07	1.10E-06	4.71E-07	5.11E-06	6.36E-06	1.10E-06	-5.60E-07

Table B-19. Mass ratios calculated for the corresponding SLD values.

Exposure time, min	QPC mass ratio	PMAA mass ratio	dQPC mass ratio	Water content	SLD of D-containing block, Å^{-2}
0	0.460	0.439	0.000	0.101	6.43E-07
4	0.458	0.431	0.010	0.101	7.00E-07
8	0.451	0.424	0.023	0.101	7.70E-07
24	0.436	0.414	0.049	0.101	9.12E-07
48	0.417	0.363	0.118	0.101	1.29E-06
96	0.383	0.361	0.154	0.101	1.50E-06
192	0.364	0.356	0.178	0.101	1.64E-06
394	0.361	0.333	0.205	0.101	1.78E-06

APPENDIX C

SUPPORTING MATERIAL FOR CHAPTER 5

Table C-1. Model parameters for $QPC_8/dPMAA_9/QPC_{14}^{4min}$ film.

Layer	***Nb* (Å^{-2})**	***d* (Å)**	**σ_{int} (Å)**
H-stack	6.430E-07	457.0	47.6
D-stack	2.330E-06	143.4	66.8
H-stack	6.430E-07	478.3	57.2
BPEI	2.500E-07	29.8	29.8
SiO2	3.200E-06	18.0	5.0
Si	2.070E-06	100.0	5.0

Table C-2. Model parameters for $QPC_8/dPMAA_9/QPC_{14}^{8min}$ film.

Layer	***Nb* (Å^{-2})**	***d* (Å)**	**σ_{int} (Å)**
H-stack	6.430E-07	477.4	139.0
D-stack	2.405E-06	260.0	166.0
H-stack	6.443E-07	404.0	118.8
BPEI	2.500E-07	75.0	75.0
SiO2	3.200E-06	18.0	5.0
Si	2.070E-06	100.0	5.0

Table C-3. Model parameters for $QPC_4/dPMAA_5/QPC_{10}^{16min}$ film.

Layer	***Nb* (Å^{-2})**	***d* (Å)**	**σ_{int} (Å)**
H-stack	5.33E-07	652.6	165.6
D-stack	2.30E-06	270.1	178.0
H-stack	6.39E-07	290.5	120.0
BPEI	3.12E-07	15.9	5.0
SiO2	3.40E-06	26.1	16.3
Si	2.07E-06	100.0	19.0

Table C-4. Model parameters for $QPC_4/dPMAA_5/QPC_8^{24min}$ film.

Layer	***Nb* (Å^{-2})**	***d* (Å)**	**σ_{int} (Å)**
H-stack	7.550E-07	314.0	270.6
D-stack	2.287E-06	581.7	176.2
H-stack	1.550E-06	115.5	109.9
BPEI	3.500E-07	5.0	5.0
SiO2	3.200E-06	25.0	18.0
Si	2.070E-06	100.0	25.0

Table C-5. Model parameters for $PMAA_7^{24min}$.

Layer	***Nb* (Å^{-2})**	***d* (Å)**	**σ_{int} (Å)**
H-stack	6.430E-07	540.0	65.0
BPEI	3.790E-07	28.0	5.0
SiO2	3.200E-06	19.0	10.0
Si	2.070E-06	100.0	19.0

Table C-6. Model parameters for hydrogenated $PMAA_7^{24min}$ film after 4 min exposure to a 0.2 mg/ml *d*QPC solution.

Layer	***Nb* (Å^{-2})**	***d* (Å)**	**σ_{int} (Å)**
D-stack	1.980E-06	500.5	80.0
H-stack	6.430E-07	95.0	95.0
BPEI	3.790E-07	75.0	30.6
SiO2	3.200E-06	18.7	5.0
Si	2.070E-06	100.0	18.7

Table C-7. Model parameters for hydrogenated $PMAA_7^{24min}$ film after 8 min exposure to a 0.2 mg/ml *d*QPC solution.

Layer	***Nb* (Å^{-2})**	***d* (Å)**	**σ_{int} (Å)**
D-stack	2.050E-06	506.4	79.3
H-stack	6.430E-07	88.7	88.7
BPEI	3.790E-07	75.0	30.6
SiO2	3.200E-06	18.7	5.0
Si	2.070E-06	100.0	18.7

Table C-8. Model parameters for hydrogenated $PMAA_7^{24min}$ film after 24 min exposure to a 0.2 mg/ml *d*QPC solution.

Layer	***Nb* (Å^{-2})**	***d* (Å)**	**σ_{int} (Å)**
D-stack	1.953E-06	521.6	80.7
H-stack	6.430E-07	92.0	92.0
BPEI	3.790E-07	75.0	30.0
SiO2	3.200E-06	18.7	5.0
Si	2.070E-06	100.0	18.7

Table C-9. Model parameters for hydrogenated $PMAA_{11}^{8min}$ film.

Layer	***Nb* (Å^{-2})**	***d* (Å)**	**σ_{int} (Å)**
H-Block	6.430E-07	1002.0	120.0
BPEI	3.790E-07	28.0	5.0
SiO2	3.200E-06	19.0	10.0
Si	2.070E-06	100.0	19.0

Table C-10. Model parameters for hydrogenated $PMAA_{11}^{8min}$ film after 4 min exposure to a 0.2 mg/ml *d*QPC solution.

Layer	*Nb* (Å^{-2})	*d* (Å)	σ_{int} (Å)
D-block	7.000E-07	430.5	85.0
H-block	6.430E-07	556.6	180.0
BPEI	4.500E-07	73.5	62.5
SiO2	3.400E-06	16.0	5.0
Si	2.070E-06	100.0	5.0

Table C-11. Model parameters for hydrogenated $PMAA_{11}^{8min}$ film after 8 min exposure to a 0.2 mg/ml *d*QPC solution.

Layer	*Nb* (Å^{-2})	*d* (Å)	σ_{int} (Å)
D-block	8.000E-07	589.7	100.8
H-block	6.430E-07	419.7	177.7
BPEI	5.000E-07	67.9	67.0
SiO2	3.400E-06	16.0	5.0
Si	2.070E-06	100.0	5.0

Table C-12. Model parameters for hydrogenated $PMAA_{11}^{8min}$ film after 24 min exposure to a 0.2 mg/ml *d*QPC solution.

Layer	*Nb* (Å^{-2})	*d* (Å)	σ_{int} (Å)
D-block	1.080E-06	660.0	155.0
H-block	6.430E-07	352.0	325.9
BPEI	2.700E-07	75.0	62.5
SiO2	3.400E-06	16.0	5.0
Si	2.070E-06	100.0	5.0

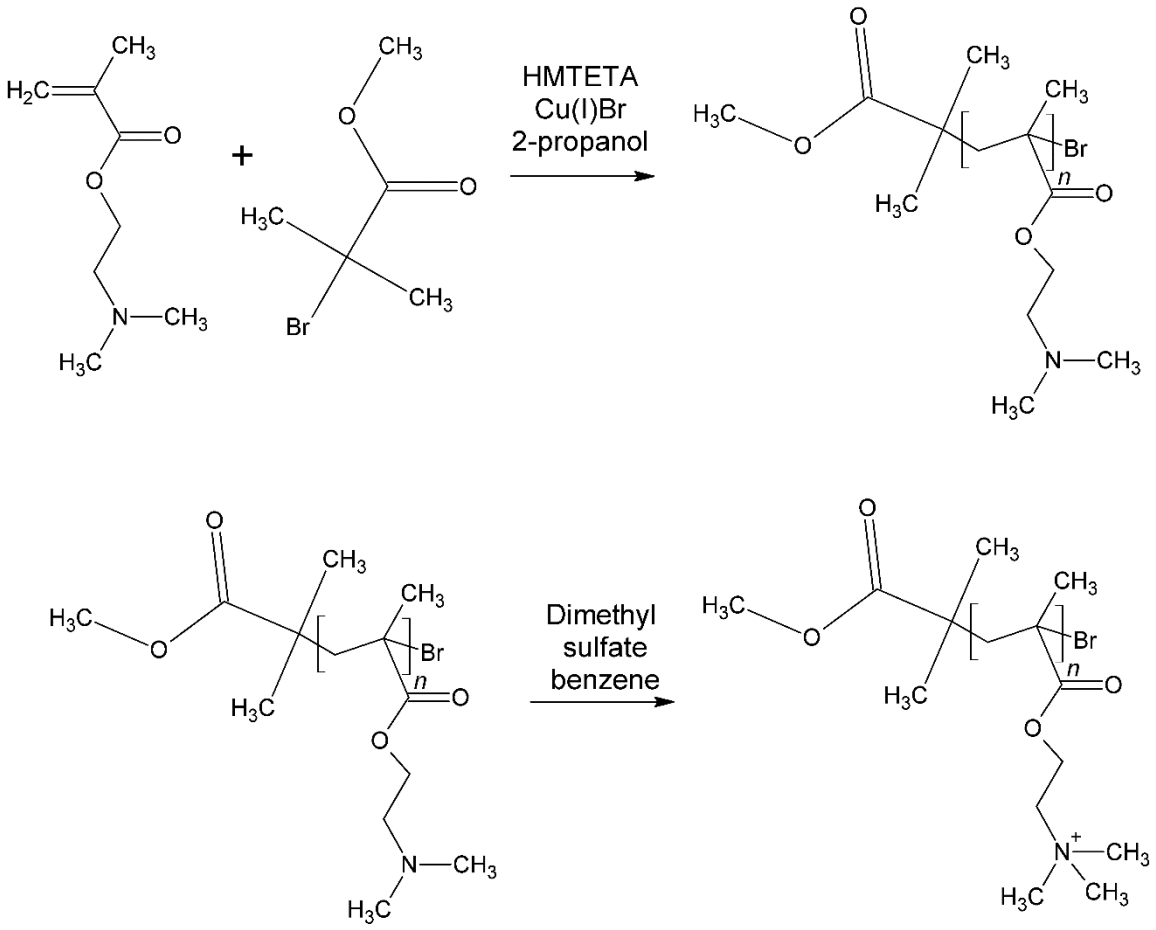

Fig C-1. Polymerization of DMAEMA (top) and quaternization of *h*PDMAEMA (bottom).

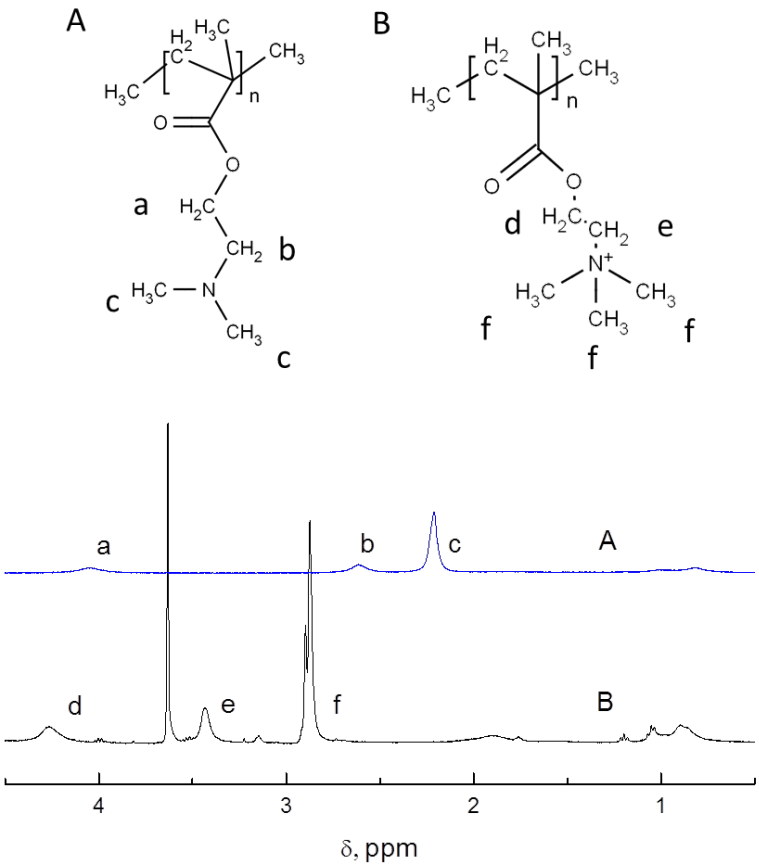

Fig. C-2. ^{1}H-NMR spectra of *h*PDMAEMA before quaternization (A) and after complete quaternization and conversion to *h*QPC (B) measured in D_2O at pH 9.